7th meeting
on Chemistry & Life

Conference Proceedings

FACULTY
OF CHEMISTRY

Faculty of Chemistry, Brno University of Technology
September 12–14, 2018
www.fch.vut.cz/chl2018

Gold and Silver Sponsors, Partners

FOSFA
Life Science

VUSTAH

TEVA

Unipetrol
ORLEN GROUP

Remarkplast
compounding

Synthon

Other Sponsors

Donators

INTERANTIONAL SCIENTIFIC BOARD

Chairman:

Martin Weiter (Brno University of Technology, Czech Republic)

Members:

Mikhail Borisover (Agriculture research organization, Volcani Center, Israel)

Pellegrino Conte (University of Palermo, Italy)

Alfred Crosby (University of Massachusetts Amherst U.S.A.)

Michal Čeppan (Slovak University of Technology in Bratislava, Slovakia)

Sabine Hild (Johannes Kepler University Linz, Austria)

Chris Holland (The University of Sheffield, England)

Josef Jancar (Brno University of Technology, Czech Republic)

Jiri Kučerík (Brno University of Technology, Czech Republic)

Tony Patti (Monash University, Australia)

Miloslav Pekař (Brno University of Technology, Czech Republic)

Jan Schwarzbauer (RWTH Aachen, Germany)

Peter Šimon (Slovak University of Technology in Bratislava, Slovakia)

František Šoukal (Brno University of Technology, Czech Republic)

Martin Tchingnabé Palou (Slovak University of Technology in Bratislava, Slovakia)

Martin Vala (Brno University of Technology, Czech Republic)

Michal Veselý (Brno University of Technology, Czech Republic)

Czech and Slovak Food Science Meeting:

Josef Balík (Mendel University in Brno, Czech Republic

František Buňka (Tomas Bata University in Zlin, Czech Republic)

Libor Červenka (University of Pardubice, Czech Republic)

Jozef Golian (Slovak University of Agriculture in Nitra, Slovakia)

Jana Hajšlová (University of Chemistry and Technology in Prague, Czech Republic)

Ivana Márová (Brno University of Technology, Czech Republic)

Zuzana Nouzovská, Director (General, National Agricultural and Food Centre, VUP Food Research Institute in Bratislava, Slovakia)

Martin Polovka (National Agricultural and Food Centre, VUP Food Research Institute in Bratislava, Slovakia)

Ján Šajbidor (Slovak University of Technology in Bratislava, Slovakia)

PHA Workshop:

Adriána Kovalčík (Brno University of Technology, Czech Republic)

Martin Koller (BOKU University, Tulln, Austria)

Ivana Márová (Brno University of Technology, Czech Republic)

Lenka Mynářová (Nafigate,Corp., a.s., Prague, Czech Republic)

Stanislav Obruča (Brno University of Technology, Czech Republic)

Radek Přikryl (Brno University of Technology, Czech Republic)

Ota Samek (Institute of Scientific Instruments in Brno, Czech Republic)

ORGANIZING COMMITTEE

Martin Vala (chairman)

Hana Alexová

Petr Dzik

Roman Hladík

Renata Komendová

Jitka Krouská

Ilona Pipková

Radek Přikryl

Eva Slaninová

Šárka Sovová

Michal Veselý

Oldřich Zmeškal

MAIN CONFERENCE TOPICS

- Environmental Chemistry and Technology
- Functional Materials
- Inorganic Materials
- Physical Chemistry & Life with special session on Advanced Fluorescence Techniques
- Photochemistry and Photocatalysis
- Organic Electronics and Bioelectronics
- Czech and Slovak Food Science Meeting dedicated to 100th anniversary of the Czechoslovak Republic establishment with special session aimed at:
  - historical perspective of 100 years in food sciences in Czech and Slovak regions,
  - trends and innovations in modern food science and technology, biotechnology and related fields.

PARALLEL EVENTS

Workshop on PHA Based Bioplastics

PHAs are a family of naturally occurring polymers produced as energy reserves of microorganisms. All members of the PHA family are fully biodegradable; not just in industrial composting equipment, but also in the soil and in the freshwater and seawater. Controlled PHA production and application belongs to the most important research topics at FCH BUT. The workshop is focused on the roundtable discussion of up to date problems regarding production of PHAs in different types of microorganisms, study of physical chemical properties of PHAs and their role in microbial cells, and possibilities to process natural PHAs into functional polymers. The key speakers will be specialists in PHA production and processing from foreign countries, cooperation institutions and FCH. PHA workshop is organized in cooperation with Institute of Scientific Instruments, The Czech Academy of Sciences under the project "Strategie AV21".

2nd GEODUST Workshop

Workshop is focused on education and training in soft skills related with scientific work and project management. The GEODUST is project of Marie Sklodowska-Curie program of H2020 that strengthens collaboration of research institutes and industrial companies in utilization of industrial by-products, esp. cement kiln bypass dust, in production of building materials.

PLENARY SPEAKERS

- Ines Fritz (BOKU University, Austria)
- Eric Glowacki (Linköping University, Sweden)
- Jose Luis Gomez-Ariza (University of Huelva, Spain)
- Marek Koutný (Tomas Bata University in Zlín, Czech Republic)
- Robert Liska (TU Wien, Austria)
- Angel Palomo (Spanish National Research Council, Spain)

INVITED SPEAKERS

- Milan Čertík (Slovak University of Technology, Slovakia)
- Sabine Hild (Johannes Kepler University Linz, Austria)
- Martin Hof (Czech Academy of Sciences, Czech Republic)
- Henryk Jelen (University Poznan, Poland)
- Tony Patti (Monash University, Australia)

LIST OF CONTRIBUTIONS

Plenary and invited lectures

Optoelectronic Stimulation of Cells with Organic Photocapacitors. *Eric Daniel Głowacki*

Combined Application of Metal Speciation and Omics in Food Quality Assessment. *Sara Ramírez-Acosta, Ana Arias-Borrego, Tamara García-Barrera, José Luis Gómez-Ariza*

Synthesis and characterization of smart hydrogel systems. *Sabine Hild*

Lipid Driven Nanodomains Are Fluid. *R. Šachl, M, Amaro, A. Koukalová, L.Veľas and M. HoF*

PHA - A Biodegradable Plastic To Solve Society Problems? *Ines Fritz*

Photopolymerization: From Biomaterials to 3D Printing. *Robert Liska*

Biodegradable Polymer Materials: Properties, Applications, and Environmental Fate. *Marek Koutný, Jana Šerá, Jan Salač*

Improved Nitrogen Fertilisers Utilising Humic Material Blends. *Biplob K. Saha, Michael T. Rose, Vanessa Wong, Timothy R. Cavagnaro and Antonio F. Patti*

Nanostructure of Cementitious Products: A MAS-NMR Approach. *Angel Palomo, Ana Fernandez-Jimenez*

PHA Workshop

Extremophiles – platform strains for sustainable production of polyhydroxyalkanoates. *Stanislav Obruca, Dan Kucera, Eva Slaninova, Iva Pernicova, Petr Sedlacek, Filip Mravec, Ivana Marova, Ota Samek, Ladislav Krzyzanek, Martin Vanek, Adriana Kovalcik, Lucie Mullerova, Aneta Chytilova, Ivana Novackova, Olga Kratochvilova, Jana Nebesarova*

Biological valorization strategy for converting spent coffee grounds into biopolymers and chemicals. *Adriana Kovalcik, Dan Kucera, Stanislav Obruca, Helena Hudeckova, Ivana Marova*

Monitoring of biotechnological production of microbial substances using Raman spectroscopy. *Ota Samek, Stanislav Obruča, Jan Ježek, Silva Bernatová, Zdeněk Pilát, Andrea Hároniková, Ivana Márová, Petr Sedláček, Dominika Gonová, Martin Šiler, Pavel Zemánek*

Environmental Chemistry and Technology

The photocatalytic decomposition of methanol over photocatalyst based on the TiO2. *Abouali galedari, Dubnová, L., Matějová, L., Reli, M., Drobná H., Čapek, L., Kočí, K.*

Urban aerosol: metals as starters of cellular stress? *Hana Barbořiková, Pavel Mikuška, Jozef Krajčovič*

Toxicity of Some Nitramines. *Karel Bednařík, Papírek Jan*

Application of Statistical Methods for Assessment of Soil Pollution. *Helena Doležalová Weissmannová, Silvie Mihočová, Petr Chovanec, Jan Brzobohatý*

Determination of PPD in Hair Dyes Collected from Local Markets in El-Bieda city – Libya. *Galal Elmanfe, Osama Khreit, Omukalthum Abduljalil and Enas S. Farag*

Anhydrous ethyl lactate synthesis by transesterification of oligomeric lactic acid. *Silvestr Figalla, Jaroslav Petruj, Tereza Švestková*

Development of New Voltammetric Approach for Determination of Plant Hormones Employing Boron-Doped Diamond Electrode as a Sensor. *Jaromíra Chýlková, Lenka Janíková, Miloš Sedlák, Jiří Váňa, Renáta Šelešovská*

Distinguishing the PET quality for its recycling. *Lucie Kabelíková, Jiří Kučerík*

Removing CO_2 from Air Masses by a Pilot-Plant Scubber Equipped With a Spiral Nozzle. *Josef Kalivoda, Tomáš Svěrák, Ondřej Krištof, Kateřina Mayerová*

Platinum nanoparticles in the environment and their impact on soil. *Renata Komendová, Michal Berka, Jiří Kučerík*

Possibilities of water and energy storage in the environment of fast-growing trees. *Kotlík, J., Půčková, H., Levek, P., Mikšík, F.*

Linking soil microbial quality indicators and thermo-oxidative stability. *Jiří Kučerík, Karel Svatoň, Stanislav Malý, Martin Brtnický, Christian Siewert*

System of efficient use of heat, water and electricity in family houses. *Petr Levek, Milada Vávrová, Josef Kotlík, Helena Půčková, František Mikšík, Silvie Kotlíková*

Preliminary Investigation into the Stimulation of Plant Growth Promoting Bacteria (Pgpb) by Soil Amendment With a Commercial Humic Acid. *Karen Little, Han Ming Gan, Michael Rose, William Roy Jackson, Timothy Cavagnaro and Antonio Patti1*

Assessment Adsorption behavior of K-Humat (Tki- Hümas) on carbon nanotubes from soil by provided E4/E6 ratios in different incubation times. *Abdelbagi Mohamedelnour, Muhittin Onur Akça, Sonay Sözüdoğru Ok*

Analysis of organic compounds in biochar produced by pyrolysis of sludge. *Ludmila Mravcová, Flávia Bittencourt Moré, Jakub Raček, Jan Ševčík, Josef Čáslavský, Milada Vávrová*

Possible solutions for process monitoring on the wastewater treatment plants. *Michal Petruľák, Josef Čáslavský*

The Role of Alkalis In Hydraulic Mixtures. *Prochazka, L.*

Environmental aspects of fast growing trees. *Puckova, H., Kotlik, J., Levek, P., Miksik, F., Kotlikova, S., Caslavsky, J.*

Artificial sweeteners in water. *Martina Repková, Nikola Dalajková, Libuše Vítková*

Spectrophotometric determination of chlorophyll in tests of phytotoxicity. *Veronika Řezáčová, Petra Rábová, Helena Zlámalová Gargošová*

From Chemistry to Technology - Biomass Gasification Product Gas Cleaning and Utilization. *Petr Seghman, Tomáš Jirout, Lukáš Krátký*

Phthalates concentration in Anzali wetland sediments, Iran. *Fatemeh Shariati, Mohammadjavad Mostafaloo, Shahab Shariati, Shayan Shariati*

The use of ion exchangers for preconcentration of platinum group metals. *Jiří Sýkora, Renata Komendová*

Determination of antidepressants and psychoactive drugs in waste water. *Vávrová Milada, Švestková Tereza, Mravcová Ludmila, Landová Pavlína, Křivánková Zuzana, Kočnar Michal*

Separation of air pollutants using different types of scrubbers. *Jaroslav Vlasák, Tomáš Svěrák, Lukáš Drevený, Josef Kalivoda*

Ecotoxicity evaluation of fire extinguishing agents. *Helena Zlámalová Gargošová, Barbora Jabandžievová*

Czech and Slovak Food Science Meeting

Lignans in foods and food fortification using 7-HMR. *Josef Balík, Pavel Híc, Jana Kulichová, Jan Tříska, Naděžda Vrchotová, Milan Houška*

DNA binding properties of p53 mutant R249S protein induced by exposure to aflatoxin in food. *Václav Brázda, Natália Vadovičová, Eva B. Jagelská, Jan Coufal*

Analysis of yeast exoproducts related to antifungal activity of Metschnikowia pulcherrima. *Emília Breierová, Dominika Šoltésová, Barbora Stratilová and Vlasta Sasinková*

Positioin of Food Fraud Prevention and Food Defence in Food Safety Management Systems. *František Buňka, Michaela Černíková*

Biotechnological Preparation of Functional Cereals-Based Food and Feed. *Milan Čertík, Tatiana Klempová, Ondrej Slaný, Miroslav Janák, Slavomír Marcinčák*

Validation of diffusive gradient in thin films technique for determination of mercury in fish sauce. *Pavel Diviš, Marek Reichstädter, Aneta Habartová and Jakub Křikala*

Diversity of Yeasts Colonizing Aboveground Plant Organs of Fruit Trees and the Soil Related to these Trees. *Hana Dudášová, Renáta Vadkertiová*

Comparison of sensitivity of DNA biochip and Real Time PCR for pork DNA in meat products. *Zuzana Drdolová, Jozef Golian*

Maldi TOF Analysis For Verification of Collection Yeasts And Classification of New Isolates. *Ágnes Horváthová, Natália Čurillová, Monika Vadkertiová, Laura Vyšehradská, Ivana Márová, Hana Dudášová, Barbora Stratilová*

Effects of conventional heating on fatty acids profile of virgin and refined olive oil. *Dani Dordevic, Lucia Hodulová, Simona Jančíková, Sanja Ćavar Zeljković*

The effect of final heating on the concentration of phthalic acid esters in sous-vide products. *Marcela Jandlová, Alžbeta Jarošová, Josef Kameník*

Pigmented yeasts as biotechnological factories for bioproducts and biofuels. *Márová I., Szotkowski M., Vanek M., Byrtusova D., Rapta M., Haronikova A., Certik M., Shapaval V*

Analytical and chemometric tools used for fruit juices authenticity evaluation. *Martin Polovka, Blanka Tobolková, Elena Belajová, Mária Kopuncová, Ján Durec*

Influence of the postfermentation technologies on selected chemical components of czech lager beer. *Jaromír Pořízka, Dominika Vopelková, Václav Štursa, Milena Vespalcová, Pavel Diviš*

Processing of pomace from chokeberry and elderberry. *Milena Vespalcová, Tereza Lošková, Zuzana Jurečková, Václav Štursa, Jaromír Pořízka, Pavel Diviš*

Influence of aroma compounds on sensory quality of processed cheese analogues. *Eva Vítová, Michal Sýkora, Martina Mahdalová, Kateřina Sůkalová*

Is rapeseed oil suitable for frying French fries? *Eva Vítová, Michal Sýkora, Martina Mahdalová, Kateřina Sůkalová*

Physical Chemistry & Life with Special Session on Advanced Fluorescence Techniques

Influence of surfactant concentration on hyaluronan hydrogel microstructure characteristics measured by FRET. *Zuzana Adamcová, Filip Mravec, Miloslav Pekař*

Förster Resonance Energy Transfer between Perylene and Fluorescein in Cationic Micellar Solutions. *Petra Holínková, Filip Mravec, Miloslav Pekař*

Preparation and research of cosmetic emulsions from solid TiO2 and emulsions prepared from dispersion of TiO2. *Sabina Jarabkova, Marcela Lastuvkova, Adam Jugl, Tomas Velcer, Jiri Smilek*

Study of Electrostatic Interactions between Hyaluronan and Amino Acids. *Adam Jugl, Miloslav Pekař, Hejná Jana*

Study of flow properties of powders in pharmaceutical industry. *Pavel Kolesa*

Sorption of Water Humidity by Selected Biopolymers by Means of Microcalorimetry *Jitka Krouská, Tomáš Bola, Vojtěch Enev, Miloslav Pekař*

Complex characterization of agarose hydrogels. *Marcela Lastuvkova, Milan Kracalik, Jiri Smilek*

Fluorescence Techniques in Hydrogel Characterization. *Filip Mravec*

Design of nanostructure models using grammatical evolution. *Pavel Osmera senior, Daniel Zuth, Anna Kucerova, Pavel Osmera junior, Monika Dosoudilová, Jan Muller, Tomas Marada, Ladislav Dobrovsky*

What keeps polyhydroxyalkanoates in bacterial cells amorphous? A contribution from stress-response experiments. *Petr Sedláček, Eva Slaninová, Stanislav Obruča*

Effects of Hydration of Sodium 3-Hydroxybutyrate on Phase Transitions Connected to Cryoprotectivity Of Microorganisms. *Eva Slaninová, Vitaly Kocherbitov, Petr Sedláček, Stanislav Obruča*

Light scattering techniques in the study on the formation of the interactions between polysaccharides and surfactants. *Michal Kalina, Šárka Sovová, Miloslav Pekař*

Organic Electronics & Photochemistry and Photocatalysis

Modification of Photocatalyst Morphology by Ball-milling and its Impact on the Physicochemical Properties of Wet Coated Layers. *Petr Dzik, Michal Veselý, Tomáš Svoboda*

Bioelectronical device for electrostimulation of stem cells. *Jiří Ehlich, Ota Salyk, Stanislav Stříteský, Lukáš Omasta, Eva Šafaříková, Jan Víteček, Lukáš Kubala, Martin Vala, Martin Weiter*

Improvement of Performance of Screen-Printed Electroluminescent Device by Reducing the Thickness of Dielectric Layer. *Michal Hrabal, Petr Dzik, Lukáš Omasta, Martin Vala, Martin Weiter*

Printed Perovskite Solar Cells with Carbon Back Electrode. *Matej Hvojnik, Michal Hatala, Barbora Krištofovičová, Pavol Gemeiner, Milan Mikula*

Optoelectronic control of single cells using organic photocapacitors. *Marie Jakešová, Malin Silverå Ejneby, Tony Schmidt, Johan Brask, Vedran Derek, Magnus Berggren, Rainer Schindl, Fredrik Elinder, Daniel Simon, Eric Daniel Głowacki*

Implementation of polycyclic cycloalkane systems: a path to high-performing, soluble, versatile and sustainable organic semiconducting materials. *Alexander Kovalenko, Cigdem Yumusak, Patricie Heihrichova, Stanislav Stritesky, Martin Vala, Martin Weiter Niyazi Serdar Sariciftci and Jozef Krajcovic*

Alkyl substitutions a powerful tool for tailormade properties of soluble and versatile organic semiconducting materials. *Jozef Krajčovič, Alexander Kovalenko, Martin Vala, Martin Weiter, Cigdem Yumusak, Niyazi Serdar Sariciftci*

Conductive polymers integrated into a textile matrix designed for sensor elements. *Kubáč, L., Pretl, S., Josefík, F., Martinková, L., Hamacek, A.*

Time-resolved kinetics of excitons, polarons and polaron pairs in organized thin films of conducting polymers. *Miroslav Menšík, David Rais, Jiří Pfleger, Petr Toman*

Screen Printed Biocompatible Photoresist as a mean to Enhance Performance of Organic Electrochemical Transistors. *Lukáš Omasta, Jiří Ehlich, Stanislav Stříteský, Michal Hrabal, Ota Salyk, Martin Vala, Martin Weiter, Milan Matejka*

High-k dielectrics for organic electronic devices. *Jiří Pfleger, Francesco Piana, Bartosz Paruzel, Yadu Ram Panthi*

Organic Solar Cells with an Inkjet Printed Hole-Extracting Graphene Oxide Layer. *Jan Pospisil, Alexander Kovalenko, Oldrich Zmeskal, Martin Vala*

Flashing light at the "dark" triplet states in organic semiconductors. *David Rais, Jiří Pfleger, Petr Toman, Miroslav Menšík, Yaduram Panthi, Martin Vala, Jozef Krajčovič, Stanislav Stříteský, Martin Weiter*

New bio-inspired organic semiconductors for bio-organic electronics. *Jan Richtar, Alexander Kovalenko, Martin Weiter, and Jozef Krajčovič*

Charge Carrier Mobility in Lamellar Structure of Conjugated Polymers. *Petr Toman, Miroslav Menšík, Jiří Pfleger*

Disposable Printed Ozone Dosimeter. *Michal Veselý, Petr Dzik, Zuzana Petříčková*

Contact resistance effects in organic field-effect transistors. *Martin Weis*

Artificial Photosynthesis: Learning from Nature. *Dong Ryeol Whang*

Organic field effect transistors based on hydrogen-bonded semiconductor pigments. *Cigdem Yumusak*

Inorganic Materials

Hybrid binder from recycled concrete powder and BPCKD. *Bílek, V.*

Preparation and characterization of electroless Ni-P coating on wrought ZE10 magnesium alloy. *Martin Buchtík, Petr Kosár, Jakub Tkacz, Pavel Doležal, Jaromír Wasserbauer*

Use of infrared spectroscopy as a tool for the identification and analysis of inorganic materials. *Jan Hajzler, Tomáš Opravil, Petr Ptáček, Petr Sedláček*

Durability of basalt fibres under the alkaline conditions. *Hrubý, P., Kalina, L., Másilko, J., Pořízka J.*

Alkali-activated slag-based systems with cement bypass dust incorporation. *Lukáš Kalina, Vlastimil Bílek Jr., František Šoukal, Tomáš Opravil*

Application of the theoretical knowledge of material engineering to building practice. *Konarik, J.*

Anhydrite stabilization in refractory materials. *Kotrla Jan, Šoukal František, Švec Jiří,*

Resistance of cementitious composites against ballistic loading. *Koutný Ondřej, Kratochvíl Jiří, Krátký Josef*

Basics of ballistic protection design. *Jiří Kratochvíl, Ondřej Koutný, Jiří Švec, Josef Krátký*

Ash – the raw material base for the future. *Marko M., Opravil, T., Šoukal F., Pořízka J.*

Development of heavyweight concrete for an eventual gamma and neutron-rays shielding application. *Janette Dragomirová, Martin Palou*

Formation of clinker containing lithium. *Theodor Staněk, Alexandra Rybová, Anežka Zezulová, Martin Boháč*

Differences in use of isothermal and isoperibolic calorimetry to assess the effect of zinc on hydration of cement blended with ground blast furnace slag and silica fume. *Pavel Šiler, Iva Kolářová, Jiří Dobiáš, Radoslav Novotný, Jiří Másilko, Jiří Švec, Jan Bednárek, Martin Janča, Tomáš Opravil*

Portland clinker characterization by scanning electron microscopy with BSE, EDS, WDS and EBSD. *Šoukal, F., Opravil, T., Ptáček P., Staněk T.*

Porous hydroxyapatite/alumina composites intended for bone tissue engineering. *Jan Vojtisek, Eva Bartonickova, Juliana Drabikova, Jaromir Porizka*

Functional Materials

Processing stabilization of poly(3-hydroxybutyrate)/poly(lactic acid) blends with oligomeric carbodiimide. *Veronika Melcova, Radek Prikryl, Premysl Mencik, Jiri Tochacek*

Biodegradable composite materials based on poly(3 hydroxybutyrate) for 3D printing applications. *Premysl Mencik, Veronika Melcova, Radek Prikryl, Sona Kontarova, Jano Bockaj, Pavol Alexy*

Adhesion and Mechanical Properties of a-CSi:H Thin Films Prepared from Tetravinylsilane Monomer by Plasma Polymerization. *Tomas Plichta, Martin Branecky, Vladimir Cech*

Synthesis of lactic acid-based thermosetting bio-polyester. *Tomáš Porubský, Mikael Skrifvars, Jaroslav Petrůj*

The Effect of Bioactive Additives on Morphology and Biological Properties of Collagen-Based Nanostructured

Resorbable Skin Substitutes. *Lucy Vojtova, Johana Babrnakova, Veronika Pavlinakova, Lucie Vistejnova, Veronika Stepankova, Eva Filova, Martin Knoz, Bretislav Lipovy, Jakub Holoubek, Zdenek Pavlovsky, Martin Faldyna, Eduard Göpfert, Jiri Damborsky, Vanessa Hearnden*

Young Researchers Forum

Cytotoxic activity of liposome particles with natural source of antioxidants for food and cosmetic application. *Jitka Bokrova, Ivana Maslonkova, Renata Pavelkova, Petra Matouskova, Ivana Marova*

High-ordered adamantane-substituted industrial organic dyes for organic semiconducting materials. *Martin Ciganek, Jozef Krajcovic*

Antibacterial 3D Porous Collagen Scaffolds for Soft Tissue Regeneration. *Jana Dorazilová, Johana Babrnáková, Kristýna Šmerková, Pavel Kopel, Silvia Kočiová, Pavel Diviš4, Vojtěch Adam3, Lucy Vojtová*

Polylysine Coated Magnetic Nanoparticles As A Tool For DNA Isolation From Real Samples. *Lenka Fialova, Alena Spanova, Bohuslav Rittich*

Characterization of adsorption properties of probiotic bacteria. *Eva Fryšová, Klára Černá, Eva Slaninová, Stanislav Obruča, Aneta Chytilová*

The Effect Of Antibacterial Selenium Nanoparticles On The Properties Of Polymer-Phosphate Bone Fillers. *Veronika Grézlová, Lenka Michlovská, Kristýna Šmerková, Pavel Kopel, Vojtěch Adam, Silvia Kočiová, Petr Bábor, Pavel Diviš, Petr Poláček, Lucy Vojtová*

The comparison of platinum metal contaminations of the environment in Brno, Czech Republic and Moscow, Russia. *Stanislav Ježek, Renata Komendová*

Improving the Stability of Perovskite Solar Cells. *Matouš Kratochvíl, Dávid Strachala, Adam Gajdoš, Martin Weiter*

Thermal properties of electro insulating papers. *Lucie Marackova, Veronika Melcova, Josef Samek, Oldrich Zmeskal*

Single Cell Analysis And Use Of Autofluorescence In Pha Synthesising Bacteria. *Lucie Müllerová, Stanislav Obruča, Filip Mravec, Kateřina Bílková*

The Use of Natural Extracts in Cosmetics and Subsequent Detection of Plants DNA Using Moleculat Diagnostic Methods. *Renata Pavelková, Denisa Romanovská, Monika Plachá, Anna Plášková, Petra Matoušková, Andrea Hároniková, Ivana Márová*

Screening of biosurfactants excretion among selected bacteria. *Iva Pernicová, Olga Kratochvílová, Dan Kučera, Stanislav Obruča*

Stability of methylated humic acids. *Jan Rybárik, Vojtěch Enev, Martina Klučáková*

Organic Transistors Towards Bio-electronic Applications. *Stanislav Stříteský, Lukáš Omasta, Jiří Ehlich, Šárka Tumová, Aneta Marková, Eva Šafaříková, Jan Víteček, Lukáš Kubala, Lubomír Kubáč, Ota Salyk, Martin Vala, Martin Weiter*

Monitoring of the fatty acid content in Swiss type cheese. *Michal Sýkora, Eva Vítová*

Study of potencial use and production of carotenoid, lipid enriched biomass using extremophilic algae isolated from Rio Tinto, Spain. *Martin Szotkowski, Carlos Vilchez Lobato, Ivana Márová*

Removal of sulfonamides antibiotics by wood-decay fungi from water matrix. *Suková Petra, Žižlavská Adéla, Švestková Tereza, Vávrová Milada*

Modelling of Bioelectronic devices. *Truksa, J.*

Modification of PEDOT:PSS Surface by RGD Peptide. *Šárka Tumová, Romana Malečková, Vojtěch Enev, Stanislav Stříteský, Martin Vala, Martin Weiter*

Thixotropic Polymer-Composite Bone Cement. *Kristýna Valová, Lenka Michlovská, Klára Částková, Lucy Vojtová*

On Mixing and Separation During Polyhydroxyalkanoates Extraction – Yield and Purity Optimization. *Martin Vanek, Libor Tomala, Martin Szotkowski, Ivana Novackova, Stanislav Obruca*

Psychoactive pharmaceuticals in water. *Petra Venská, Martina Repková, Milada Vávrová*

Analysis of Betaglucans in selected commercial products and higher funghi with their possibility use in pharmaceutical industry. *Marie Vysoká, Dana Byrtusová, H. Thra Phan, P. Matoušková, I. Márová*

TABLE OF CONTENTS

Preface: Dear Attendees, Colleagues and Friends

The Meeting on Chemistry and Life has a rich tradition of bringing together students, innovators, and leaders in chemistry into a vibrant and highly integrative forum that is conducive to sharing information, gaining knowledge, strengthening collaborations and moving forward the chemical science and technology in basic and applied research.

This year's technical programme encompassed six areas that covered the broad spectrum of activities in materials, environmental and food chemistry and technology, biotechnology, physical chemistry and applied chemistry and provided a unique opportunity to share and discuss the latest developments.

A special forum was dedicated to Czech and Slovak food science on the occasion of the 100th anniversary of the establishment of the independent Czechoslovak Republic. In addition to an exceptional technical programme, Chemistry & Life 2018 gathered the attendees to educational and outreach activities; including an exciting Workshop on PHA based bioplastics and GEODUST Workshop focused on education and training in soft skills related to scientific work and project management.

Finally, we thank all of you for attending and bringing your expertise to this conference. You as the leaders of this field, have a vision, the knowledge, and the experience to pave the way into the chemistry and life future. Through this conference, we had a chance to share our visions and help to shape the future of chemical science and technology.

Martin Weiter
Conference Chair

Martin Vala
Organizing Committee Chair

The conference was held under the auspices of the rector of Brno University of Technology, professor Petr Štěpánek on the occasion of the 120th establishment of the Brno University of Technology.

FÖRSTER DISTANCE BETWEEN PERYLENE AND FLUORESCEIN IN CATIONIC MICELLAR SOLUTION

PETRA HOLÍNKOVÁ*, MILOSLAV PEKAŘ

Materials Research Centre, Faculty of Chemistry, Brno University of Technology, Purkyňova 118, 612 00 Brno, xcucekajova@fch.vut.cz

Abstract

Fluorescence energy transfer via Förster mechanism occurs by a radiationless, coulombic, dipole-dipole interaction between two molecules (donor and acceptor) and is active over a range from 1 to 10 nm. This process is dependent upon the donor-acceptor distance. Therefore, energy transfer has been proposed as a spectroscopic measure for determination of interchromophore distances in macromolecules and microheterogeneous systems. This makes it a well suited technique to probe nanoscale processes. This paper deals with determination of critical transfer distance called Förster distance between perylene (donor) and fluorescein (acceptor) in two cationic micellar solutions (CTAB, Septonex) as the basis for further experimental work.

Introduction

Förster energy transfer (FRET)[1] is a physical phenomenon describing the radiationless energy transfer between two molecules of fluorophores – donor (D) and acceptor (A). This coulombic, dipole-dipole interaction is active over a range from 10 to 100 Å[2], which makes it well suited to follow molecular interactions and determine distances on the nanometer scale.

FRET requires spectral overlap between the donor emission and acceptor's absorption, along with the suitable orientation of their transition dipoles[1]. Also FRET is dependent on quantum yield of donor and distance between donors and acceptors. The strength of spectral overlap of donor emission and acceptor absorption is characterized by the overlap integral *J*, which can be expressed as

$$J = (\int_0^\infty I_D(\lambda)\, \varepsilon_A(\lambda)\, \lambda^4\, d\lambda)/(\int_0^\infty I_D(\lambda)\, d\lambda) \qquad (1)$$

where $I_D(\lambda)$ is fluorescence intensity of donor, $\varepsilon_A(\lambda)$ is absorption molar coefficient of acceptor and λ is wavelength. This contributes to the critical transfer distance known as the Förster distance R_0, which is the distance at which energy transfer between donor and acceptor is 50% efficient. This distance is characteristic for donor-acceptor pair and its formula is given below.

$$R_0 = 0.2108\, [n^{-4}\, \phi_D\, \kappa^2\, J]^{1/6} \qquad (2)$$

where *n* is refractive index, ϕ_D is donor fluorescence quantum yield and κ^2 is orientation factor for the transition dipoles, which is 2/3 for a random orientation.

Generally, surfactants are amphiphilic molecules with relatively long hydrophobic tails and short hydrophilic heads. This special structure of surfactant is responsible for self-organizing in water, which leads to form aggregates called micelles. Studied of energy transfer in micelles[3] are especially interesting because these systems provide a structure where it is possible to get high local concentration and spatial proximity between donor and acceptor molecules.

This paper is focused on determination of Förster distance for perylen as a donor and fluorescein as an acceptor in two cationic micellar (CTAB and Septonex). Perylene is located in hydrophobic core of these micelles, while fluorescein is micellized in the inner part of the Stern region[4].

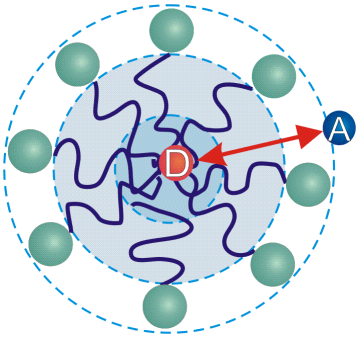

Fig. 1. **Localization of perylene (D) and fluorescein (A) in the cationic micelle.**

Experimental

Materials. The cationic surfactant Septonex (carbethopendecinium bromide, Czech Pharmacopoeia quality) was purchased from GBNchem, Czech Republic, and cetyltrimethylammonium bromide (CTAB, purity ≥ 99.0%) from Sigma-Aldrich, Czech Republic. Experiments were carried out using perylene (purity ≥ 99.0%, Fluka, Czech Republic) and fluorescein (purity ≥ 99.0%, Sigma-Aldrich, Czech Republic) as a fluorescence probes. All chemicals were of the best available quality and used as received without further purification. Deionised water was used throughout this study (PURELAB Option R7/15; ELGA, Great Britain).

Preparation of samples. A stock solution of perylene and fluorescein was prepared in acetone. Stock solutions of CTAB and Septonex were prepared in water. An appropriate amount of fluorescence probe stock solution was added to glass vials and the acetone was evaporated under reduced pressure. Subsequently, the surfactant stock solution and water were added. All samples were stirred overnight at laboratory temperature.

Fluorescein has increasing concentration from $1 \cdot 10^{-6}$ M to $2.5 \cdot 10^{-5}$ M in the series of samples for determination of fluorescein molar absorption coefficient in 2 mM surfactant solutions without perylene. The quantum yield of perylene was established in 2 mM Septonex and 2 mM CTAB solutions. The perylene concentration was chosen to $5 \cdot 10^{-6}$ M based on the measurement of absorbance. The refractive index was measured for 2 mM pure micellar solution of Septonex or CTAB.

Measurement. Fluorescein absorption spectra with a wavelength range of 300–700 nm were recorded on a Varian Cary 50 Probe UV-VIS spectrophotometer. Fluorescence spectra were measured on a Flurolog spectrofluorimeter (Horiba Scientific). Emission spectra of perylene were recorded between

420–620 nm with the excitation wavelength set to 389 nm. The absolute quantum yield of perylene was determined using the integration sphere Quanta-ϕ on Fluorolog. All measurements were performed at 25 ± 1 °C.

Results and disccussion

Fig. 2 shows absorption fluorescein spectra in micellar solutions of CTAB and Septonex. The molar absorption coefficient of fluorescein was determined from the slopes of dependences of the maximum fluorescein absorbance (502 nm) at the fluorescein concentration in the sample. The value of fluorescein absorption coefficient was determined as $\varepsilon_{A,Sept}$ = 55 289 dm^3 mol^{-1} cm^{-1} and $\varepsilon_{A,CTAB}$ = 35 044 dm^3 mol^{-1} cm^{-1}.

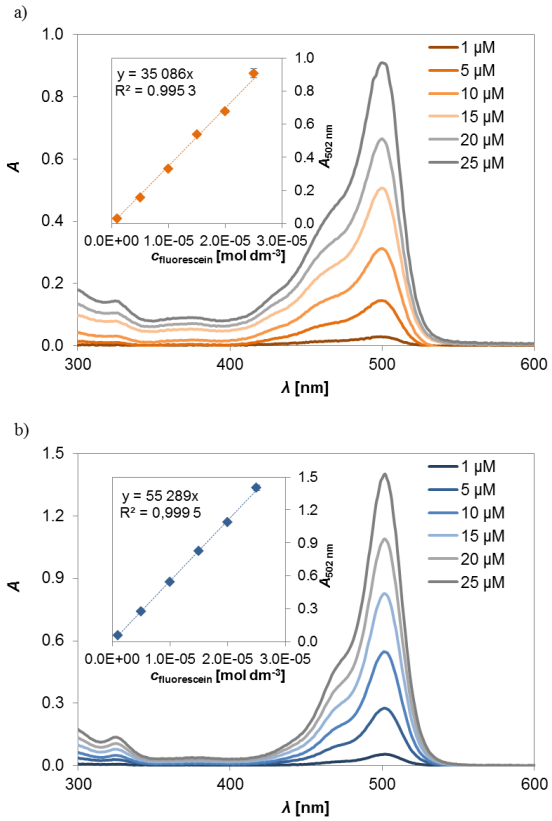

Fig. 2. **Absorption spectra of two cationic micellar solutions with varying concentration of fluorescein. a) 2 mM CTAB, b) 2 mM Septonex.**

The main condition of Förster resonance energy transfer is the spectral overlap of donor emission and acceptor absorption. Fig. 3 shows the overlap of fluorescence spectra of perylene and absorption spectra of fluorescein in cationic micelles. The perylene-fluorescein pair is suitable for energy transfer process because besides presenting a considerable overlap it is possible to excite the donor without exciting the acceptor.

The value of overlap integral J was calculated according to the equation 1. The value for this parameter was found to be $J_{CTAB} = 8.30 \cdot 10^{14}$ dm^3 cm^3 mol^{-1} and $J_{Sept} = 8.59 \cdot 10^{14}$ dm^3 cm^3 mol^{-1}.

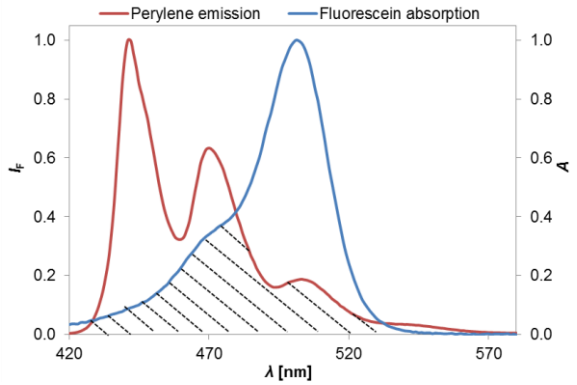

Fig. 3. **Emission spectra of perylene and absorption spectra of fluorescein in 2 mM Septonex solution.**

The refractive indexes of used micellar solutions was determined to be n_{CTAB} = 1.3313 and n_{Sept} = 1.3316. The quantum yield of perylene fluorescence was found to be $\phi_{D,CTAB}$ = 0.861 for 2 mM CTAB solution and $\phi_{D,Sept}$ = 0.921 for Septonex micellar solution.

The Förster distance for perylene-fluorescein pair was calculated according to equation 2. We obtained the values $R_{0,CTAB}$ = 4.87 nm and $R_{0,Sept}$ = 4.91 nm. These values of Förster distance for perylene-fluorescein in different micellar media are in good agreement with each other.

Conclusion

In this paper we investigated the Förster distance between perylen as a donor and fluorescein as an acceptor in two cationic micellar solutions. We obtained the values 4.87 nm for CTAB micellar solution and 4.91 nm for Septonex micellar solution. These results are in good agreement with each other.

This work was supported by Materials Research Centre at FCH BUT- Sustainability and Development, REG LO1211, with financial support from National Programme for Sustainability I (Ministry of Education, Youth and Sports).

REFERENCES

1. Dos Remedios C.: J. Struct. Biol. *115*, 175 (1995).
2. Förster T.: Radiat. Res. Suppl. *2*, 326 (1960).
3. Kalyanasundaram K.: *Photochemistry in microheterogeneous systems*, Academic Press, Orlando 1987.
4. Sánchez F.G., Ruiz C.C.: J. Lumin. *69*, 179 (1986).

PRINTED PEROVSKITE SOLAR CELLS WITH CARBON BACK ELECTRODE

MATEJ HVOJNIK*, MICHAL HATALA, BARBORA KRIŠTOFOVIČOVÁ, MICHAELA PAVLIČKOVÁ, PAVOL GEMEINER, MILAN MIKULA

Department of Printing Arts Technology and Photochemistry, Faculty of Chemical and Food Technology STU in Bratislava, Radlinského 9, 812 37, Bratislava, matej.hvojnik@gmail.com

Electricity generation is based on the combustion of coal, oil and natural gases which are non-renewable energy sources. It has been found that combustion increases the concentration of harmful gases in the air, which can lead to global warming, destruction of the ozone layer and acid rains. An alternative is renewable sources such as sun, wind, water, geothermal resources, etc. The sun is the unexhausted source with the key role for our life on the Earth. Solar cells represent a direct way to transform solar energy into electricity, create no harmful substances, and therefore represent an excellent alternative to conventional sources of electricity. At present crystalline silicon solar cells dominate due to a high efficiency and stability. Their disadvantage is high production costs, so they are used in small quantities. Thin film solar cells based on CIGS and CdTe are cheaper, but they are still expensive in terms of electricity costs and ecologically harmful. Organic solar cells, dye-sensitized solar cells, and solar cells with quantum dots have considerable potential due to their low supposed cost and easier preparation, but their performance does not reach till yet values like their inorganic counterparts.

Organometal trihalide perovskite solar cells (PSCs) have been much enhanced in the past few years as an interesting alternative due to their simple and low-cost solution-processed fabrication techniques. Many variations of PSCs were found to improve preparation process, efficiency and stability. Among them, carbon-based C-PSCs without hole transport materials[1] seem to be very promising for the stability because carbon materials are stable, water-resistant and inert to ion migration from perovskite and electrodes.

C-based systems use mesoporous oxide (TiO_2) electrodes and porous scaffold space and separating layers (Al_2O_3, ZrO_2) through which the perovskite precursores are infiltrated. The system originates from dye sensitized solar cell (DSSC) where mesoporous layers were standardly printed with nano-oxide pastes[2] and where also C-based materials including conductive polymers and nanotubes were used as a counter-electrode[3].

In this work printable perovskite cells with a C-based back electrode were prepared using low-temperature and high-temperature processes of mesoporous oxide layers application and using different hole blocking compact TiO_2 layers. Oxide layers were screen printed and carbon layers doctor bladed. Moreover, the functionality of the cells prepared with our pastes was compared with the cells prepared with commercial pastes from Solaronix.

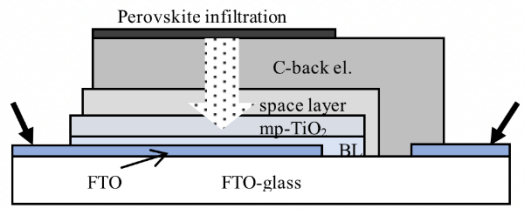

Fig. 1. **Carbon based perovskite solar cell structure**

In the first step, low-temperature perovskite solar cells (PSCs) were prepared on commercial FTO/glass substrates, onto which three different blocking layers (BL) were first applied: i) the blocking layer prepared from 0.2 M $TiCl_4$ solution by spontaneous growth, ii) by a spin coating of 1.8 wt% titanium diisopropoxide bis(acetylacetonate) (TiAcAc) solution in isopropanol and of iii) TiAcAc (1.8 wt%) with TiO_2 nanoparticles (0.4 wt%, 20 nm, P25 Degussa). $TiCl_4$ was hydrolyzed in water at 70°C for 1, 1.5 2h, resulting in the formation of crystalline TiO_2 (rutile) nanoparticles[4]. Next, mesoporous TiO_2 oxide layer and the cover TiO_2 layer was applied on the oxide layers by spontaneous growth from the 0.06 M $TiCl_4$ solution (70°C, 0.5 h reacting time). Finaly porous scaffold space and separating layer Al_2O_3 were applied onto the whole oxide system. Mesoporous and porous layer were applied by a spin coating at laboratory conditions. These layers enable perovskite infiltration and suppress disruptions occurring in the blocking layers. A two-step deposition process was used to grow the $CH_3NH_3PbI_3$ perovskite layer. The procedure consists of spin coating of 32.9 wt% PbI_2 solution in dimethylformamide (DMF) onto the oxide surface, followed by immersion of the PbI_2 coated substrate into a 1 wt% solution of CH_3NH_3I in isopropanol. Finally thick low-temperature (120° C) carbon back electrode was applied by the doctor blade technique on the system (perovskite). Carbon back electrode was prepared from carbon black and grafit particles (1:3) in chlorobenzene (20 wt%).

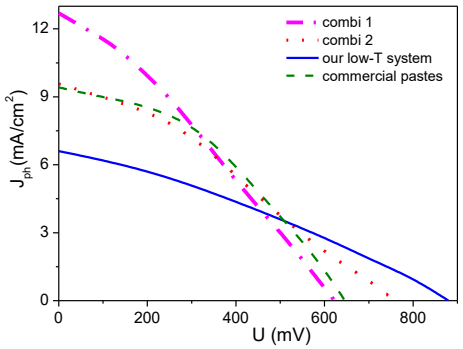

Fig. 2. **V-A loading photocurves of cells (defined in Tab. I) under standard day-ligh**

The conversion efficiency of solar to electric energy was determined measuring photocurrent-voltage load characteristics under 1000 W/m^2 of standard day light exposition.

PSCs with TiAcAc and the TiAcAc + P25 blocking layer have shown a minimal, eventually zero photocurrent, probably due to microdefects in blocking layers, low curing temperature, and also due to high series resistance of the carbon paste layer. Another reason may be the high roughness of the FTO layer, where we apparently could not prepare a compact blocking layer of the TiAcAc and TiAcAc + P25 type. The best efficiency 1.8 % was achieved by mesoporous PSCs employing the rutile TiO_2 blocking layer prepared from 0.2 M $TiCl_4$ with 2h of reaction time which is more compact with less of defects than coated blocking layers, due to its spontaneous uniform growth. Another reason is that the FTO layer has the same rutile crystalline structure as the blocking layer and so creates better interfacial contact. In the next preparation of solar cells, just blocking layers prepared from solution $TiCl_4$ were used.

In the next step, there were prepared high-temperature perovskite solar cells from commercial Solaronix pastes with the structure shown in Figure 1. The solaronix system is fully printable with screen printing techniqe except for the perovskite layer. For perovskite infiltration we used one step methods. The infiltration of the perovskite layer followed after the C-layer was sintered. To the commercial blocking layer of this system, we additionally incorporated also the TiO_2 blocking layers prepared from 0.2M $TiCl_4$ solution with 1.5 and 2h reacting time.

Systems with deposited $TiCl_4$ layers had a lower fill factor compared with the Solaronix system that is caused by high series and low paralel resistences resulting in the linearity of V - A curves (Tab. I, Fig. 2). Nevertheless, the cells with $TiCl_4$ layer achieved a higher short circiut photo-current and/or higher open circuit voltages. With the system Solaronix, we anticipated better parameters than we have achieved. The cause may be in the preparation condition and environment leading to high level of microdefects in layers and finaly short-circuits inside the cells. Under our laboratory conditions we can not provide the kind of thorough cleanliness and boxes that are required in the preparation of solar cells. The deffects can be seen already within the optical microscope characterization of the layers, below (Fig. 4, 5).

Table I, Parameters of V-A curves of different solar systems

System	Low T	Solaronix (commercial pastes)	Solaronix 0,2 M $TiCl_4$ 2 h (combi 1)	Solaronix 0,2 M $TiCl_4$ 1.5 h (combi 2)
U_{oc} [mV]	883	646	623	683
I_{sc} [mA]	1.316	2.83	3.81	2.77
Jsc [mA/cm^2]	6.58	9.42	12.70	9.22
P_{max} [mW/cm^2]	1803	2447	2333	1723
FF	0.31	0.40	0.29	0.27
η [%]	1.80	2.45	2.33	1.72

Table II, Parameters of V-A curves of the cells with Solaronix pastes

System	Solaronix (commercial pastes)	Solaronix (commercial pastes)
Active area [cm^2]	0.30	0.06
U_{oc} [mV]	646	810
I_{sc} [mA]	2.83	0.816
Jsc [mA/cm^2]	9.42	13.60
P_{max} [mW/cm^2]	2447	4080
FF	0.40	0.48
η [%]	2.45	5.25

Later on, by reducing the active area of solar cells from 0.30 cm^2 to 0.06 cm^2, we have succeeded in increasing the efficiency of the commercial Solaronix pastes system from 2.45 % to 5.25 % (Table II). Efficiency has increased probably due to a smaller occurrence of micro defects in the functional layers.

The individual layers were characterized by microscopic and spectroscopic methods. From the microscopic images taken, it can be concluded that the individual blocking layers are relatively homogeneous, without large breakdowns, cracks or layer breaks, but with a considerable amount of micro-defects.

Mesoporous layers were characterized by atomic force microscopy (AFM, Fig. 6). The AFM scan of TiO_2 layer shows many agregates and micro-defects.

On mesoporous Al_2O_3 layers (Fig. 7), there are minor impurities in the layer that could have an impact on the efficiency of the solar cells. Legible interferences show that the layer is sufficiently homogeneous in thickness.

The mesoporous ZrO_2 layer (Fig. 8) had the biggest and optically visibly roughness, but rather homogeneous.

AFM and UV-VIS microscopy were used to determine the roughness Rq and the thickness of mesoporous layers.

In case of AFM the thicknesses of the mesoporous layers were estimated scanning the edge of a mechanically made groove, as follows (Table III).

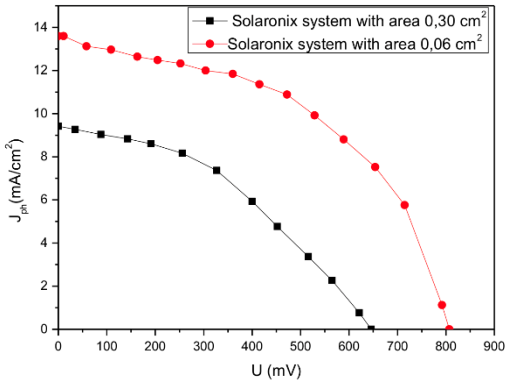

Fig. 3. **V-A photocurves of Solaronix systems under standard day-light**

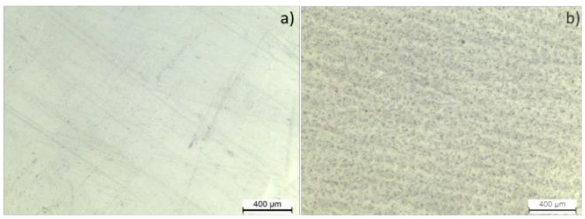

Fig. 4. **a) Optical micro-photos: BL TiAcAc on FTO/glass, b) BL TiAcAc+P25 on FTO/glass**

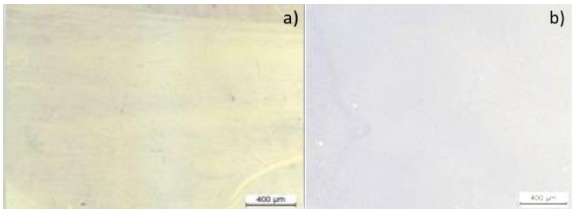

Fig. 5. **a) Optical micro-photos: BL 0,2 M $TiCl_4$ with 1 h reacting time on FTO/glass, b) BL 0,2 M $TiCl_4$ with 2 h reacting time on FTO/glass**

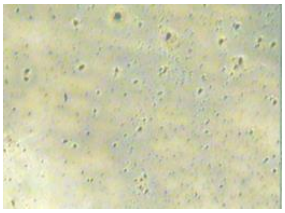

Fig. 6. **Microscopic optical image of the mesoporous TiO_2 layer with the area of 400 x 300 nm**

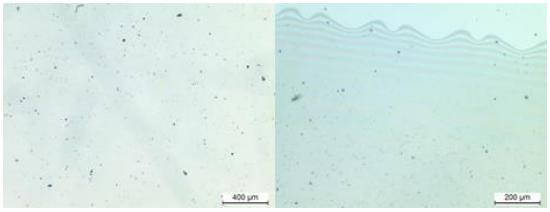

Fig. 7. **Microscopic optical images of mesoporous Al_2O_3 layers**

Fig. 8. **Microscopic optical image of the mesoporous ZrO_2 layer with area 400 x 300 nm**

Table III, The parameters of the mesoporous layers estimated by the AFM

Mesoporous layer	Rq [nm]	Thickness [μm]
our TiO_2	55	0.1-0.15
Al_2O_3	32	1.1
ZrO_2	100	1.2

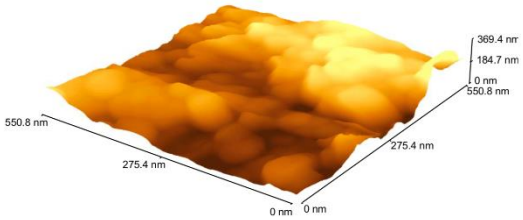

Fig. 9. **AFM image of the mesoporous TiO_2 layer**

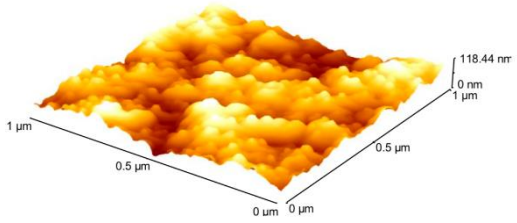

Fig. 10. **AFM image of the mesoporous Al_2O_3 layer**

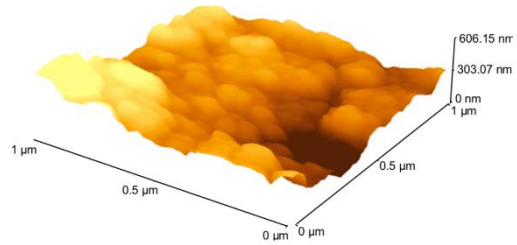

Fig. 11. **AFM image of the mesoporous ZrO_2 layer**

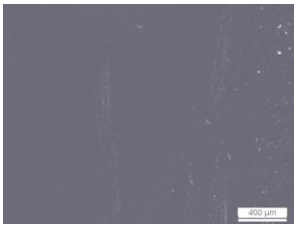

Fig. 13. **Optical micro-images of the perovskit layer surface**

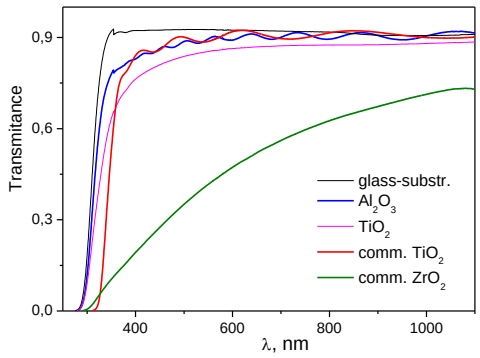

Fig. 12. **UV-Vis spectra for mesoporous layers**

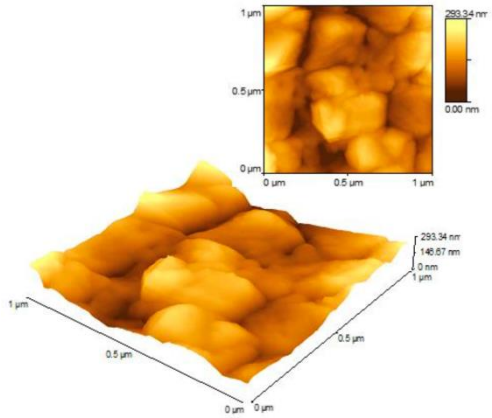

Fig. 14. **AFM topography of the perovskite capping layer**

Layer thicknesses were estimated also by the UV-Vis spectroscopy from interference in UV-Vis transmission spectra with using equation (1) (Figure 12).

$$\Delta\nu = \frac{1}{2nd} \quad (1)$$

Where: *n* is the refractive index and *d* is the thickness of the layer.

Only mp-Al_2O_3 and commercial mp-TiO_2 layers interfere in the UV-Vis area. The commercial mp-ZrO_2 layer was too roughness, strongly dispersing. The thicknesses of mesoporous layers are shown in the table IV.

The perovskite layers (Fig. 13) were black, homogeneous, but in some cases, slots and defects were formed. This defects can decrease the efficiency of solar cells.

The AFM was used for display the surface. The perovskite layer has a complex surface structure with visible crystals around 200 nm (Figure 14).

The surface of the carbon layer is shown in Figure 15., The thickness and roghness of the carbon layer was estimated to 15 μm and 1.7 μm respectively, while the resistance did not exceed 20 Ω / sq.

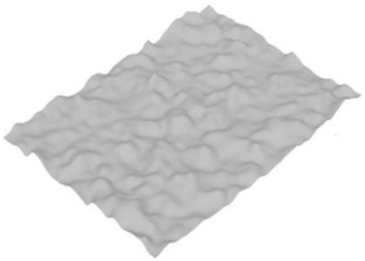

Fig. 15. **Optical 3D micro-image of the carbon layer surface**

The authors thank for financial assistance from the Slovak Grant Agency, VEGA 1/0900/16 and Development Agency under the contract APVV-15-0460.

REFERENCES

1. Chen H., Yang S.: Advanced Materials *29*, 1603994 (2017).
2. Gemeiner P., Mikula M.: Materials Science in Semiconductor Processing *30*, 605 (2015).
3. Gemeiner P., Kuliček J., Mikula M., Hatala M., Švorc Ľ., Hlavatá L., Mičušík M., Omastová M.: Synthetic Metals *210*, 323 (2015).
4. Mikula M., Beková Z., Hvojnik M., Hatala M., Mikolášek M., Mullerová J., Jergel M., Gemeiner P.: Applied Surface Science *461*, 54 (2018).

PREPARATION AND RESEARCH OF COSMETIC EMULSIONS FROM SOLID TIO_2 AND EMULSIONS PREPARED FROM DISPERSION OF TIO_2

SABÍNA JARÁBKOVÁ, MARCELA LAŠTŮVKOVÁ, ADAM JUGL, TOMÁŠ VELCER, JIŘÍ SMILEK

Brno University of Technology, Faculty of Chemistry, Purkyňova 464/118, 612 00 Brno, Czech Republic, xcjarabkova@fch.vut.cz

Keywords: cosmetic emulsion, TiO_2, sun protection factor, SPF determination, sunscreens, UV filters, stability tests

Introduction

The skin is the body's first line of defence for external exposure. Although sun radiation is vital, it can cause damage in excessive amounts. Every year, about one million people are diagnosed with skin cancer and about 10.000 die from malignant melanoma. Most skin cancer occurs on the areas of the body that are most frequently exposed to the sun, such as the face, neck, head and back of the hands (SAX, 2000). The harmful effects of solar radiation are caused predominantly by the ultraviolet (UV) region of the electromagnetic spectrum, which can be divided into three regions: UVA, from 320 to 400 nm; UVB, from 290 to 320 nm and UVC, from 200 to 290 nm. UVC radiation is

filtered by the atmosphere before reaching earth. UVB radiation is not completely filtered out by the ozone layer and is responsible for the damage due to sunburn. UVA radiation reaches the deeper layers of the epidermis and dermis and provokes the premature aging of the skin. Ultraviolet radiations have been implicated as a causative factor of skin cancer. To prevent those undesirable effects, scientists formulated sunprotectors in forms of creams, lotions or emulsions. These substances contain active ingredients to protect the skin from absorbing the sun radiation. The molecules in sunscreen absorb most of the UVB and prevent it from reaching the skin.

Nowadays there is an extensive list of active ingredients that can be used as additives for various cosmetic emulsions. The choice is limited by the laws of the state in which the final product is to be placed on market[1].

The main aim of this work is preparation and characterization of cosmetic emulsions with different addition of TiO_2 and different sun protection factor (SPF). TiO_2 is the main component (main UV filter) of all emulsions in this study and was used in dispersed form and in the powder form.

Spectrophotometric measurement and SPF determination

The efficacy of a sunscreen product has been recognized as an important public health issue and it is usually expressed by the sun protection factor (SPF).

$$SPF = \frac{MED\ (protected\ skin)}{MED\ (unprotected\ skin)} \qquad (1)$$

SPF is defined as the UV energy required producing a minimal erythema dose (MED) on protected skin, divided by the UV energy required to produce a MED on unprotected skin. The minimal erythemal dose (MED) is defined as the lowest time interval or dosage of UV light irradiation sufficient to produce a minimal, perceptible erythema on unprotected skin. The higher the SPF, the more effective is the product in preventing sunburn. This method is called *in vivo* and is ideally determined by phototesting the human volunteers.

In this study, the *in vitro* method was used. The protective factors of the emulsions were determined by measuring the absorption spectra of samples in the range from 290 to 320 nm. Measured absorbance values were recalculated in MATLAB using the Mansur equation:

$$SPF_{spectrophotometric} = CF \times \sum_{290}^{320} EE(\lambda) \times I(\lambda) \times Abs(\lambda) \qquad (2)$$

where EE: erythemal effect spectrum; I: solar intensity spectrum; Abs: absorbance of sunscreen product; CF: correction factor (= 10) (cit.[2]).

The values of EE x I are constants and showed in Table I.

Table I, Normalized product function used in the calculation of SPF[3]

Wavelength [nm]	EE x I [normalized]
290	0.0150
295	0.0817
300	0.2874
305	0.3278
310	0.1864
315	0.0837
320	0.0180
Total	1

The whole experiment was performed on the defined roughness Poly(methyl methacrylate) plates on which the product was spread in amount of 2 $mg \cdot cm^{-2}$. These plates must be UV transparent, inert to all components contained in the product, photo-stable, and must not be fluorescent when irradiated. A spectrophotometer Hitachi U-3900 H was used in the classical and the integration sphere method[4]. To evaluate the results, the samples had to be measured right after preparation and 30 minutes after UV exposition as well. Glycerol (2 $mg \cdot cm^{-2}$/plate) was used as a blank sample. To determine the accuracy of our measurements, we compared them with the spectrophotometric SPF values of the commercial products.

Samples preparation

Preparation method is the same for all the samples, it varies only in ratios of used ingredients.

First of all, water, glycerol, xanthan, PEG and carbomer 940 were mixed together and warmed up to 75 °C in water bath. In case of undissolved carbomer 940, the beaker was put to dispergator for 30 seconds. The second mixture, which was warmed also to 75 °C, contained TiO_2 in oil, mineral oil, oxabenzone, benzyl salicylate, cocamide dea and cetylalcohol. When water and oil phase reached the same temperature, they were mixed together in order oil to water. The mixture was put into the dispergator for 8-10 minutes with simultaneous addition of triethylamine. As an outcome, the white cream was gained. The viscosity of the product was relatively low, thus it could be well spread on the skin.

Results and discussion

Commercial sunscreens with different declared SPF were measured to determine the accuracy and suitability of either integration sphere or classical method. Results showed in Table II proved that integration sphere method presented the highest deviations from declared values, thus it has not been used for further measurements. Classical method evinced more precise results with exception of sample no. 4 and 5. These inaccuracies could be caused by inappropriate amount of cream on the plates (case no. 4). On the other hand as for the sample 5 the results could be considered right, because of high values of absorbance. Also the maximal SPF on commercial product is declared as 50.

Table II, SPF values of commercial products

Sample	Declared SPF	Classical method SPF	Integration sphere SPF
1	6	6.60	2.62
2	20	19.38	14.34
3	30	29.39	10.38
4	30	17.78	11.90
5	50	83.62	25.63

Inconvenience of integration sphere method is also described on Fig. 1 and Fig. 2. Both of them show major differences in comparison of the methods. Representatives were selected as commercial product (SPF=30) and laboratory-prepared product (theoretical SPF=20, contain TiO_2 of 20 wt% and octyl salicylate of 2 wt%)

Laboratory-prepared samples are compared in Table III. Samples differ in composition and it is seen that the highest SPF is evinced by sample no. 2 (SPF=48.94). This can be caused by the biggest amount of used UV filters (5 % of titanium dioxide, benzyl salicylate 7.5 %, stearic acid 6 %, glycerol 6 %, PEG-100 stearate 3 %, panthenol 3 %, octyl salicylate 3 %, oxybenzone 3 %, cetearyl alcohol 3 %, jojoba oil 3 %, xanthan gum 1 %, almond oil 1 %, methylparaben 1 %) in comparison with others. This emulsion also managed a long-term stability test on analytical centrifuges.

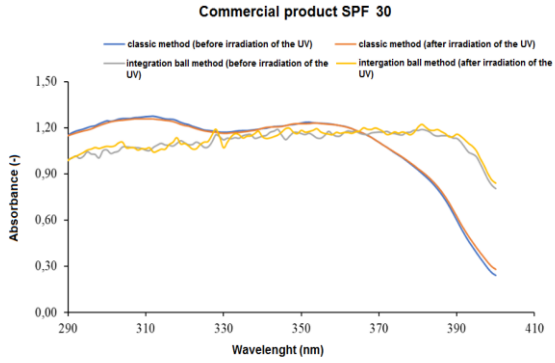

Fig. 1. **Example of absorbance measurement with a classical method and the integration sphere method for a commercial product.**

Table III, SPF values of laboratory-prepared products

Sample	Theoretical SPF	Classical method SPF	Integration sphere SPF
1	20	25.24	2.54
2	30	48.94	3.36
3	45	31.52	3.46

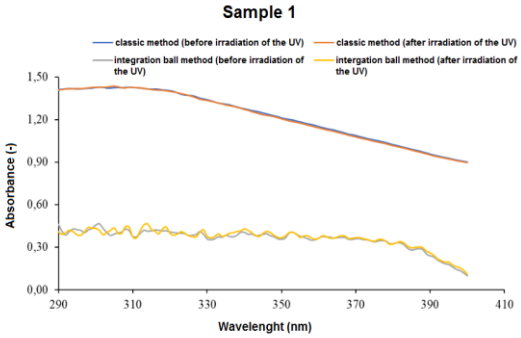

Fig. 2. **Example of absorbance measurement using a classical method and an integration sphere method for a laboratory-prepared emulsion**

Conclusion

Wide range of protective cosmetic emulsions with the addition of titanium dioxide as a physical blocker have been prepared and characterized. The protective factors of the individual emulsions were determined *"in vitro"* by emulsion deposition on the PMMA plates and absorbance was measured using a spectrophotometer. From the measurement of commercial preparations, it is obvious that the more accurate method of determining the protective factor was the classical method compared to the integration sphere method, which is however considered by many as the more accurate one. Problems could been caused by installation of the integration sphere into the spectrophotometer and its own calibration. Another issues could arised from spreading the sunscreen over the plate, since the layers were not always 100 % homogenous. That's why it should be desired to perform more measurements so that this method would stand as more optimized. After all this could replace the *"in vivo"* method which provides even less reliable results and may be not so pleasant for patients.

This work has been supported by the project LO1211 from National Programme for Sustainability I (Ministry of Education, Youth and Sports).

REFERENCES

1. Dutra A. E., Oliveira D. A. G., Kedor-Hackmann E. R. M., Santoro M. I. R. M.: Braz. J. Pharm. Sci. *40*, 381 (2004).
2. Mbanga L., Mulenga M., Mpiana P. T., Bokolo K., Mumbwa M., Mvingu K.: IJARCS *1*, 7 (2014).
3. Sayre R. M., Agin P. P., LeVee G. J., Marlowe E.: Photochem. Photobiol. *29*, 559 (1979).
4. Springsteen A., Yurek R., Frazier M., Carr K. F: Anal. Chim. Acta. *380*, 155 (1999).

STUDY OF ELECTROSTATIC INTERACTIONS BETWEEN HYALURONAN AND AMINO AICDS

ADAM JUGL*, JANA HEJNÁ, MILOSLAV PEKAŘ

Brno University of Technology, Faculty of Chemistry, Purkyňova 118, 61200 Brno
xcjugl@fch.vutbr.cz

Keywords: hyaluronan, polyarginine, nanoparticles, high resolurion ultrasonic spectroscopy, dynamic light scattering

Abstract

This paper focuses mainly on the use of high resolution ultrasonic spectroscopy (HRUS) for the study of interactions between the negatively charged polysaccharide hyaluronan and positively charged amino acids.

Interaction between hyaluronan (9 kDa and 1.39 MDa) and arginine in monohydrochloride forms with different molecular weights were studied. Amino acid solutions were titrated to hyaluronan solutions of various molecular weights. The relative velocity change during the titration was monitored. The concentrations were set such that the amount of charges, which carry the amino acids was nearly eight times higher in the end of the titration than the number of charges in a solution of hyaluronate.

It has been discovered that the molecular weight of the polyarginine chain plays a significant role in interacting with hyaluronan, and that the molecular weight of hyaluronan itself does not influence the interaction.

If the length of the poly amino acid chain length is sufficiently prolonged, hyaluronan begins to aggregate with the amino acid forming nanoparticles. The second part of this work is focused on the preparation and characterization of nanoparticles formed by electrostatic interactions using negatively charged polymer hyaluronan and polyarginine of molecular weight ranging from 5 to 15 kDa in hydrochloride form.

Unlike the previous study[1], where the effect of PBS on nanoparticles was studied, we decided to study nanoparticles in terms of stability by addition of sodium chloride and by lyophilization and re-dissolving. NaCl was added to the prepared solution of nanoparticles to a concentration of 0.15 M to simulate physiological environment. The results show that the particles in both cases increased their size.

Due to the composition of nanoparticles from biodegradable materials, particles may be attractive for medical applications. Particle size was studied using dynamic light scattering.

Introduction

Hyaluronan is a well-known and body's own negatively charged polysaccharide, which is of great interest in targeted drug distribution, especially anti-cancer[2]. In contrast, positively charged polyamino acids such as polyarginine consist of a body's own amino acids and their molecules are similar to molecules of peptides that are readily degradable in the body. Due to the opposite charge of the two polymers, the nanoparticles formed by the electrostatic forces between the polymers occur when they are mixed[1, 3]. Previous experiments have already confirmed the possibility of preparing such nanoparticles[1], which can be used as an instrument for targeted drug distribution. These experiments are followed by our work to simplify the preparation of nanoparticles and characterize them.

For a more thorough examination of electrostatic interactions, we also studied the interactions between hyaluronan and oligomers of arginine hydrochloride using High Resolution Ultrasonic Spectroscopy (HRUS). The intensity of interactions was studied, depending on the length of the interacting oligomer and the molecular weight of hyaluronan. HRUS has been chosen as a characterization technique because of its sensitivity to the molecular organization in the sample. For example due to the sensitivity of HRUS, one of the studies revealed up to 6 different types of hyaluronan-tenside complexes[4].

Preparation of Nanoparticles

Micro and nano particles were prepared by simply mixing hyaluronan solution of proper concentration and solution of polyarginine at room temperature in one-to-one volume ratio. Hyaluronan (sodium salt) (Hya) of molecular weight of 137 kDa (Contipro Group s.r.o.) and poly-*L*-argininehydrochloride (PArg) of molecular weight ranging from 5 to 15 kDa (Sigma Aldrich) were used to prepare the particles. PArg solutions of concentration 0.5 $g \cdot l^{-1}$ were prepared in deionized water (Purelab Flex, ELGA) and hya solutions were also prepared in deionized water in concentrations 0.44, 1.67 and 2.67 $g \cdot l^{-1}$. Size of the particles was measured by Zetasizer Nano ZS from Malvern Instruments.

Study of Electrostatic Interactions

Interactions between Hya 9 kDa, 1.39 MDa (Contipro Group) and oligomers of arginine in the monohydrochloride form (each arginine residue carries one positive charge) with chain length 4, 8 (Vidia) and 30 arginine residues (Alamanda polymers) were investigated using HRUS. Abbreviations for the corresponding length of the polyarginine chain are 4Arg.HCl, 8Arg.HCl, 30Arg.HCl.

Aqueous solutions of hyaluronan were prepared by dissolving hyaluronan so that the resulting concentration of monomer units of hyaluronan was 2.4919 mM. Aqueous solutions of arginine oligomers were prepared by dissolving oligomers so that the resulting concentration of monomers was 30 mM.

Interactions between hyaluronan and oligomers were investigated by titrating the oligomer solution into a solution of hyaluronan using HRUS to observe changes in the molecular configuration. To a solution of hyaluronan 1 ml, individual oligomer solutions were titrated with addition of 10 µl and total volume of 0.6 ml. A change of relative velocity was measured. From the titration results of the hyaluronan-oligomer the results of the blind titration of oligomer to water were subtracted.

Measurements were carried out at 6 frequencies. Results are frequency-independent therefore the results are only shown

for frequency 11.6 MHz. All measurements were carried out at 25 °C.

Study of Electrostatic Interactions: Results and Discussion

HRUS gives, as its output, the difference in velocity or attenuation measured between the sample and reference cells, in our case, the difference between the value in the sample and the values in water. For this study seems particularly interesting results of measuring changes in sound velocity of the sample.

Graphs in Fig. 1. and Fig. 2. show the titration curves of the individual oligomers to a solution of hyaluronan. The charge ratio is chosen as the axis since full dissociation of the carboxyl groups of hyaluronan is assumed and in the case of oligomer sone positive charge on each arginine residue occurs.

Measurements were carried out with hyaluronan of two different molecular weights. However, the studied interactions were found not to be dependent on the molecular weight of the hyaluronan. Therefore, only results for hyaluronan of molecular weight 9 kDa are shown.

Unlike the molecular weight of hyaluronan, the molecular weight of oligomers is critical for the interaction. During titration, the shape of the relative velocity profile is decreasing,

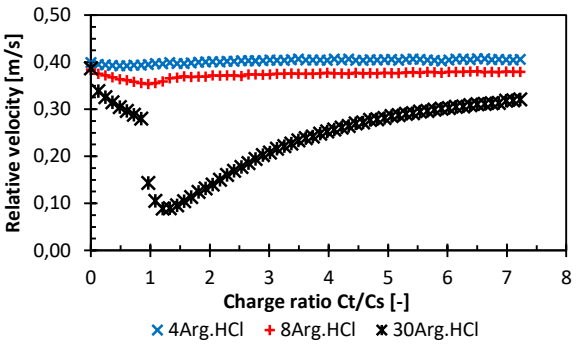

Fig. 1. **Graph showing titration curves of individual oligomers to hyaluronan 9 kDa in water, frequency 11.6 MHz.**

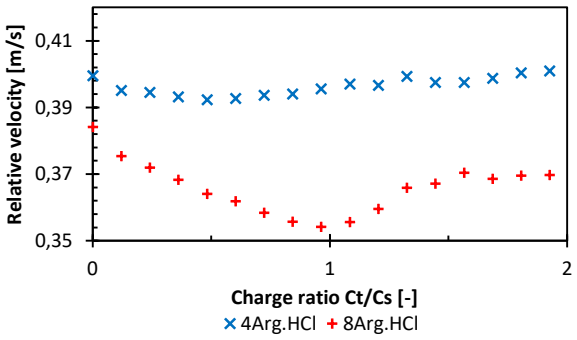

Fig. 2. **Graph showing a more detailed view of titration curve of oligomers to hyaluronan 9 kDa in water, frequency 11.6 MHz.**

until equal charge ratio is reached (Fig. 1. and 2.). Then there is an increase in relative velocity values. This applies to 8Arg.HCl and 30Arg.HCl. Although in the case of 8Arg.HCl the change in relative velocity is much smaller. In the case of 4Arg.HCl, this change does not occur and during the titration the relative speed is constant. It can also be noticed that with the increasing molecular weight of the oligomer, the minimum of the titration curve is shifted to a higher charge ratio. This decrease in relative velocity could mean the presence of interactions in the system.

Nanoparticles: Results and Discussion

Size of the particles was measured in a several cases. In the first case (Table I), 1 ml of prepared solution with particles was taken and centrifuged for 30 min with 20 µl of glycerol (Sigma Aldrich). In the next step supernatant was removed and particles with glycerol were mixed with 1 ml of deionized water. Particle size was measured in both the supernatant and the glycerol/water mixture. In the second case (Table II), the particles were measured after mixing the solutions of Hya and PArg without further processing.

It is apparent that samples labeled as supernatant and centrifuged have very similar particle size values. Also, the samples labeled as glycerol and non-centrifuged have corresponding particle size. With these simple experiments was found that the glycerol had no significant effect on the size of the centrifuged particles, therefore, in other experiments, particles were prepared with centrifugation but in the absence of glycerol.

The influence of ionic strength on the particle size was tested by adding NaCl (Lach-Ner s.r.o.) to solutions formed by mixing solutions of hyaluronan and polyarginine. NaCl was added in such a quantity that the final concentration was 0.15 M. Unlike the previous study[2], where the effect of PBS on nanoparticles was studied, we decided to study nanoparticles only in 0.15 M NaCl. Samples of nanoparticles of the Hya-PArg system were subjected to a stability test of NaCl addition. The influence of ionic strength on the particle size in the solution was determined by measuring particle size. We found that the addition of NaCl leads to a significant increase in particle size (Table III). After addition of NaCl to all solutions, all samples became immediately turbid. This fact was not described in the previous article[1].

Lyophilization and subsequent dissolution of the samples resulted in an increase of the particle size. A larger increase of particle size occurred in the sample dissolved after lyophilization in 0.15 M NaCl solution (Table IV). It took

Table I, Measured values of particle sizes of nanoparticles composed of Hya and PArg with further processign at different concentration ratios

Cencentration [g·l^{-1}] Hya + PArg	Particle size [nm] Hya + PArg + glycerol + centrifugation	
	Supernatant	Glycerol part
0.44 + 0.5	44 ± 10	70 ± 6
1.67 + 0.5	42 ± 2	69 ± 11
2.67 + 0.5	61 ± 2	91 ± 3

Table II, Measured values of particle sizes of nanoparticles composed of Hya and PArg without further processign at different concentration ratios

Cencentration [g·l^{-1}] Hya + PArg	Particle size [nm] Hya + PArg	
	Centrifuged	Non-centrifuged
0.44 + 0.5	44 ± 10	70 ± 6
1.67 + 0.5	42 ± 2	69 ± 11
2.67 + 0.5	61 ± 2	91 ± 3

Table III, Measured particle sizes of the systems subjected to the NaCl stability test

Concentration [g·l^{-1}] Hya + PArg	Particle size [nm] After addition of NaCl
0.44 + 0.5	245 ± 78
1.67 + 0.5	566 ± 14
2.67 + 0.5	424 ± 6

relatively long time to dissolve samples after the lyophilization. The sample, which was dissolved in 0.15 M NaCl solution, had to be placed in an ultrasonic bath to dissolve. Experiments with other concentrations (0.44 g·l^{-1}, 2.67 g·l^{-1}) of Hya solutions were also performed. Similar results were achieved (results not shown).

Conclusion

Using the HRUS method, it has been discovered that the molecular weight of the polyarginine chain plays a significant role in interacting with hyaluronan, and that the molecular weight of hyaluronan itself does not influence the interaction.

It is important to realize that ultrasonic spectroscopy is an indirect method and interpretation of the cause for changing the relative velocity is primarily a matter of knowledge of the issues and experiences with this technique. Given the fact that we can only use information from similar systems[4] to evaluate data, it might be advisable for further work to add other techniques (for example ITC) to the HRUS method, which could help clarify the system more thoroughly.

Nanoparticles based on hyaluronan and polyarginine were prepared simply by mixing the appropriate solutions. It has been found that glycerol does not provide any advantage during the preparation over the preparation of nanoparticles without the glycerol. Particle stability was examined by lyophilization, re-dissolving and by addition of NaCl to simulate the ionic strength of the physiological environment. The results show that the particles in both cases increased their size, but prevent it from falling apart. It was also found that the addition of NaCl to the system causes the turbidity of the system. After lyophilization and redissolving or addition of NaCl, particle size values have exceeded the limits when it would be safe to use them as intravenous drug carriers, but other applications such as topical or mucoadhesive remain interesting.

Table IV, Particle sizes of the lyophilized systems

Concentration [g·l^{-1}] Hya + PArg	Dissolved in	Particle size [nm] After lyophilization
1.67 + 0.5	water	226 ± 14
1.67 + 0.5	0.15 [M] NaCl	523 ± 85

This work has been supported by the project LO1211 from National Programme for Sustainability I (Ministry of Education, Youth and Sports).

REFERENCES

1. Oyarzun-Ampuero F. A., Goycoolea F. M., Torres D., Alonso M. J.: Eur. J. Pharm. Biopharm. *79*, 54 (2011).
2. Almond A.: Cell. Mol. Life. Sci. *64*, 1591 (2007).
3. Kim E., Shim G., Kim K., Kwon I. Ch., Oh Y., Shim Ch.: J. Gene. Med. *11*, 791 (2009).
4. Kargerová A., Pekař M.: Langmuir. *30*, 11866 (2014).

STUDY OF FLOW PROPERTIES OF POWDERS IN PHARMACEUTICAL INDUSTRY

PAVEL KOLESA[a,b], MARTINA KLUČÁKOVÁ[a], ALEŠ GAVENDA[b]

[a] Faculty of Chemistry, Brno University of Technology, Material Research Centre, Purkyňova 464/118, 612 00 Brno
[b] R&D department, Teva Czech Industries s.r.o., Ostravská 305/29, 747 70 Opava, Komárov
xckolesa@fch.vutbr.cz

Introduction

Since many industries are focused on production of solid materials, powder flowability is a critical parameter for movement of product, production efficiency and other operations connected with bulk solid handling. Due to this fact, it is necessary to study flow properties of powders in order to better understand behavior of powders in different systems. The importance of these properties in pharmaceutical industry is well known and plays a significant role in production and handling as well as it influences key properties of final drug product itself.

The powders of APIs (Active Pharmaceutical Ingredients) and their intermediates are usually stored in a large scale for a long time at different conditions due to logistical reasons and this storage or transport may negatively affect flow properties (e.g. compactation and agglometarion of bulk API). An adverse impact on agglomeration of particles is generally referred to as caking and is mainly caused by moisture migration in the bulk of powders. This water content affects behavior of APIs by inducing the formation of soft or hard lumps. Powders including small particles make it harder to achieve content of humidity which is required and which is not suitable for lumps formation. Molecules of water may exist at least three stages between the crystals: a hydroscopic stage which forms thin adsorption layers on the surface of crystals, a pendular stage formed by liquid bridges between individual particles and a saturation stage in which all pores are filled with water[1].

The main purpose of presented work is study of two model batches of APIs which were characterized by different flow properties (especially different tendency to caking). Immunosuppressant drug Mycophenolic Acid (MPA) was selected such as model substance for this study, because this API has issues in production due to presence of large lumps which clogged the hopper and it was very difficult to transport the sample through the pipeline. This issue had an adverse impact on production efficiency and it was necessary to find the relevant properties and parameters which affect lumps creation. Therefore many physico-chemical techniques were used for investigation of MPA in order to identify root cause of caking tendency.

Experimental part

Materials and methods

Two production lots of immunosuppressant drug Mycophenolic Acid (MPA) were provided by Teva Czech Industries s.r.o. One of these batches (#A) showed a large tendency to lumps creation and caused a lot of issues in production due to poor flow properties. The second batch of MPA used for this study (#B) did not show any tendency to lump creation and showed suitable flow properties for handling and other pharmaceutical processing, especially for preparation of final dosage form.

Since flow properties of powders and tendency to lump creation is very complex phenomenon and may be affected by a several properties of powders itself as well as storage conditions, a lot of instrumental techniques have to be used for characterization each of them.

X-Ray Powder Diffraction

Most of API exhibit polymorphism and different polymorphic forms have different properties, such as morphology, hygroscopicity, cohesivity etc. X-Ray Powder Diffraction method (XRPD) was used for determination of crystalline form of both samples which were used for this study.

Small amount of API was gently grinded in an agate mortar with the pestle and powder was filled in the round cavity of sample-holder by pressing with a glass plate to form smooth surface.

X-Ray Powder Diffractometer PANalytical X'Pert PRO with X'Celerator detector was used for this analysis with the following parameters:

Scan rate 3 deg/min; measuring range 3 – 40 °2Theta; step size 0.0131 deg; Cu tube.

Dynamic Vapor Sorption

As was already mentioned moisture content and hygroscopicity of substances play a major role in creation of the lumps and have a negative impact on flow properties of API as well as final drug product quality may be affected by this phenomenon. Dynamic Vapor Sorption (DVS) is a gravimetric technique that measures how quickly and how much is solvent (in this case water) absorbed by a sample using specified relative humidity cycles.

DVS analyzer Advantage 1 (Surface Measurement Systems Ltd., UK) was used for study of water sorption. Basic measurement included 2 humidity cycles at 25 °C with humidity range 0 – 90 % relative humidity (RH), step 10 % RH and condition for the next step is: dm/dt 0.002.

Based on application list provided by Surface Measurement Systems Ltd. is possible to study tendency of powders to caking using series of short cycles which could simulate the daily fluctuations in relative humidities. For study of MPA caking was used a method of twelve cycles 30 – 80 % RH, step size 50 % RH and time of step is 120 min[2].

Particle size distribution (PSD) by laser diffraction

Flow properties of powders are very affected by particle size. A pendular state of water reported above is characterized by creating intensive forces between two individual particles due to tension of surface and pressure differences between liquid and air pressure across the liquid bridge interface, called capillary pressure. Cohesion forces between particles depend on number of liquid bridges which are affected by particle size. The presence of small solid particles influence the water retention and cohesion forces between particles are increased[1]. This is the reason why it is necessary to study particle size distribution of chosen MPA batches.

Malvern Mastersizer 2000 with Hydro 2000s Unit was used for determination of PSD of Mycophenolic acid using following parameters:

Meas. range: 0.02 – 2000 μm, Fraunhofer model, dispersion medium: 1 % (w/w) Tween 80 in water, measuring medium: water, ultrasonic time 50 sec, sample weight about 150 mg.

Scanning electron microscopy (SEM)

One of the most important parameter which influence flow properties of API is morphology, especially particles shape. Really wide range of particles shape may be observed in pharmaceutical industry. Some of them are regular e.g. needles, plates, laths, equant but also particles with irregular shape are commonly observed. This parameter may be modified and controlled by using relevant crystallization techniques. For purpose of this measurement was used scanning electron microscope Hitachi 3030TM Plus. Samples were fixed on an aluminum stub with conductive double sided adhesive tape and coated by a gold layer using sputter coater Quorum SC7620 (working current: 10 mA, time: 2 min).

Thermogravimetric analysis (TGA)

The production batches of Mycophenolic Acid are anhydrous (also confirmed by XRPD analysis) so it was suitable to use thermogravimetric technique for moisture content determination. Small amount of sample (about 6 mg) was loaded to the 100 μl aluminum pan and measured by TGA instrument TA Discovery using following parameters:

Temperature range: 25 – 250 °C, heat. rate: 10 °C/min with nitrogen gas flow 25 cm^3/min.

Differential Scanning Calorimetry (DSC)

DSC technique was used as a complementary technique to TGA (for moisture content determination based on enthalpy of evaporation detection) and XRPD (for polymorph identification based on enthalpy of melting). DSC instrument TA Discovery was used for characterization of chosen batches of MPA. About 4 mg of MPA samples were loaded to the 40 µl aluminum T-zero pans. The same temperature range and heating rate as was reported above for TGA was set. Nitrogen was used as a purging gas with flow rate 50 cm^3/min.

Specific Surface Area (SSA)

Specific surface area is an additional technique for characterization and quantification of particle size, shape and porosity of the sample. All of these parameters affect the value of specific surface area. Surface area can be estimated from particle size distribution but only for regular geometric shape of particles[3]. But this is not a case of Mycophenolic acid which contains predominantly irregular porous particles.

Specific surface area analyzer Micromeritics Tristar II Plus 3030 was used for determination of specific surface area of Mycophenolic acid. Samples were degassed in vacuum at 40 °C for 30 min and measured with the following parameters:

Adsorptive gas: N_2, analysis bath temperature: – 196 °C, equilibration interval: 10 s.

Powder rheology

One of the most important technique for study of flow properties of solid particles is powder rheology, in this case measured by FT4 powder rheometer (Freeman technology). There are a lot of parameters which can be chosen for characterization of flow properties e.g. flow function, basic flowability energy, cohesion or Pesch level of cohesion. Based on some previous measurement were chosen two parameters – Flow Function (FF) and Basic Flowability Energy (BFE). FF parameter is measured using one of the basic tests called Shear test and it characterize flow properties of API in initial state. On the other hand BFE test is measured in 25 ml glass cell and therefore may be used for combination with some stress conditions, such as temperature, humidity, mechanical pressure etc. In the presented experiment stress conditions included mechanical load of the sample in glass cell using 50 g of weights at room temperature and exposed to 60 % of relative humidity. MPA samples were placed in these conditions for 5 days and then measured by FT4 powder rheometer using BFE test. The obtained results were compared with the BFE results of initial samples before application stress conditions.

Another test used for characterization of flow properties of MPA was compressibility test in which the sample is compressed in a glass vial using steel piston (mechanical pressure 1-15 kPa).

Results

Since many parameters which affect flow properties of powders and tendency to lumps creation are connected with polymorphism, X-Ray Powder Diffraction method was used as a first technique for characterization of two production lots of Mycophenolic Acid. XRPD pattern of both batches showed the same crystalline form which was compared with crystalline forms in Cambridge Structural Database (CSD). This polymorphic form corresponds to one anhydrous form reported in Journal of Chemical Society[4], CSD ref. name: MYCPHA. Overlaid XRPD patterns are shown below in Fig. 1.

The influence of moisture and water vapor in the bulk material was already discussed in the previous chapters. Thermogravimetric analysis was used for determination of moisture content in both samples (#A and #B). But the analysis did not show any relevant content of water in the samples. Results are summarized in the table below (Tab. II).

Another thermal technique for characterization of API was used Differential Scanning Calorimetry which confirmed results of XRPD and TGA, because no further event except melting was observed. Maximum of the DSC melting peak was detected at 143.6 °C for both samples.

Tendency to moisture absorption and hygroscopic properties of MPA samples were studied using Dynamic Vapor Sorption. Two basic isothermic cycles in the humidity range 0 – 90 % RH showed relatively large differences between both samples of Mycophenolic Acid. The production batch #A which showed a large tendency to lump creation absorbed much more water (more than six times) than the sample #B which did not show any tendency to lump creation.

P. T. Attwool described an application of DVS instrument for lump creation study. He used a short relative humidity cycles (30 – 80 % RH) which simulated the daily fluctuations in relative humidities. Based on this research article series of humidity cycles were performed (method parameters are described above in the previous chapter)[2]. Anyway due to small water absorption of both samples no significant results were observed. The results are summarized in the table below (Tab. II).

Morphology of the samples were studied using elektron microscope Hitachi TM3030 Plus. Sample #B showed more regular shaped particles than #A and also presence of larger particles were observed in the sample #B. Detailed micrographs of individual particles showed that batch #B contained significantly smoother surface of particles. Different surface

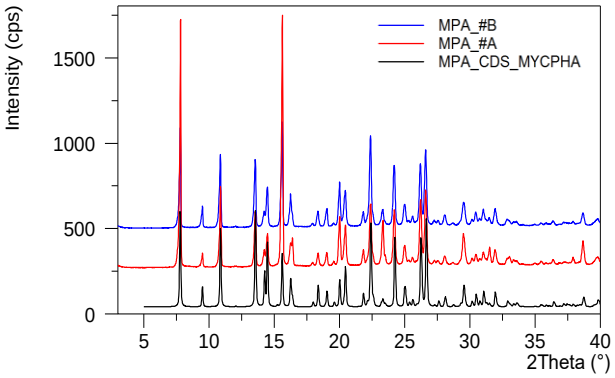

Fig. 1. **Overlaid XRPD patterns of two production lots of Mycophenolic acid compared with polymorphic form reported in CSD (Journal of Chemical Society, 1974)[4].**

roughness may affect capillary condensation which contributes to water sorption[5]. Electron micrographs of both production lots are shown in figures below (Fig. 2, Fig. 3).

A pendular state of water is affected by a particle size due to liquid bridge interface. This liquid interface is responsible for increasing of cohesion forces and therefore has an adverse effect on flow properties of particles. C. Moduno et. al described in their study parameter d_{50} as the most relevant PSD value for determination of tendency of powders to caking. Based on this article d_{50} parameters obtained by laser diffraction method were compared for both batches. Results are summarized in the table below (Tab. II). It was found that the sample of MPA #A has a lower d_{50} parameter but the largest differences was found for d_{90} parameter. Presence of larger particles in the sample #B was also confirmed by electron microscope.

Different particle size and roughnes of surface should be studied using Specific Surface Area analyzer. But all SSA measurements of MPA batches showed very small value of specific surface area which can not be precisely measured by

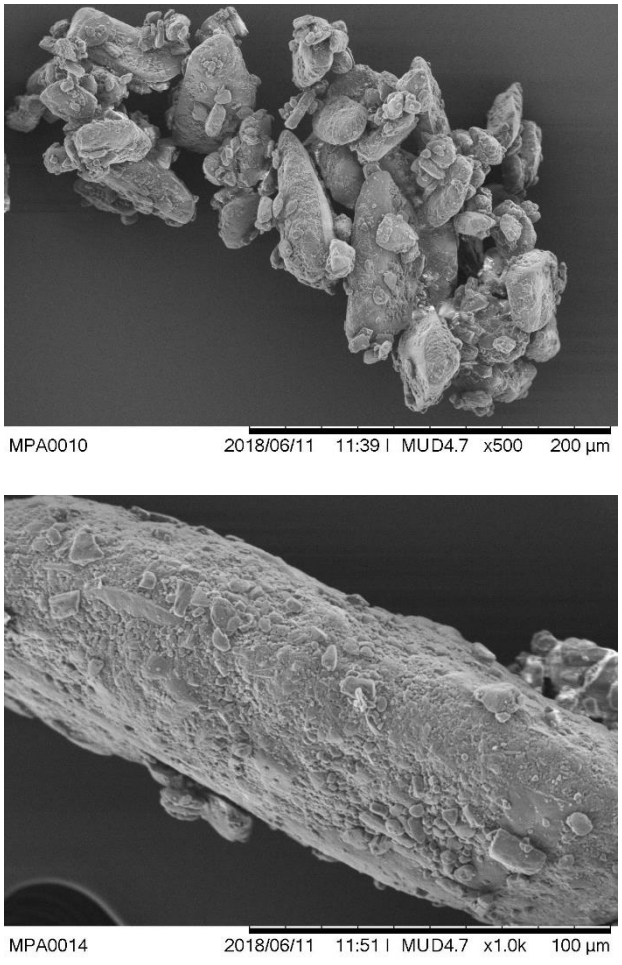

Fig. 2. **Electron micrographs of MPA #A**

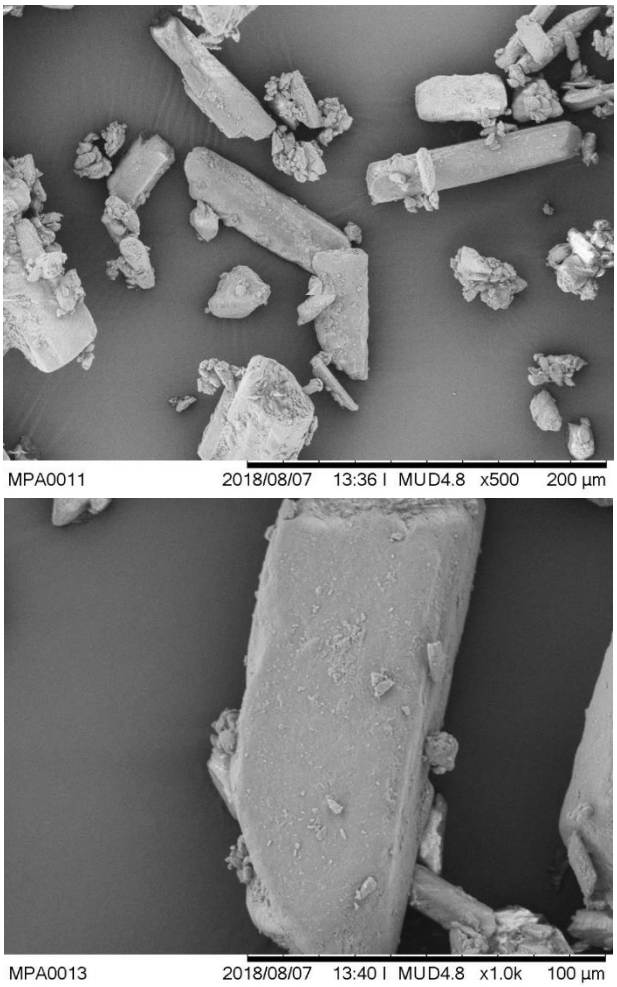

Fig. 3. **Electron micrographs of MPA #B**

used instrument configuration. The sensitivity and accuracy of the nitrogen sorption for measurement of relatively small specific surface areas is insufficient for pharmaceutical industry. For SSA value determination of small surfaces is commonly used sorption of krypton instead of nitrogen. But this configuration was not available so value of specific surface area less than 0.5 m^2 was reported for both lots in this study.

Flow properties of MPA samples were studied and quantified using powder rheometer FT4. As was already mentioned in previous chapter above two different type of measurement were used. The first test called Shear test was used for initial sample and obtained parameter Flow Function (FF) characterize flow properties of the sample using small amount of powder (1 ml Shear cell). Flow Function was described by Jenike A. W. in his study from 1964 and is considered to be the most relevant indicator of the powder's ability to flow. Classification of powder flowability after Jenike is summarized in the table below (Tab. I)[6].

Tab. I: Classification of powder flowability after Jenike[6].

Type of flow:	Flow Function (FF):
Free-flowing	10 < FF
Easy-flowing	4 < FF < 10
Cohesive	2 < FF < 4
Very cohesive and non-flowing	FF < 2

Flow function value of the batch #A (FF = 3.62) corresponds to cohesive powder while FF of the sample #B (FF = 4.26) corresponds to easy-flowing powders based on clasification table above (Tab. I).

Powder rheometer can be used to study the effect of stress conditions (temperature, humidity, mechanical pressure) on flow properties. T. Freeman and his colleague from Freeman Technology Ltd. studied measurement and quantification of caking in powders using FT4 rheometer. Based on this article stress conditions simulating storage and handling were used. These conditions including mechanical load of the sample in glass cell using 50 g of weights at room temperature and exposed to 60 % of relative humidity. After five days were samples measured by FT4 powder rheometer using BFE test. BFE test measure Basic Flowability Energy which is an energy required to establish a particular flow pattern in a glass cell. It corresponds with flow properties of powders[7].

The obtained results were compared with the BFE results of initial samples before application stress conditions (Tab. II). As expected sample #A showed much worse flow properties (in initial and stress state) than the second one #B. Prior to all rheometric analysis both samples were sieved using 1 mm sieve. Even so sample #A after several days storage contained significant number of (see Fig.4).

Compressibility of the MPA samples was also tested by FT4 rheometer. Initial method load range was set for pressure 1-15 kPa using steel piston. Sample #B was better copressible than #A. The differences between both lots are most probably caused by presence of hard lumps in the sample #A.

Fig. 4. **Sieved sample #A after several days storage at room temperature.**

Tab. II: Results summary table for two production batches of Mycophenolic acid.

Sample batch:		#A	#B
Problematic batch		big lumps, relatively fragile	no lumps, good flow properties
XRPD		crystalline (csd ref. MYCPHA)	crystalline (csd ref. MYCPHA)
DVS [w/w at 90 % RH]		1. cycle 0.44 % 2. cycle 0.44 % XRD after DVS: crystalline	1. cycle 0.07 % 2. cycle 0.07 % XRD after DVS: crystalline
DSC maximum of peak and enthalpy		143.6 °C (-106 J/g)	143.6 °C (-113 J/g)
TGA		0.15 % w/w (25-130°C)	0.15 % w/w (25-130°C)
SEM		irregular shaped particles, rough surface	almost lath shaped particles, smooth surface, presence of larger particles
PSD [μm]	d_{10}	10.6	10.8
	d_{50}	60.8	71.1
	d_{90}	157.0	232.1
Flowability	BFE [mJ]	272	209
	BFE stress test 60 % RH 50 g load 5D [mJ]	783	576
	Shear test – FF	3.62	4.26
	Compressibility [% at 15 kPa]	33.2	24.5
	Bulk density by FT4 [g/cm^3]	0.45	0.58
SSA [m^2/g]		less than 0.5	less than 0.5

Conclusion

The presented work showed a comprehensive view to flow properties and physico-chemical methods which can be used for characterization of API. It was found that particle size distribution and different morphology may significantly affect flow properties, especially tendency to lump creation through water sorption. The presence of the lumps has been proven by powder rheometer FT4 using BFE and shear tests. Both test showed that higher energy is required for movment of the sample which caused several issues during the production.

Mycophenolic acid will be further tested using the other methods and techniques (e.g. specific surface energy by inverse gass chromatography (IGC), SSA with krypton configuration, etc…). For better understanding to lump creation of MPA it is neccessary to study more production batches with different flow properties. Based on this study was recommended to focuse on particle size distribution of final material and morphology using controlled crystallization in suitable solvent system. This may help to produce Mycophenolic acid with appropriate properties which will be suitable for final dossage form and formulation.

I would like to thank to Teva Czech Industries s.r.o. for providing API, resources, instruments and opportunity to conduct the above research. This research was supported by Material Research Centre, Brno University of Technology.

REFERENCES

1. Modugno C., Paterson H. J., Mcleod J.: Procedia Engineering. *102*, 114 (2015).
2. Attwool P. T.: SMS Application list. *20*, (2012).
3. Lowell S., Shields J. E., Thomas M. A., Thommes M.: *Characterization of porous solids and powders: surface area, pore size, and density*. Springer, Boston 2006.
4. Harrison W., Shearer H. M. M., Trotter J.: Journal of the Chemical Society. *11*, 1542 (1972).
5. Stoklasa A. M., Lipasek R. A., Taylor L. S. a Mauer L. J.: Food Research International. *49*, 783 (2012).
6. Jenike A. W. in bulletin 123: *Storage and Flow of Solids*, University of Utah, Utah 1964.
7. Freeman T., Brockbank K., Armstrong B.: Procedia Engineering. *102*, 35 (2015).

STUDY OF PEROVSKITE SOLAR CELLS DEGRADATION IN THE PRESENCE OF MOISTURE

MATOUŠ KRATOCHVÍL[a]*, DÁVID STRACHALA[b], ADAM GAJDOŠ[b], LADISLAV CHLADIL[b] AND MARTIN WEITER[a]

[a]*Faculty of Chemistry, Brno University of Technology, Purkyňova 464/118, 612 00 Brno*
[b]*Faculty of Electrical Engineering and Communication, Brno University of Technology, Technická 3058/10, 616 00 Brno*
xckratochvilm@fch.vut.cz

Abstract

Degradation study of perovskite solar cells in presence of moisture was conducted. In perovskite solar cells was observed the influence of moisture on photoconversion efficiency. In order to explain the degradation of cells, the perovskite itself was studied as well. The degradation was investigated using X-ray diffraction (XRD) and atomic force microscopy (AFM). The results of these measurements were subsequently compared and were in good agreement, showing that decrease of cells' photoconversion efficiency is caused by decomposition of perovskite crystal to lead iodide.

Introduction

Interest in renewable energy is growing since the beginning of the millennium and photovoltaics has established itself as one of the leading sources of renewable energy. To date silicon is the most widely used material in photovoltaic cells. Owing to extensive research silicon photovoltaic cells have almost achieved their theoretical limits. On the other hand, because of financially and energetically expensive processing of silicon it is important to look for other materials suitable for solar cells fabrication. In 2009 organometal halide perovskites emerged as suitable candidates with first reported use in solar cell[1]. Since then perovskite solar cells have experienced unprecedented progress with to-date record efficiencies exceeding 22 %[2, 3, 4]. The outstanding performance of perovskite solar cells coupled with the possibility to prepare them from liquid precursors makes this technology promising alternative to silicon photovoltaics. To fulfil the potential of perovskite photovoltaics it is necessary to ensure long-term stability. This, along with the use of toxic lead, is the main drawback standing in the way of commercial exploitation of the perovskite photovoltaic technology. The overall stability issues were comprehensively reviewed by D. Wang et al.[5]. As stated in this review, one of the main causes of degradation of organometal halide perovskite materials is moisture and oxygen. A possible pathway of this degradation was suggested by G. Niu et al.[6] who propose degradation process as follows:

$$CH_3NH_3PbI_3\ (s) + H_2O \leftrightarrow PbI_2\ (s) + CH_3NH_3I\ (aq) \quad (1)$$

$$CH_3NH_3I\ (aq) \leftrightarrow CH_3NH_2\ (aq) + HI\ (aq) \quad (2)$$

$$4HI\ (aq) + O_2 \leftrightarrow 2I_2\ (s) + 2\ H_2O\ (l) \quad (3)$$

$$2HI\ (aq) + h\nu \leftrightarrow H_2\ (g) + I_2\ (s) \quad (4)$$

Reactions (3) and (4) are the two possible ways of decomposition of hydrogen iodide in the cell structure. The first one proceeds in presence of oxygen while the other is photochemical reaction induced by UV radiation. An important product of this degradation process is water soluble lead iodide (PbI_2) which creates possible environmental threats. The aim of this work is to study the influence of the humidity on photovoltaic conversion efficiency of perovskite solar cells and simultaneously study the influence of the moisture on degradation of the perovskite itself by XRD and AFM techniques. Comprehensive understanding of the processes that take place during degradation opens a way to propose possible solutions to this problem.

Materials and Methods

In order to assess the influence of moisture and to study degradation of perovskite materials, perovskite thin films and planar perovskite solar cells with inverted structure were prepared. All materials used in experiments were purchased from commercial suppliers. The used materials are specified in following description of preparation process.

As a substrate for the solar cells Ossila ITO (indium tin oxide) patterned glass (S101) was used. To clean the substrates following procedure was implemented: 10 minutes sonication in ~2% Neodisher solution, rinsing with distilled water, 10 minutes sonication in isopropyl alcohol (IPA), rinsing with ethanol and drying with compressed air. The next step was deposition of PEDOT:PSS (Heraeus Clevios P VP AI 4083) layer by static spin-coating at 4500 RPM for 30 s. Substrates were then laid on a hotplate set to 120 °C and left there for at least 10 minutes. The temperature of hotplate was afterwards decreased to 90 °C. The perovskite layers were deposited using Ossila perovskite precursor ink for deposition in air (I101) and deposition was carried out in dry glovebox with relative humidity (RH) ~15 %. The precursor ink was first heated to 70 °C for at least 120 min and left to cool to room temperature afterwards. Perovskite precursor ink was dynamically spin-coated at speed of 4000 RPM and left to spin for 30 s. After the deposition samples were put on 90 °C hotplate for 120 min to let the perovskite crystals form. For solar cells, next deposited layer was $PC_{70}BM$ (Ossila M113, dissolved in chlorobenzene, concentration 50 mg/ml). Deposition of PCBM was carried out in nitrogen filled glovebox by dynamic spin-coating at 1000 RPM for 30 s. Samples were then transported to vacuum evaporator chamber, where 5 nm thick layer of calcium and subsequently 100 nm thick layer of aluminium were deposited as cathode. Cells were encapsulated by Ossila E132 epoxy resin cured with UV radiation for 20 s to shield them from environmental effects.

As a result planar perovskite solar cells with inverted structure were prepared. Complete multi-layered structure is Glass|ITO|PEDOT:PSS|$CH_3NH_3PbI_{3-x}Cl_x$|$PC_{70}BM$|Ca|Al. Schematic depiction of solar cell is shown in Fig. 1.

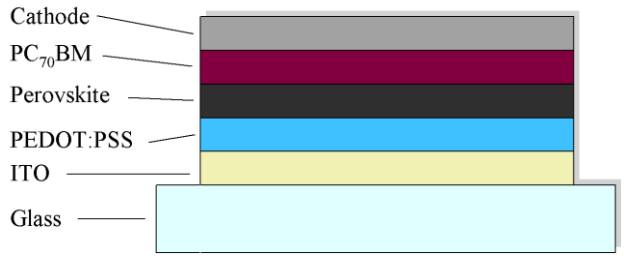

Fig. 1. **Schematic depiction of structure of prepared solar cells.**

The photoconversion efficiency of prepared cells was characterized by current-voltage characteristics. Measurements were carried out using Keithley 2601B electrometer and LOT-Oriel LSO916 solar simulator with irradiance 850 W/m^2 at room temperature.

For XRD and AFM measurements only partial samples were prepared, to ensure accessibility of perovskite. The preparation process was identical but only to the point of deposition of perovskite layer. Other layers were not deposited in samples for XRD and AFM measurements. To eliminate premature degradation samples were kept under nitrogen atmosphere until the beginning of experiment.

In order to achieve accelerated degradation and to secure controlled environment climatic chamber Climacell 111 was used for studying influence of moisture on perovskite. The XRD measurements were carried out using Rigaku miniflex 600 HR. The obtained spectra were analysed using PDXL software. For the purpose of detailed quantitative study the measured data was analyzed by Rietveld refinement. After final analysis the error parameter R_{wp} was always under 12%. AFM measurements were carried out using Agilent 5500 Scanning Probe Microscope.

Results and discussion

In order to assess the influence of moisture, the perovskite solar cells were left in the ambient atmosphere and changes in photoconversion efficiency were observed. The I-V characteristics (Fig. 2) of the cells were recorded right after preparation, after four days and after eight days. The results are summarized in Table I. The given parameters are averaged results over all measured electrodes. Stated uncertainty is sample standard deviation of averaged values.

From obtained results it can be seen, that energy conversion efficiency (η) has dropped in course of eight days. This loss of efficiency is mainly due to the decrease in current density (J_{sc}). This result is consistent with other published studies and has been ascribed to increasing content of PbI_2 in the perovskite layer[7]. In order to verify this conclusion, XRD and AFM investigation of perovskite layer was carried out.

The climatic chamber was used to secure a controlled environment and to accelerate the degradation process of the perovskite layer for XRD and AFM measurements.

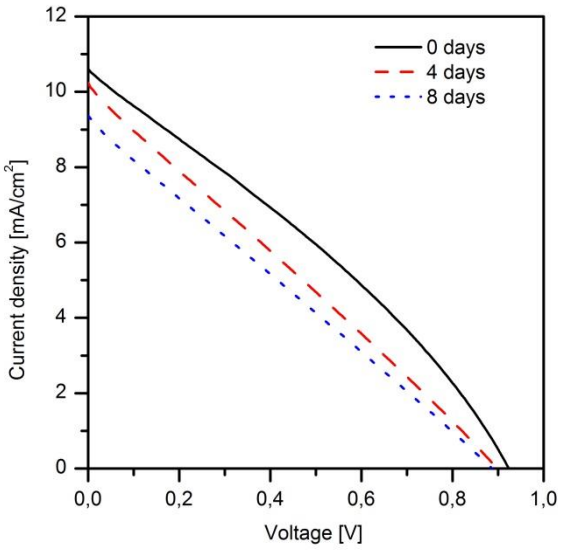

Fig. 2. I-V **characteristic of selected electrode of the perovskite solar cell aged in ambient environment for 0 days (black line), 4 days (red dashed line) and 8 days (blue dotted line).**

Table I, Parameters of prepared perovskite solar cells.

Ageing [days]	J_{sc} [mA/cm^2]	V_{oc} [V]	*FF* [%]	η [%]	R_{series} [Ω·cm^2]
0	10 ± 2	890 ± 30	29,1 ± 1,4	2,6 ± 0,7	60 ± 20
4	9 ± 3	840 ± 50	25,7 ± 0,3	2,0 ± 0,7	80 ± 30
8	8 ± 3	820 ± 60	25,3 ± 0,4	1,8 ± 0,6	90 ± 40

The prepared samples were placed into a climatic chamber with set 60% RH and temperature set to 25 °C. The measurement was conducted on samples after preparation, after 24 and after 48 hours ageing in the climatic chamber. The diffraction spectra are shown in Fig. 3. The diffraction patterns were normalized to the perovskite peak at 14,06° as maximum and intensity converted to a logarithmic scale for better observation of minor peaks.

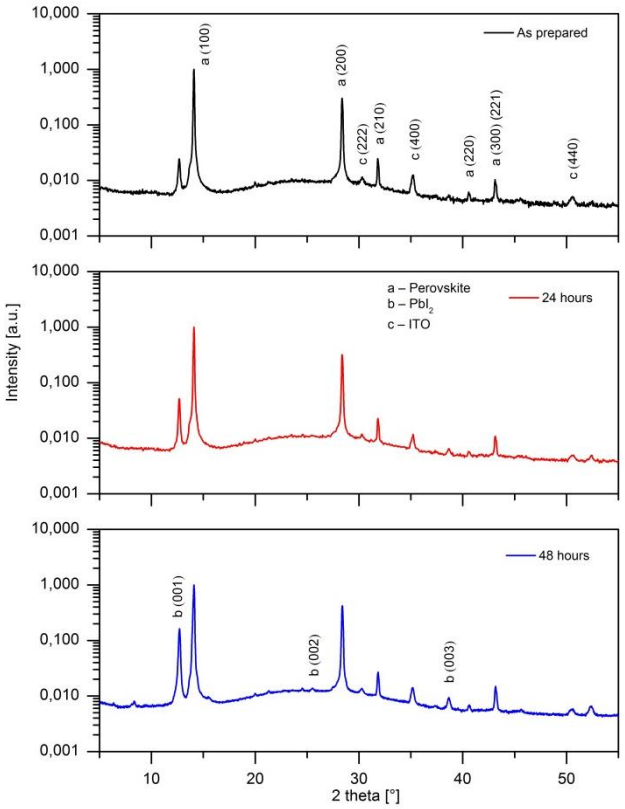

Fig. 3. **XRD patterns of perovskite film exposed to moisture in climatic chamber at 25 °C and 60% RH. Figure shows patterns of film as prepared (top), after 24 hour (centre) and 48 hours exposure (bottom). Peaks corresponding to different compounds are marked a (perovskite), b (PbI_2) and c (ITO).**

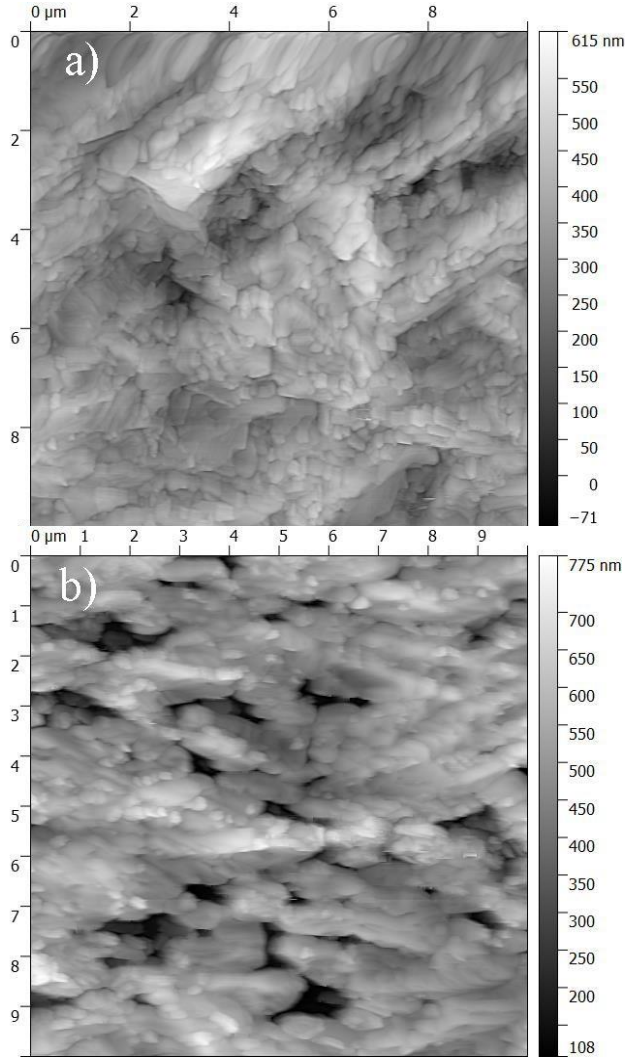

Fig. 4. **AFM images of perovskite layer a) as prepared and b) after 48 hours in climate chamber (25 °C, 60% RH).**

In measured patterns three distinct compounds were identified – indium tin oxide (ITO), perovskite and lead iodide (PbI_2). The amount of lead iodide was gradually increasing with the time the samples spent in the climatic chamber. The increase is in good accordance with the proposed degradation process[6]. The quantitative results of analysis (Table II) revealed that in as prepared perovskite already 8 molar % of PbI_2 is present. After 24 hours lead iodide content increased by 6 molar % and after another 24 hours, the content more than doubled. It seems that speed of degradation was increasing in time.

The sizes of respective crystals have been calculated from diffraction patterns from the peaks with the highest intensity using Debye-Scherrer formula. Resulting sizes were approximately 62 nm and 259 nm for PbI_2 and perovskite respectively.

Table II, Perovskite and lead iodide molar percentage content in studied sample.

	As prepared	24 hours	48 hours
PbI_2 [mol%]	8.3	14.0	30.3
$CH_3NH_3PbI_3$ [mol%]	91.7	86.0	69.7

In order to assess effects of exposure to moisture also on the perovskite layer morphology AFM measurements were conducted on the samples aged in the climatic chamber. Measurements were carried out after preparation and after 48 hours in the climatic chamber with parameters set to 60% RH and 25 °C. The results are shown in Fig. 4.

It is evident from the measurement that moisture led to coarser layer and even possible pinholes formation. This is due to decomposition of perovskite crystal to lead iodide. As our XRD measurements have shown, the size of PbI_2 crystals is approximately four times lower than that of the perovskite ones. The decomposition then creates voids in perovskite layer.

Conclusions

The degradation of perovskite material in perovskite solar cells in the presence of moisture was studied. The study was carried out using three different methods – current-voltage measurements of complete solar cells and XRD and AFM measurements of perovskite material itself in partial structure of the solar cell aged in a controlled environment of a climatic chamber. Results have shown that deterioration of energy conversion efficiency of solar cells is caused by decomposition of perovskite crystals and formation of lead iodide. This conclusion was supported by results of XRD and AFM measurements which were in good agreement showing an increase in PbI_2 content in the perovskite layer.

This research was conducted at Materials Research Centre (MRC). Research infrastructure was supported by National Program for Sustainability I (MEYS CR), projects No. REG LO1211 and LO1210. Authors gratefully acknowledge financial support under BUT projects No. FCH/FEKT-J-18-5427, FCH-S-18-5194, FEKT-S-17-4595 and No. FEKT-S-17-4626. M. Kratochvíl was supported by the Statutory City of Brno through Brno PhD. Talent program.

REFERENCES

1. Kojima A., Teshima K., Shirai Y., Miyasaka T.: J. Am. Chem. Soc. *131*, 6050 (2009).
2. Yang W. S., Park B.-W., Jung E. H., Jeon N. J., Kim Y. C., Lee D. U., Shin S. S., Seo J., Kim E. K., Noh J. H., Seok S. I.: Science *356*, 1376 (2017).
3. Yang W. S., Noh J. H., Jeon N. J., Kim Y. C., Ryu S., Seo J., Seok S. I.: Science *348*, 1234 (2015).
4. Jeon N. J., Noh J. H., Yang W. S., Kim Y. C., Ryu S., Seo J., Seok S. I.: Nature *517*, 476 (2015).
5. Wang D., Wright M., Elumalai N. K., Uddin A.: Sol. Energ. Mat. Sol. C. *147*, 255 (2016).
6. Niu G., Li, W., Meng F., Wang L., Dong H., Qiu Y.: J. Mater. Chem. A *2*, 705 (2014).
7. Gujar T. P., Unger T., Schönleber A., Fried M., Panzer F., van Smaalen S., Köhler A., Thelakkat M.: Phys. Chem. Chem. Phys. *20*, 605 (2018).

SCREEN PRINTED BIOCOMPATIBLE PHOTORESIST AS A MEAN TO ENHANCE PERFORMANCE OF ORGANIC ELECTROCHEMICAL TRANSISTORS

LUKÁŠ OMASTA[a], JIŘÍ EHLICH[a], STANISLAV STŘÍTESKÝ[a], MICHAL HRABAL[a], OTA SALYK[a], MARTIN VALA[a], MARTIN WEITER[a], MILAN MATEJKA[b]

[a]Materials Research Centre, Brno University of Technology, Purkyňova 118, 612 00 Brno, Czech Republic
[b]Institute of Scientific Instruments of the Czech Academy of Sciece, Královopolská 147, 612 64 Brno, Czech Republic
xcomastal@fch.vut.cz

Keywords OECT; screen printing; organic electrochemical transistor; PEDOT:PSS; SU-8 photoresist; multi-electrode array; cell culture

Abstract

Human cell cultures provide a potentially powerful means for pharmacological and toxicological research. A microplate pattern with a multielectrode array of organic electrochemical transistors (OECTs) based on the semiconductive polymer poly(3,4-ethylenedioxythio-phene):poly(styrene sulfonic acid) PEDOT:PSS was developed and fabricated using conventional printing methods (screen printing) together with standard lithographic procedures. The devices were designed for electrogenic cell monitoring and stimulation[1].

In this study, the screen printing process of commercially available and biocompatible photoresist SU-8 was optimized. SU-8 is an epoxy-based negative photoresist commonly used in the printed circuit board (PCB) industry. A layer of photoresist prepared in this study had the thickness of 30 μm thick, and we photolithographically produced patterns with the resolution better than 50 μm. This layer was intended as a mask to cover the underlying printed OECT array sensor consisting of gold electrodes and the active layer of PEDOT:PSS.

Output, transfer and transient characteristics of prepared devices were evaluated. The devices were tested in a simulated model for the response of the drain current to the voltage pulses applied to the gate electrode up to 300 μV. The reaction to such gate voltage renders the device to be sensitive enough to detect the electrical signal of pulsing cardiomyocytes. The transconductance up to 2.5 mS and the time constant of 150 ms was achieved. Further development is directed towards higher time resolution through miniaturization of the transistor channel.

Introduction

The high electrical conductivity of polyacetylene and other organic compounds with conjugated bonds, discovered by Hideki Shirakawa, Alan Heeger, and Alan MacDiarmid led to considerable interest in the use of organics in electronics. This discovery was acknowledged by the Nobel Prize in Chemistry in 2000[2]. The following branches made considerable effort into the related research: photovoltaics, photoluminescence, and bioelectronics as the brand new field of science. In 1989 the first polymer-based light emitting diode (LED) was discovered using PPV as the emissive layer[3]. The printable properties of organic semiconductors lead to the development of so-called printed electronics.

The biocompatibility of organic semiconductors, predominantly polymers, predetermined their application in biosensors and bio-actuators in biology and medicine as an ideal bio-interface[4]. In 1984 White et al. fabricated the first organic electrochemical transistor (OECT) based on polyaniline (PANI)[5].

The recent course in toxicology and pharmacology concentrates on the replacement of laboratory animals with in-vitro cell-based methods and models. This replacement requires the introduction of strategies for the real-time ascertainment of cell physiology. To this end device such as electrochemical sensors can be used. The use of organic semiconductors provides the inexpensive production of disposable sensors in large quantities. One of the most suitable materials among organic semiconductors for bioelectronic applications is Poly(3,4-ethylenedioxythio-phene) mixed with poly(styrene sulfonic acid)—(PEDOT:PSS).

In 1992 Heywang and Jonas[6] reported the electrochemical polymerization of a new conducting polymer, poly(3,4-ethylenedioxythiphene) (PEDOT). After that in the year, 1995 Yamato et al. showed the superiority of Poly(3,4-ethylenedioxythiophene)-poly(styrenesulfonate)
(PEDOT + PSS) at stability against pH and applied potential in comparison to PANI[7]. Soon after that, this polymer became widespread in bioelectronics as active transistor channels and other fields as conductive thin film semitransparent wiring. This material is attractive mainly due to its high conductivity, biocompatibility, and availability.

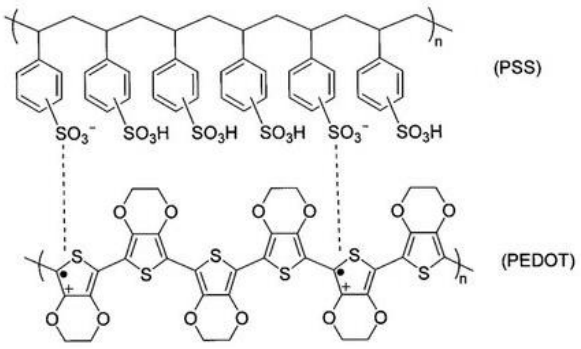

Fig. 1. **Chemical structure of PEDOT:PSS. The "dot'' and "plus'' represent the unpaired electron and positive charge on the PEDOT chain, respectively**

For the measurement of the electrical response of electrogenic cells, OECTs are excellent instruments. The potential of the cell membrane spreads into the surrounding electrolyte, in this case, phosphate-buffered saline (PBS) and therefore affects the OECTs channel electrode. Moreover, the change in the cell membrane potential can be simulated by the modulation of the OECT gate voltage VG and hence various stimuli could be detected.

In good agreement with previously published works improvement of the transconductance and time constant of prepared devices can be achieved by decreasing the OECT dimensions[8]. The increase in the parameters mentioned above is done by shortening the gate-channel distance and minimizing the channel-electrolyte charge electrical double layer (EDL) capacitance by reducing the channel area. The miniaturization and optimization were done via photolithography using SU-8 photoresist.

Screen printing is a cheap and versatile fabrication process for material deposition on nearly any surface. It enables minimizing waste throughout deposition unlike spin-coating and physical vapor deposition (PVD). It is a robust, simple, accurate, high-throughput and low-cost technique which is well fitted for mass production. Screen printing is broadly employed in the microelectronic industry for fabrication of printed circuit boards, in solar cell industry, display, and electronic industries[9].

SU-8 was produced by IBM in the late 1980s[10] and is nowadays extensively used in the manufacture of microstructures in electrowetting displays[11] and microelectromechanical (MEMS) devices. The typical and most popular application method of SU-8 is spin-coating. Nevertheless, this approach is somewhat unsuitable for large areas due to edge bead effects[12] and geometric defects due to the solvent evaporation[13]. Increased material consumption renders this technique inadequate for large area production. Screen-printing of SU-8 was reported by J. Klavins et. al[14].

Materials and Methods

The goal of this study is to improve the previously manufactured and published OECTs arrays based on PEDOT:PSS[1].

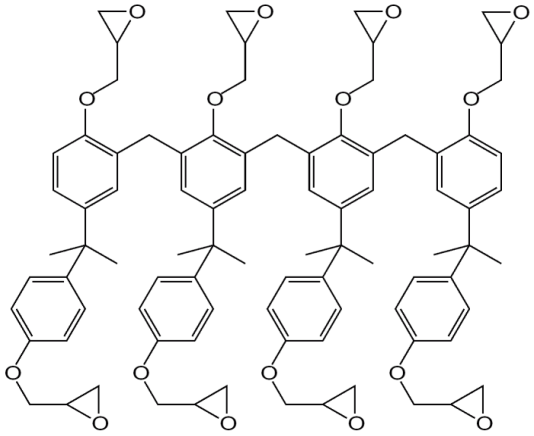

Fig. 2. **Structure of the SU-8 molecule**

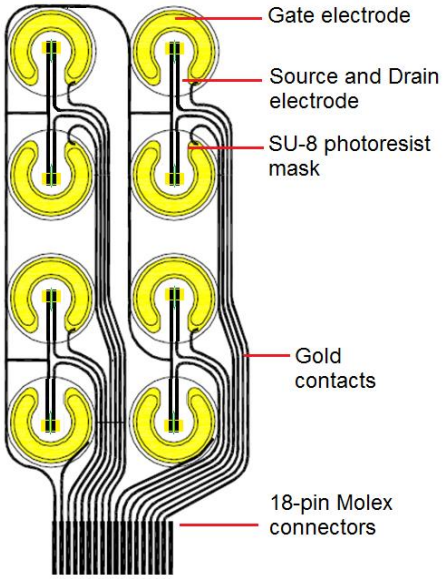

Fig. 3 **Detail of the designed OECT array**

The prototype (Fig. **3**) was designed to fit into a 96-well polystyrene microplate (chimney-well, no bottom) from Greiner Bio-One (GmbH Frickenhausen, Frickenhausen, Germany), for the automatic investigation of a multitude of substances. We manufactured the prototype with the array of 8 Organic Electrochemical Transistors (OECT) based on the Poly(3,4-ethylenedioxythiophene) polystyrene sulfonate (PEDOT:PSS) polymer (Clevios™ S V3, Heraeus Holding GmbH, Hanau, Germany).

The combination of photolithographic techniques together with screen-printing method was employed for the device assembly. Printed organic electronic technology has generated the possibility of printing biosensor patterns on biocompatible polymer foils such as PEN (Poly(Ethylene 2,6-Naphthalate) which was employed in our study. The copper laminates on a PEN-film backing with a thickness of 50 µm (AKAFLEX PENCL HT provided by Gatema a.s, Boskovice, CZ), was used to photolithographically pattern flexible circuits. The PEN variant was chosen due to its superior stability at high temperatures compared to PET laminates and enables processing at a temperature of up to 150 °C. On top of the patterned electrolytic copper foil (thickness of 17 µm) was galvanically applied a thin layer of gold (tens of nanometers) with an interlayer of nickel for better adhesion.

The PEDOT: PSS layer was printed from commercially available Clevios S V3 screen printing pastes (Heraeus Holding GmbH). The PEDOT:PSS pattern created a functional OECT gate and channel. The paste was first stirred intensively before printing in order to obtain a lower viscosity, better homogeneity and higher conductivity of the resulting film, as we described previously (cit). The stirring slightly decreased also the final thickness of the layer by an average of 20 %, from 250 nm to 200 nm. IT also improved the thickness homogeneity in roughness from 25 nm to 18 nm and waviness from 25 nm to 10 nm. These parameters were measured by a DektakXT Stylus Profiler (Bruker, Billerica, MA, USA).

PEDOT:PSS was screen-printed in the form of a rectangular channel connecting two parallel gold electrodes with a width of 250 µm and 200 µm gap between them. The channel was surrounded by a planar circular gate electrode also from a screen-printed PEDOT:PSS with an outer diameter of 6 mm. The rotary symmetry was selected to improve the field distribution[1].

The device was masked and sealed by the layer of an epoxy-based negative photoresist SU-8 (MicroChem Corp. Westborough, MA, USA). This layer insulated the gold conducting paths from the electrolyte environment and created a narrow active channel.

For screen printing the RokuPrint Screen printing machine, SD 05 was used together with custom-made polyethylene screens 36/31 (36 µm - size of mesh opening, 31 µm – the size of thread diameter) for screen printing of Clevios S V3 PEDOT:PSS and 140/65 screen for screen printing of SU-8 photoresist. The layers of approximately 200 nm of PEDOT:PSS and 30 µm of SU-8 was obtained. To this end, the SU-8 2015 with a viscosity of 1250 cSt had to be diluted by cyclopentanone to the viscosity of approximately 250 cSt (Fig. **4**). An ARG2 rheometer (TA Instruments, New Castle, DE, USA) was used for viscosity measurement at the fixed temperature of 25 °C.

The prepared screen-printed layer was firstly dried on a hot plate at 95 ° C for 5 minutes (soft bake). This step was necessary in order to minimize the amount of solvent in the layer of SU-8 before exposure. The resulting photoresist layer was 30 µm thick. The unexposed photoresist substrate was then aligned under a microscope with a chrome photomask made by electron-beam lithography and placed in the Suss Microtech MA6 / BA6 adjuster. The photoresist was exposed to UV radiation of 5,6 mW/cm^2 for 120 seconds. This step was followed by another heat curring on a hot plate for 5 minutes at 100 °C (post exposure bake). This step is necessary for the development of the desired pattern. Subsequently, the photoresist was submerged for 1 minute in the developer, rinsed with isopropyl alcohol and dried with a stream of nitrogen.

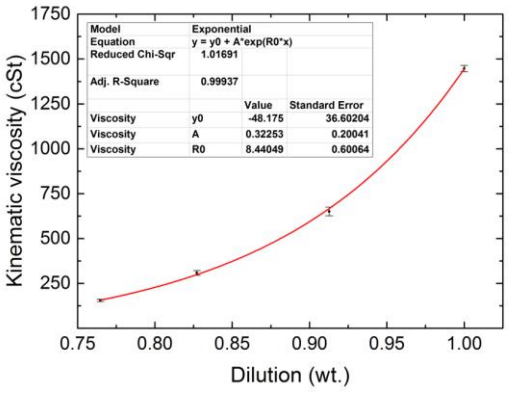

Fig. 4 **SU-8 kinematic viscosity dependance on cyclopentanone content.**

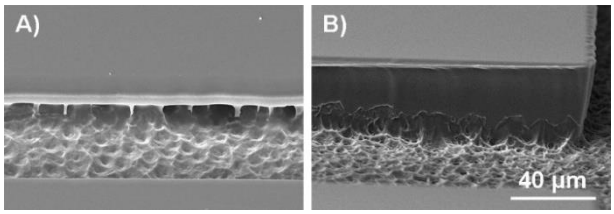

Fig. 5 **The difference between using printed pattern on the foil A) and chrome photomask B) to produce the photolithographic pattern**

The difference between the usage of the foil with a printed pattern and the photomask made by electron-beam lithography to photolithographically produce 50 µm thin channel is shown in Fig. **5**. Using the foil, we were not able to produce adequately exposed patterns due to the random scattering of the incident UV light passing through the foil and due to the inherently not well-defined edges. The usage of foil led to underexposed edges in the vicinity of several micrometers around our designed channel and even to the outright short circuit due to the exposed golden Source and Drain electrodes. Switching to the chrome photomask solved this problem.

The screen printed and the photolithographically patterned layer of SU-8 covers the surface of the whole OECT sensing array as can be seen in Fig. **6**.

Only parts of the sensor that comes in contact with the electrolyte (active channel and gate electrode) are exposed. The exposed channel area had the dimension of L = 50 µm and a width of W = 600 µm as shown in Fig. **7**. The typical resistance of the channel was 200-300 Ω.

The electrical circuitry designed for OECT testing in schematic form is depicted in Fig. **8**. The contact array on the microplate foil was contacted by 18-pin Molex connectors and 18-wire ribbon conductors so that a single connector connected eight OECTs and individual OECTs could be selected from the array by a proper couple of microswitches.

Results

The initial test determined the OECTs parameters such as output characteristics Fig. **9** and transfer Fig. **10** characteristics, and from them, the highest derived transconductance g = 2.5 mS.

The next experiment investigated the response of an OECT's channel current on a simulated signal of electrogenic cells. The standard PBS solution was used as an electrolyte. In looking for the optimum working point of the OECT with the highest transconductance, the gate voltage V_G was set to 0.2 V and the voltage between Source and Drain electrode was set to V_D = -0.4 V. The rectangular pulses of 1 mVpp at a 1 second period were modulated. Typical response on such pulse together with filtered data using FFT bandpass from 0 to 25 Hz and determined value of the time constant can be seen inFig. **11**.

3T3 fibroblasts were used to test the biocompatibility of the sensor. Cells were able to grow on top of the sensor to the same degree as in control (standard cell culture plastics). The cell viability was similar to the control and was typically around 90-95 %. The unimpaired viability indicated that a high level of biocompatibility was reached. The unimpaired viability indicated that a high level of biocompatibility was reached. All the biocompatibility tests were done by the Institute of the Biophysics of the Czech Academy of Sciences.

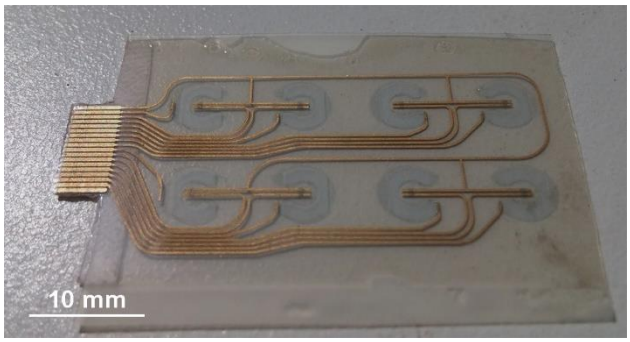

Fig. 6 **Screen-ptinted and photolithographically patterned OECT sensor array**

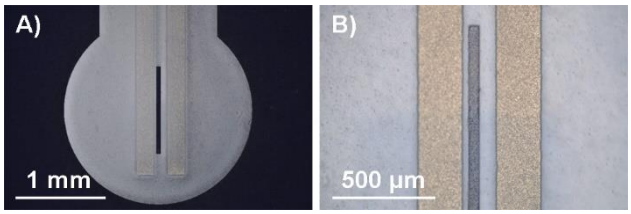

Fig. 7 **Detail of one sensor channel patterned using SU-8 photoresist**

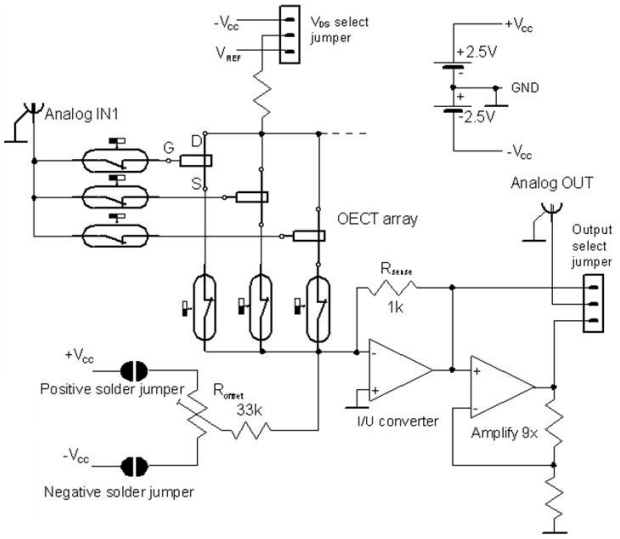

Fig. 8 **The amplifier - current/voltage converter for the OECTs testing**

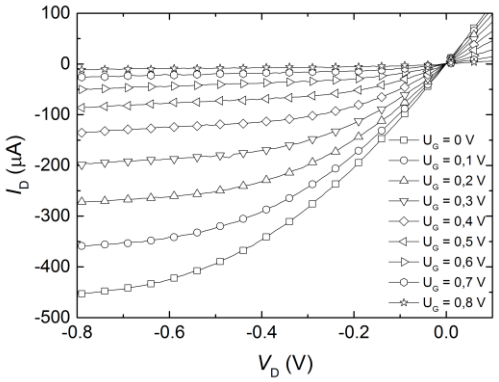

Fig. 9 **Output characteristics of prepared OECTs**

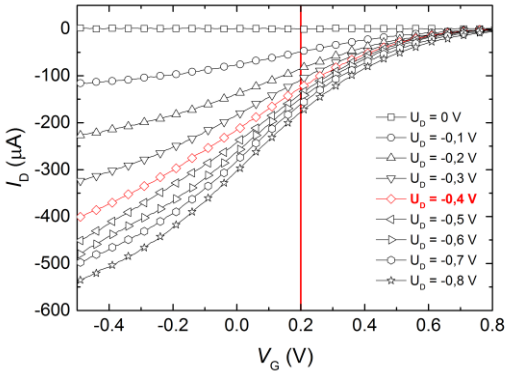

Fig. 10 **Transfer characteristics with the illustration of set point and the slope dependent on the drain potential**

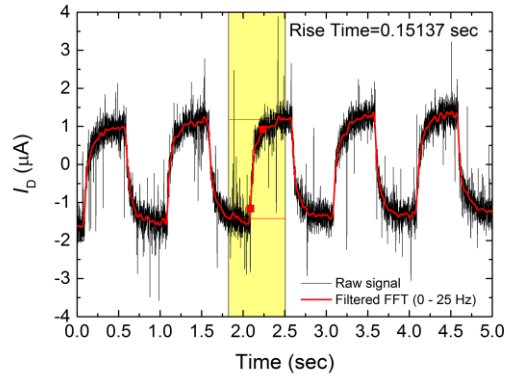

Fig. 11 **Response of OECT on 1 mVpp gate rectangular signal at setting point V_D = -0.4 V, V_G = 0.2 V. The derived transconductance gives g = 2.5 mS and time constant τ = 0.15 s.**

Conclusion

The screen printing process of commercially available and biocompatible photoresist SU-8 was optimized and successfully implemented into previously adapted OECT sensors based on PEDOT:PSS. Using the photolithographic process the pattern of 50 mm thin active channel was achieved. Signal amplification was shown employing an electrogenic cell pulsation simulation, where the constant gate offset potential was modulated by a 1.0 Hz, 1.0 mVpp rectangular signal. The resulting Source-Drain current response I_D was 2.5 µA, and the corresponding achieved transconductance 2.5 mS. The upper-frequency limit 7 Hz was concluded from the OECT gate circuit time constant of 0.15 s. Additional improvement of the device speed and amplification could be obtained by reducing the OECT channel dimensions, mainly by the shortening of the gate-channel distance and reducing the EDL capacitance by decreasing the channel area.

This work was supported by Czech Science Foundation via project No. 17-24707S, research infrastructures was supported by projects MŠMT No. LO1211 from the National Programme for Sustainability I (MEYS CR) and J. Ehlich was supported by the student project of Faculty of chemistry BUT under project No. FCH-S-18-5194.

REFERENCES

1. Salyk O., Víteček J., Omasta L., Šafaříková E., Stříteský S., Vala M., Weiter M.: Appl. Sci. *7*, 998 (2017).
2. Heeger A. J.: Rev. Mod. Phys. *73*, 681 (2001).
3. Burroughes J. H., Bradley D. D. C., Brown A. R., Marks R. N., Mackay K., Friend R. H., Burns P. L., Holmes A. B.: Nature *347*, 539 (1990).
4. Strakosas X., Bongo M., Owens R. M.: J. Appl. Polym. Sci. *132*, 41735 (2015).
5. White H. S., Kittlesen G. P., Wrighton M. S.: J. Am. Chem. Soc. *106*, 5375 (1984).
6. Heywang G., Jonas F.: Adv. Mater. *4*, 116 (1992).
7. Yamato, H.; Ohwa, M.; Wernet, W., J. Electroanal. Chem. *397*, 163 (1995).
8. Stříteský S., Marková A., Víteček J., Šafaříková E., Hrabal M., Kubáč L., Kubala L., Weiter M., Vala M.: J. Biomed. Mater. Res., Part A *106*, 1121 (2018).
9. Yue W., Li C. W., Xu T., Yang M.: Biosens. Bioelectron, *15*, 675 (2013).
10. Gelorme J. D., Cox R. J., Gurrierez S. A.: IBMCorp. US4882245A.
11. You H., Steck A. J.: J. Soc. Inf. Disp. *21*, 192 (2013).
12. Luurtsema G. A.: *Master thesis*. University of California, Berkeley 1997.
13. Garcano G., Ceriani M., Soglio F.: Microelectron. Int. *10*, 12 (1993).
14. Klavins J., Mozolevskis G., Ozols A. A., Nitiss E., Rutkis M.: Latv. J. Phys. Tech. Sci. *52*, 58 (2015).

ANALYTICAL AND CHEMOMETRIC TOOLS USED FOR FRUIT JUICES AUTHENTICITY EVALUATION

MARTIN POLOVKA[a]*, BLANKA TOBOLKOVÁ[a], ELENA BELAJOVÁ[a], MÁRIA KOPUNCOVÁ[a], JÁN DUREC[b]

[a] National Agricultural and Food Centre, VUP Food Research Institute, Department of Chemistry and Food Analysis, Priemyselná 4, SK-824 75 Bratislava, Slovak Republic,
[b] McCarter, Bajkalská 25, SK-821 01 Bratislava, Slovak Republic; production premises: Budovateľská 1247/7, SK-92901 Dunajská Streda, Slovak Republic
polovka@vup.sk

Abstract

Fruit juices authenticity is an important issue in terms of the producers and consumer's protection against illegal practices as well as in terms of products quality maintenance. In this contribution, complex physico-chemical characterisation of raw pineapple and orange juice samples of well-defined origin (feedstock), most typically used for fruit juices production is presented. The analytical data from spectroscopic (EPR, UV-VIS) and chromatographic (GC, LC-MS, LC/DAD/RID) measurements were processed by chemometric tools involving the methods of multivariate statistics. Both, region/country of origin as well as season of production were recognised as crucial factors affecting juice quality. The developed model for juice authenticity was tested via analytical data of sets of commercial samples with known origin of fruit. Prediction ability tests proved that the proposed model represents reliable tool for operational control of juice feedstock quality.

Introduction

Fruit juices belong to the most popular drinks all over the world mostly thanks to their unique flavour and aroma. They are rich source of a number of biologically active substances, including polyphenols with proven health benefits. The antioxidant properties of juices are also well described and are related to these components[1].

Properties of fruit juices important for consumers are influenced by several factors, of which the most important are the type and quality of the fruit used for its preparation (particularly, maturity, mutual sugar/acid ratio and the composition and concentration of flavouring substances), way of fruit harvesting and post-harvest treatment, processing and finalization[2,3]. Last but not least, the quality of fruit juices is significantly affected by the variety and origin of the fruit used for its production. In addition, from our previous experiments, it is clear that important factors with direct impact on the quality of fruit juices are also the seasonally/seasoning effects (year of production).

Frequently, fruit/raw juice producers or sellers use blending of fruit/juice of different origin and quality to obtain the "averaged" feedstock, which is then offered to juice producers to be used for the production of the end-products. This aspect greatly affects the quality of production, but also has a financial impact on both, juice producer and consumers, who may thus be misled.

Composition of fruit juices, as well as composition of dehydrated fruit juices and fruit nectars, their reserved name/s, way of production and labelling of their properties are subjected to specific legislation, which is at EU level regulated by the Directive 2001/112/EC relating to fruit juices and certain similar products intended for human consumption, updated by the Directive 2012/12/EU of the European Parliament and of the Council of 19 April 2012[4].

Products fulfilling the criteria set by the legislation are considered authentic, while those different are non-authentic, false or adulterated. Adulteration practices may also affect the quality of the feedstock and thus of the whole production process and the final product[2].

With the aim to protect both, the producers of fruit juices as well as the consumers against illegal practices, there is an active movement towards collecting the characteristic markers of original foods and drinks including juices and thus, set the standards typical for the authentic products.

To verify the authenticity of fruit juices, different analytical and chemometric methods and/or their combinations are used. For this purposes, analysis of well-defined juices including the feedstock of known origin and composition is necessary. Involvement of combination of highly sensitive analytical methods/assays is a logic consequence, as well.

In this contribution, the correlations between the orange and pineapple fruit juice feedstocks origin, and their physicochemical properties are presented. The correlations between the feedstock quality and seasoning effect are discussed. The model suitable to test the origin/quality of the feedstock developer on the basis of analytical characteristics obtained by EPR, UV-VIS and chromatographic techniques was introduced and its functionality verified via analysis and subsequent processing of data of sets of commercial samples.

Materials and methods

Samples. Samples of fresh fruit juice of well-defined origin from Costa Rica, Ecuador, South Africa, Colombia, Ghana and Mauritius (pineapple) and from Greece, Mexico and Brazil (orange) were subjected to analysis. Samples were delivered to the laboratory in a frozen state, in dark containers, i.e., in conditions, keeping their properties unaffected.

Besides the samples of well-defined origin, also the group of commercially available orange (5) and pineapple juices (4) were subjected to analysis.

Experimental Spectroscopic (EPR and UV-VIS) and chromatographic (GC-GC/MS-GC-olfactometry, LC) techniques were used. Concentration of polyphenols, selected antioxidants and antioxidant properties, colour parameters, profile of selected organic acids, amino acids and metals, but also sugars and hydroxymethylfurfural were evaluated. To obtain complex information, basic characteristics comprising pH, °Brix, relative density, titratable acidity and formol number were also monitored. The methods and assays were applied following the procedures previously described by Belajová et al.[5].

Statistical evaluation The obtained experimental characteristics were processed by statistical analysis involving ANOVA Tukey HSD test and multivariate statistics (involving the methods of principal component analysis (PCA), canonical discrimination (CDA) and factor analysis (FA)) in order to evaluate the mutual relationships and correlations between the feedstock origin and their properties. Using the CDA, the recognition ability was calculated as the percentage of correctly classified samples in the original data set in which all the samples were of known properties (in terms of their origin) for the classification model.

Prediction ability tests were performed to test the suitability of the evaluated model for the classification of samples of unknown origin. For this purpose, sets of commercial pineapple and orange juice samples were subjected to analysis under the identical conditions.

Results and discussion

Analysis of qualitative parameters of the feedstock

The results of the determination of basic physicochemical parameters of pineapple and orange juices of different origin were compared to qualitative requirements of the Australian Fruit Juice Association (AFJA) and Association of the Industry of Juices and Nectars (AIJN)[6,7]. It is apparent, that all the analysed (model) pineapple and orange juices meet the quality requirements of these associations. An exception is the formol number of the Mexican orange sample (13.94 ± 0.29). Taking into account the AIJN criteria, it can be supposed that the lower value of the formol number may result from the lower maturity of the oranges, or their frost damage or similar pre-harvest event.

From the statistical point of view, both between the pineapple and the orange juice samples (analysed separately) were found significant differences ($P < 0.05$) for all the monitored parameters, including colour characteristics and antioxidant properties. The statistical analysis of both types of juices showed a strong correlation of individual colour characteristics as well as of parameters characterising antioxidant properties (GAE, AAE and TEAC).

Determination of the profile of amino acids was performed by LC-MS using a mixed composite standard of 22 amino acids. Results obtained (not presented) clearly showed high variability of the concentration of practically every unique amino acid. For the purposes of differentiation of samples on the basis of their origin/ authenticity it is apparent from the results that the amino acid profile is sufficiently different for every sample under study and thus, it can serve as one of characteristic markers. Although there is scare information on amino acids profile of fruit juice, the obtained results are consistent with those previously published by Passos, et al.[8].

For the purposes of complex characterisation of juices, the concentration of selected organic acids (L-ascorbic, citric, L-malic) as well as sugars (fructose, glucose and sucrose) and the glucose/fructose (G/F) ratio were monitored. As a reference, limit values of AFJA and AIJN were taken, for pineapple and orange juices, respectively.

As follows from the results, the glucose and fructose content in pineapple from Costa Rica (2017) was slightly higher than the reference values, however, the G/F ratio in this juice was within the expected range. Slightly exceeded was also the upper limit of sucrose in pineapple juice from South Africa and Mauritius. Statistical analysis showed significant differences ($P < 0.05$) in almost all of the compared parameters.

In case of orange juices, besides the acids and sugars concentration, also the concentration of the most typical flavonoid, hesperidin was analysed (accepted as one of the quality/authenticity markers of orange juices). In juices from Greece and Mexico, the content of hesperidin was below the lower AIJN reference value[6]. ANOVA test showed an insignificant difference in concentration of hesperidin in both these juices ($p > 0.05$ for ME-GR). Differences in other parameters, except for G/F ratio values, were statistically significant.

5-hydroxymethyl-2-furaldehyde (HMF) content is a good indicator of the quality of feedstock. Its formation at stable/stabilised feedstock processing temperatures is dependent on the quality of the feedstock. The results of the experiments showed that in all samples analysed the pineapple juice was the HMF concentration less than 0.16 mg / kg. For orange juices, HMF concentrations of 0.5 mg/kg - 0.75 mg/kg were determined. These values are in good agreement with the established standards for fruit juices according to AIJN, although there is no specific limit for pineapple (for apple juice the proposed limit is 20 mg/l and for orange juices of 10 mg/l)[9,10]. These findings confirm good hygiene practice as well as qualitative standards of the juice producer.

One of the main aims of the study is the monitoring of the quality of feedstock and within this effort, obtaining markers suitable for monitoring and control of the authenticity and origin of juice feedstock.

Processing of data by multivariate statistical tools

a) feedstock of defined origin The entire dataset of the experimental characteristics obtained for feedstock of orange and pineapple juice of well-defined origin (altogether 22 parameters) was processed by multivariate statistical tools to develop the model enabling verification of the feedstock origin, separately for pineapple and orange. The data of pineapple samples from altogether 6, most typical regions/countries, representing the major producers of this type of juice were obtained. In case of orange juices, the number of samples (3 countries) is still limited, affected beside the other factors also the climatic/weather conditions in major producing regions (e.g., Florida hurricanes in 2017, with direct impact on feedstock quality and price).

Methods of principal components analysis, canonical discrimination analysis and factor analysis were involved.

By means of PCA, all samples were differentiated according to their country of origin. Apparent are also the regional similarities/differences as in the plot of principal components (Figure 1), samples are also grouped according to the geographical regions. Obvious is also the seasoning effect, present for samples of pineapple juices from Costa Rica 2016 and 2017, eigenvectors of which laying the same quadrant but are separated in space.

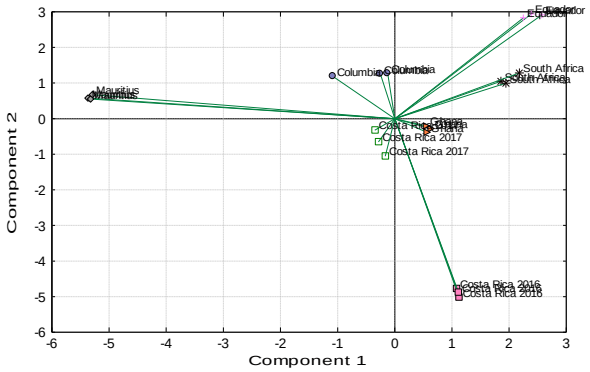

Fig. 1. **Plot of principal components constructed from 22 experimental characteristics of feedstock of pineapple juices from Costa Rica (2016, 2017), Ecuador, South Africa, Colombia, Ghana and Mauritius.**

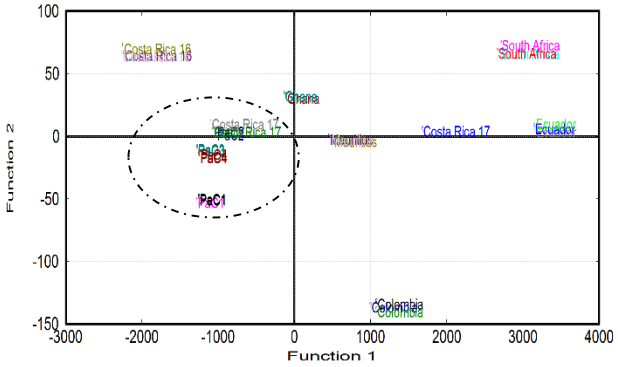

Fig. 2. **Discrimination analysis of samples of pineapple juices of known origin from Costa Rica (2016, 2017), Ecuador, South Africa, Colombia, Ghana and Mauritius and commercial samples (PaC1-PaC4, surrounded by dash-dot line) performed on the basis of 22 experimental characteristics.**

As the PCA analysis is indifferent to any factor (origin, species, etc.), the obtained trends indicate a close link between the origin of samples and their characteristics and/or the suitability to use of those characteristics for the purposes of this study. First three principal components in the PCA analysis account for about 82% of the total variability. In the same way, the results of the cluster analysis in the Euclidean space demonstrated the existence of 7 well-defined clusters on the basis of the origin of the analysed samples. The TEAC, AAE and TPC values play the dominant role in the first principal component, in the second, glucose and citric acid concentration, and in the third one, sugar content (°Brix) and sucrose.

Discrimination analysis was used to discriminate the samples according to their origin. Both, for pineapple and orange samples, 100 % discrimination scores were reached. However, it is necessary to stress low variability of particularly orange feedstock samples, which can therefore influence the discrimination.

b) Test of reliability of the discrimination model To test the applicability of the developed discrimination model based on the databases of the experimental characteristics of well-defined model samples, the analysis of commercial samples of pineapple and orange juice was performed under the identical conditions.

First of all, prediction ability tests were performed using the leave-multiple-out approach, in which a set of samples (approx. 15%) of known origin is assigned as unknown and in turns classified by CDA. Using this approach, 100 % correctness of classification was achieved.

As the developed model is intended for the prediction of attributes of unknown samples, its prediction ability, i. e., the ability to classify the samples of unknown origin was tested. For these purposes, analytical data of five commercial samples of orange juices and four samples of pineapple juices were used. The so-performed classification into groups performed by CDA lead to the conclusion, that all the analysed orange juice samples were prepared from the feedstock of Brazilian origin, whereas those of pineapple were classified as originating from Costa Rica (2017), as is depicted on Figure 2.

These results are very promising, however, it is important to stress, that the ambition and urgent need is to spread out the databases of markers of known samples as well as to count in the additional effects, e.g., variety and season.

Conclusion

On the basis of the presented results, general conclusion can be made, that the proposed authentication model based on the databases of experimental characteristics of pineapple and orange fruit juices represents suitable tool to test the quality of orange and/or pineapple juices in terms of the quality/origin of the feedstock. Additional experiments are in progress in order to expand the number of well characterised samples and thus, to spread out the internal variability and reliability of the model.

This contribution is the result of the project APVV-15-0023 "Quality and authenticity of fruit juices – study of relationships between the origin of feedstock, processing technology and quality of fruit juices" and of the project ITMS 26220220175 "Improvement of nutritional and sensorial parameters of fruity and vegetable drinks via an inert gases application" implementation, supported by the Research & Development Operational Programme funded by the ERDF.

REFERENCES

1. Donado-Pestana C.M., Caldas Moura M.H., de Araujo R.L., de Lima Santiago G., de Moraes Barros H.R., Genovese M.I.: Curr. Opin. Food Sci *19*, 42 (2018).
2. F.A.I.M. - Food Authenticity - Issues and Methodologies. Michele Lees (ed.): Eurofins Scientific (1998). ISBN 2-9512051-0-4.
3. Sinha N.K., Sidhu J.S., Barta J., Wu J.S.B., Cano M.P.: Handbook of fruits and fruit processing. 1st ed. Oxford: John Wiley & Sons, Chichester, 2012.
4. Directive 2012/12/EU of the European Parliament and of the Council.

5. Belajová E., Tobolková B., Daško Ľ., Polovka, M., Durec, J.: J. Food Nutr. Res *56*, 4 (2017).
6. Standard Nutrient Values for Fruit Juices and Guideline on Traceability. AIJN European Fruit Juices Association (2003). Available online: www.aijn.org.
7. Australian Fruit Juices Parameters. AFJA Reference Guideline. Australian Fruit Juice Association (2015).
8. Moretti Passos H., Cieslarova Z., Colnaghi Simionato A.V.: Electrophoresis *37*, 13 (2016).
9. Eller K.I, Pimenova V.V, Kon I: Vopr. Pitan (Russ). *70*, 3 (2001).

STABILITY OF METHYLATED HUMIC ACID

JAN RYBÁRIK*, MARTINA KLUČÁKOVÁ, VOJTĚCH ENEV

Material Research Center, Faculty of Chemistry, Brno University of Technology, Purkyňova 464/118, 612 00 Brno, Czech Republic
xcrybarik@fch.vutbr.cz

Key words: Humic substances, methylation, humic acid, methylated humic acid, FT-IR

Introduction

Humic substances and humic acids are a very broad class of organic compounds which are formed by the gradual decomposition of plant residues and living organisms They contain many times more organic carbon than we find in living organisms. Humic acids (HK) contain a large number of different functional groups, in particular carboxyl groups - COOH. We can find them at almost any ecosystem (soil, water) at different rates.[1]

Humic substances are able to bind various pollutants from Industrial production, agriculture and other human activities (like heavy metals, pesticides, herbicides, dyes, etc.). The interaction possibilities can be different: ion exchange, hydrogen bridge formation, coulombic interactions, hydrogen bridges, van der Waals interactions, hydrophobic interactions, absorption, etc. [1]

By methylation, the carboxyl groups are blocked and interactions with pollutants are avoided at these active sites. Thus, it is possible to distinguish methylated humic acid from normal humic acids. The aim of this work was to assess the stability of the modified humic acids and its possible demethylation.[1]

Experimental part

Humic acids were prepared by extraction from finely granulated South Moravian lignite. 60 g of ground lignite was mixed with 1 dm^3 of 0.1 M hydrochloric acid solution and the suspension was left for 1 hour on the shaker. The decalcified lignite was washed with sufficient distilled water to remove chloride ions. The lignite thus prepared was transferred to a plastic container with an extraction agent (0.1M sodium hydroxide and 0.1M anhydrous pyrophosphate). The bottle with the extraction agent was left in the shaker for 12 hours.[1]

Fig. 1. **Color difference between humic acid (one the left) and methylated humic acid (on the right)**

The suspension was centrifuged and the supernatant (the humic acid solution was filtered before filtering), the filtrate was acidified with hydrochloric acid up to pH=2. After two hours, all humic acids were precipitated and transferred to dialysis membrane, which were immersed in distilled water, the distilled water was regularly replaced with a test for the presence of chloride ions (test with $AgNO_3$) and after clear test were solved in dialysis membrane and lyophilized.

Half of the sample of prepared humic acid was subjected to selective methylation. To each 1 g of humic acids was added 4 cm^3 of chloroform and 2 cm^3 of methanol. Subsequently, 4 cm^3 of a 2M solution of trimethylsilyl diazomethane in hexane (TMS-DM) was added. The mixture was stirred for less than 2 hours on a mixer in the hood. An additional 0.75 cm^3 TMS-N21 was added after the growth.

It was necessary to evaporate the unreacted reagent from obtained methylated humic acid simple. The sample was dried overnight in the digester at room temperature. The photos of the samples and their color difference can be seen in Figure 1.

Extracted humic acid and selectively methylated humic acid were analyzed by FTIR Nicolet iS50 spectrophotometer using the ATR method to determine the humic acid spectrum and also to verify the successful methylation of the prepared sample of methylated humic acids.

Humic acids are soluble in 0.01M NaOH, but higher concentrations of NaOH are required to dissolve methylated humic acid. The methylated humic acid was dissolved in 0.05M NaOH.

The prepared sample of the dissolved methylated humic acid was divided into 4 parts, then we tried to obtain methylated humic acid by following four ways:

Sample (a) was immediately precipitated with concentrated hydrochloric acid (to pH=1) after dissolution, followed by centrifugation, washing with MQ with water and lyophilization, FTIR analysis,

Sample (b) was immediately precipitated with 0.1 M hydrochloric acid (to pH=3) after dissolution, followed by centrifugation, washing with MQ with water and lyophilization, FTIR analysis,

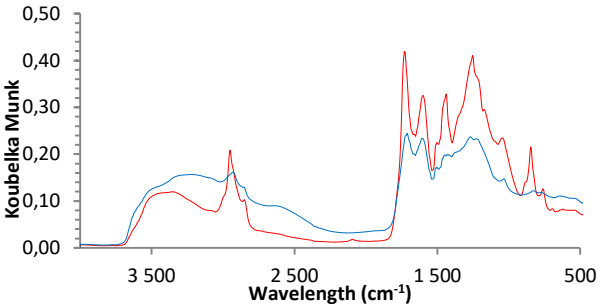

Fig. 2. **FTIR spectrum - humic acids (blue curve), methylated humic acid (red curve)**

Sample c) The methylated humic acid solution was lyophilized without any treatment, followed by analysis of FTIR,

Sample d) The methylated humic acid solution was subjected to free evaporation on a Petri dish in an oven at 40 °C, FTIR analysis.

Results and discussions

In a sample of humic acids that has been undergone selective methylation, successful methylation by the FITR method has been confirmed.

According to the spectrum in Figure 2, it is clear that the methylation of functional groups leads to changes in FTIR skeletons characteristic for esters. The width of a wide peak of about 3500 cm^{-1} was reduced by methylation and the shallow strip at 2580 cm^{-1} was completely absent. The absorption band corresponding to the valency vibration of the -C = O group was shifted after methylation to a higher wavelength after methylation (1720 cm^{-1} to 1735 cm^{-1}) and its insensity increased. These observed changes in the spectrum caused by methylation of the sample correspond to our results published in the articles.[2,3]

Figure 3 shows that the changes in the spectrum caused by the methylation of the humic acid sample above are missing for all 4 samples. The FTIR method therefore confirmed that methylamine acid in the solution is unstable and demethylation occurs.

Conclusion

During the experiments, we failed to recover the dissolved methylene acid humic from the solution in the methylated form.

pH=1 and pH=3 values were used for precipitation of methylated humic acid. Then freeze-dried lyophilization and free evaporation. From the results, it is clear that, in all cases, sample extraction from the solution resulted in the demethylation of the sample, so the methylated humic acid in the solution is unstable.

The question now remains, what is the rate of demethylation, which method to use to prevent demethylation when it is obtained from the solution.

pH = 1 and pH = 3 values were used for the precipitation of methylated humic acid and as well freeze-dried lyophilization and free evaporation. From the results, it is clear that, in all

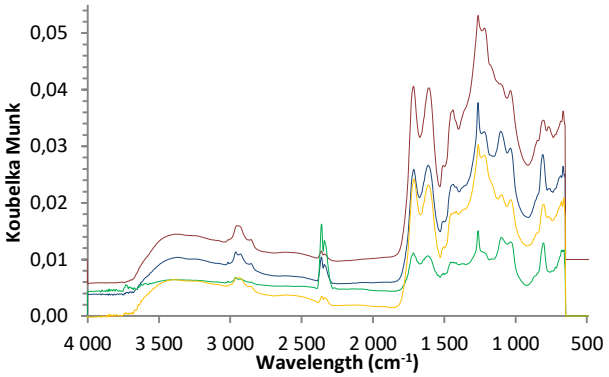

Fig. 3. **FTIR spectrum - 4 samples of methylated humic acids. Blue curve (sample a), brown curve (sample b), yellow curve (sample c), green curve (sample d)**

cases, the sample extraction resulted in the demethylation of the sample, so the methylated humic acid in the solution is unstable.

The question now remains, what is the rate of demethylation, which method to use to prevent demethylation when it is obtained from the solution.

This work was created in the Material Research Center of the Faculty of Chemistry, Brno University of Technology. Project LO1211 is funded in support of the Ministry of Education, Youth and Sports of the Czech Republic.

REFERENCES

1. Rybárik J.: *Strukturní a termodynamické aspekty interakcí biopolymerů s organickými ionty.* Vysoké učení technické v Brně Fakulta chemická, Brno 2016.
2. Klučáková M., Kalina M., Sedláček P., Graset L.: Journal of Soil and Sediments *14*, 368 (2014).
3. Klučáková M., Kalina M.: Colloids and Surfaces, A: Physiochemical and Engineering Aspects *483*, 162 (2015).

BIOMASS GASIFICATION PRODUCT GAS CLEANING AND UTILIZATION – IMPORTANT CRITERIA FOR SUITABLE TECHNOLOGY SELECTION

PETR SEGHMAN, LUKÁŠ KRÁTKÝ, TOMÁŠ JIROUT

Department of Process Engineering, Faculty of Mechanical Engineering, CTU in Prague, 160 00 Prague
Petr.Seghman@fs.cvut.cz

The amount of produced waste has been annually growing. Eventhough amount of mixed ordinary waste is almost constant (apprx. 290 mil. t y^{-1})[1], amount of other types of waste significantly increases every year – sewage sludge production grew from 15 t_{ds} y^{-1} in 2004 to over 18,5 t_{ds} y^{-1} reported in 2014[1].

As the numbers keep growing, new waste treatment and utilization methods must be developed and utilized. Biomass gasification is one of the perspective technologies that transform waste into useful products such as fuels and chemicals. This technology also helps to reduce the amount of CO_2 in the atmosphere.

The following paper presents the outcome of initial study, presenting brief information about which criteria must be studied for suitable syngas utilization technology selection. Goals for future studies are mentioned in the paper aswel.

Biomass gasification is a thermochemical process that converts feedstock into gases. Along with the syngas (main product containing mostly H_2, CO, CO_2 and CH_4), several other products are formed – ash (an unconvertible part of the biomass and bed material particulates), char (a convertible part of the biomass that stays unconverted due to incomplete conversion) and tars (higher hydrocarbons, that are liquid at normal state).

Knowledge of the composition of the produced mixture (product gas) and percentage of each of the mentioned substances is one of the most important qualities that must be known and is crucial for a suitable downstream and utilization technologies selection. For this purpose, a prediction tool for product gas composition is being developed. In the tool, available data on product gas composition dependence on various parameters is gathered. Feedstock composition, gasification temperature and pressure, agent used and agent-to-biomass ratio, catalyst used, and gasifier type are the main parameters whose effect on the product gas (and syngas) composition is observed.

In the table (Table I) bellow, different combinations of feedstock, gasifier agent, temperature and other parameters along with the produced gas composition are shown to demonstrate the variety of possible outcomes. Data were obtained from different sources[2-5].

In the Table I, following abbreviation were used: CFB - circulating fluidized bed, DFB – dual fluidized bed, FB – fixed bed, Sw.gr. – switch grass, Al.sh – almond shells, Lign. – lignite.

The presented data are involved in the prediction tool that will be presented in winter 2018/2019. The tool will according to the user specified parameters compute the most probable syngas composition based on the available data gathered in the database.

Table I, Different combinantions of gasification conditions and syngas composition, at atmospheric pressure conditions[2,3,4,5]

Feedstock	Wood[2]	Sw.gr.[3]	Al.sh.[4]	Lign.[5]
T [°C]	805	875	830	850
Gasifier	CFB	DFB	FB	DFB
Agent	Air	Steam	Steam	Steam
H2 [%mol]	16,7	25,2	62,1	54,5
CO [%mol]	28,3	35,7	22,7	23,0
CO2 [%mol]	51,7	20,8	15,2	17,2
CH4 [%mol]	3,4	18,3	0,0	5,3

Table II, Available syngas utilization technologies overview – main advantages and disadvantages of each technology

Technology	Advantages	Disadvantages
F.-T. sth.	+ One reactor + Possibility of different products	- High purity of input required (catalyst)
H_2 production	+ Can process impure gas + High demand for H_2 in the market	- High operational costs (PSA) - Storage of H_2 complicated
Methanol sth.	+ Methanol can be further transformed into other chemicals	- High operating pressures - Methanol being toxic substance -High purity of input required (catalysts)
Methane pr.	+ Low operational costs + Can process impure gas	- Slow reaction (biological) - Product only for energetic use

Another field of study of the initial research are the utilization technologies themselves. For the syngas utilization following methods were chosen: Fischer-Tropsch synthesis (liquid fuels production from syngas), Methanol synthesis (direct synthesis of CH_3OH from syngas), Hydrogen separation and Methane production (via fermentation of the syngas).

Many parameters of the technologies must be known before starting the design itself. Firstly, the partial steps of each of the technologies must be known, along with their energetic nature and main process parameters (such as temperature and pressure). Secondly, input requirements (purity, temperature) must be known. One of the important parameters of the input material is the presence and amount of the impurities in the gas. Some of the impurities, as H_2S or sulfurous oxides, are catalytic poisons for catalysts used in some of the technologies. Other technologies require absence of methane in the mixture. A summary of some of the advantages and disadvantages obtained from the initial study are shown in the Table II.

Along with the technologies themselves, final products properties and parameters must be known. Some of the obtained information are stated in the Table III bellow – the parameters that were studied are toxicity, storage and transport complications, world annual consumption and contemporary price of the substance.

From the acquired information, every mentioned technology has a potential to be utilized for bio-syngas produced via gasification. Each of the products has its advantages and disadvantages. For example, hydrogen being the product with the highest price and high demand has problems with its storage and the cost of the pre-storage treatment can raise up to as high as 8 \$ kg^{-1} which could in worst case negate the possible profits or even generate loses[16]. Thus, also storage and product handling must be part of the techno-economical assesment and comparison of the possibilities.

Table III, Products of the mentioned technologies along wih main qualities and parameters [6-15]

Products	Qualities
Olefins (FT)	$9{,}4*10^8$ Mt y^{-1}, 1800-2310 \$ Mt^{-1} - Flammable - Toxic - Can be stored for longer period if conditions (humidity, temperature) under control - Comparable to conventional diesel
H_2	$6*10^7$ Mt y^{-1}, 1800-5200 \$ Mt^{-1}* - Higly flammable, Explosive - Expansive storage (high pressure and liquefaction or storage medium needed)
Methanol	$8*10^7$ Mt y^{-1}, 480 \$ Mt^{-1} (420 € Mt^{-1}) - Flammable - Toxic - Hygroscopic and corrosive, no other complications.
Methane	$1{,}29*10^{14}$ Mt y^{-1}, 81-162 \$ Mt^{-1} - Can be sold to NG-network (energy system) - Direct storage requires liquefaction and is not that effective

Another field that the initial research must cover is the environmental effect of each of the mentioned technologies. As one of the main reasons leading to further research of biomass gasification and other waste-utilization methods is carbon capture and utilization policy and greenhouse gases emmisions reduction, the environmental burden of building and operation of such technologies must be quantified.

One of the best ways of greenhouse gases (GHG) effect evaluation is so called Carbon Footprinting. This method involves various gases emission related to one unit of the product and involves all stages of the product lifetime, including emissions produced by technology building and manufacuring, materials obtaining and treatment, production itself and product utilization and its lifecycle.

This method is further described and covered by normative ISO 14064. In this normative, each gas is assigned a global warming potential (GWP) that reflects how other gases affect the atmosphere compared to CO_2. Using this GWP parameter, a CO_2 equivalent (CO_2e.) can be computed and this value (one number) can be used for different technologies comparison. In the Table IV bellow, several examples of GWP for different gases are shown to demonstrate the differences in severity of some emissions.[17]

As seen in the table above, several gases GWP is that high that even a small amount of emited gas can cause serious changes and problems to the atmosphere.

To have an idea about how good or bad the CO_2e. (carbon footprinting) results of the proposed technology are, carbon footprint of direct inceneration will be taken as the relative process (which would most probably be used for the feedstock treatment instead of the technology).

To sum up, several criteria are important for the most suitable syngas utilization technology – compostition of the produced syngas, demand for the final products of the technology and carbon footprint of the final product. Syngas composition can vary a lot and can make huge differences in profitability. Demand of the final product must be ensured to maintain the technology in operation. The carbon footprint of each of the technologies is the most important criteria when the elementary idea of reducing carbon emissions and storaging in various forms is considered. A technology that would produce more CO_2e. than direct inceneration of wastes would not be considered suitable even if its economic aspects would seem profitable.

Table IV, Various GHG and their GWP (represented as SAR for 100-year ekvivalent effect and 20-year equivalent effect) for comparison. The table also shows lifetime (LT) of each gas in the atmosphere[17]

Name	Formula	LT [y]	SAR*	20-y
Carbon dioxide	CO_2	-	1	1
Methane	CH_4	12,0	21	72
Nitrous oxide	N_2O	114,0	310	289
CFC-11	CCl_3F	45,0	3 800	6 730
CFC-12	CCl_2F_2	100,0	8 100	11 000
Halon-1301	$CBrF_3$	65,0	5 400	8 480
Halon-1211	$CBrClF_2$	16,0		4 750
Carbon tetrachloride	CCl_4	26,0	1 400	2 700
Methyl bromide	CH_3Br	0,7		17
Methyl chloroform	CH_3CCl_3	5,0		506

Further studies will cover both making the syngas composition prediction tool and verifying it and designing and comparison of the different combinations of feedstock, gasification and utilization technologies.

This work was supported by the Ministry of Education, Youth and Sports of the Czech Republic under OP RDE grant number CZ.02.1.01/0.0/0.0/16_019/0000753 "Research centre for low-carbon energy technologies" and by Student Grant Competition of CTU number SGS18/129.

REFERENCES

1. European Commision. Eurostat tool. [Online] [Cited: 26. 08 2018.] Av. at: https://ec.europa.eu/eurostat
2. Li X.T., Grace, J.R., et al.: Biomass and Bioenergy *26* (2004).
3. Brown R.C.: Thermochemical Processing of Biomass: Conversion into Fuels, Chemicals and Power. John Wiley & Sons, Ltd., Chichester 2011.
4. Rapagná S., Jand N., Foscolo P.U.: Hydrogen Energy *7* (1998).
5. Pfeifer C., Koppatz S., Hofbauer H.: Biomass Conv. Bioref *1* (2011).
6. Dieselnet. Fuel Regulation. *EU: Fuels: Reference Diesel Fuel*. [Online] ECOpoint Inc., 09 2012. https://www.dieselnet.com/.
7. Kim, K.S., et al.: Bioresource Technology *127*, 391 (2013).

8. UK-Government. National Statistics. [Online] 26. 07 2018. https://www.gov.uk/government/statistics/
9. Brown D.R.: Hydrogen Supply and Demand: Past, Present, and Future. [online] Av. at www.researchgate.net/publication/301959632_Hydrogen_Supply_and_Demand_Past_Present_and_Future.
10. Internationa Energy Agency. *Hydrogen production and storage.* OECD/IEA, Paris 2006.
11. Bartels J.R., Pate M.B.: *A feasibility study of implementing an Ammonia Economy.* Iowa State University, Des Moines 2008.
12. METHANEX. Our Business - Methanex posts regional contract methanol prices for North America, Europe and Asia. [Online] Av. at https://www.methanex.com/our-business/pricing
13. Atmospheric Above Ground Tank Storage of Methanol. *Methanol Safe Handling Technical Bulletin.* [Online]. Av. at http://www.methanol.org/
14. Shah S., Bergland Q.H., Bakke, R.: Scandinavian Simulation Society (2017).
15. Ostúr K., Kačur J.: IEEE (2015).
16. US Drive, Hydrogen Storage Tech Team Roadmap. [online] Av. at: https://www.energy.gov/sites/prod/files/2017/08/f36/hstt_roadmap_July2017.pdf.
17. IPCC, Publications and Data. [online] available from: http://ipcc.ch/publications_and_data/ar4/wg1/en/ch2s2-10-2.html

MODELLING OF BIOELECTRONIC DEVICES

JAN TRUKSA*, OTA SALYK

Brno University of Technology, Faculty of chemistry, Purkyňova 464/118, 612 00, Brno
xctruksa@fch.vutbr.cz

Introduction

Organic electrochemical transistors (OECTs) are currently the topic of a great amount of research in the field of bioelectronics, due to possible use as biosensors. These devices consists of three electrodes, two of which are connected by a thin layer of an elecrically conductive polymer – this layer is called the channel. The two electrodes are called the Source (S), and the Drain (D). The third electrode, called the Gate (G), is separated from the channel by electrolyte. The most frequently used material for the channel is the p-type conductor PEDOT:PSS − poly(3,4-ethylenedioxythiophene), stabilized by poly(styrene sulfonate). This polymer (see fig. 1) is relatively cheap, easy to process, and biocompatible.

Typically, the D electrode is negatively biased with a potential V_D [V] and the S electrode is grounded. In this state, electric current I_D [A] flows through the PEDOT:PSS channel. When a positive potential V_G is applied to the G electrode,

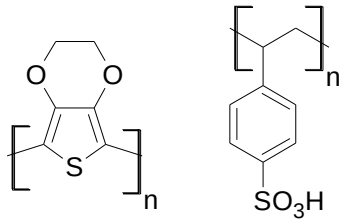

Fig. 1. **The structures of PEDOT (left) and PSS (right)**

cations from the electrolyte are pushed into the channel, where they interact with the PSS anions. This leads to recombination of the holes in PEDOT, and therefore a decrease in conductivity and a smaller I_D value. This process is referred to as dedoping. When V_G is negative, the electrolyte cations are pulled away from the channel, resulting in increased conductivity. This is called doping. If V_G = 0 V, a negligible amount of electrolyte ions may be present in the PEDOT:PSS layer[1]. The aim of this work was to create a mathematical model of an OECT, that would give output characteristics comparable to those of a real device when electric potential is applied to the D and G electrodes. The finite element method was used, with the commercial software COMSOL Multiphysics.

Electric field is governed by the Poisson equation (*1*):

$$\Delta V = -\frac{\rho_v}{\varepsilon_r \varepsilon_r}, \Delta = \frac{\partial^2}{\partial x^2} + \frac{\partial^2}{\partial y^2} + \frac{\partial^2}{\partial z^2}, \qquad (1)$$

where ε_0 is the permittivity of vacuum ($8.854 \cdot 10^{-12}$ F m^{-1}), ε_r is the relative permittivity of the used material, ρ_v is space charge density [C m^{-3}], *x*, *y*, *z* are Cartesian coordinates [m]. Space charge density in an electrolyte made up of N species is given by equation (*2*):

$$\rho_v = qN_A \sum_{i=1}^{N} z_i c_i , \qquad (2)$$

where q is the elementary charge ($1.602 \cdot 10^{-19}$ C), N_A is the Avogadro constant ($6.022 \cdot 10^{23}$ mol^{-1}), z_i is the charge number of an ion, c_i is its concentration [mol dm^{-3}]. Ion transfer in the electric double layer (EDL) directly above the channel is governed by the Nernst-Planck equation (*3*):

$$\mathbf{N}_i = -D\nabla c_i - \frac{z_i F D c_i}{RT}\nabla V, \nabla = \frac{\partial}{\partial x}\mathbf{i} + \frac{\partial}{\partial y}\mathbf{j} + \frac{\partial}{\partial z}\mathbf{k}, \qquad (3)$$

where *t* is time [s], **i**, **j**, **k** are base unit vectors, and **N** is the ion flux of some ion [mol m^{-2} s^{-1}], D is the diffusion coefficient [m^2 s^{-1}], R is the universal gas constant (8.314 J mol^{-1} K^{-1}), *T* is the temperature [K] and F is the Faraday constant (96,485.34 C mol^{-1})[2]. Equation (*2*) then serves as a coupling of the two differential equations.

Experimental

Charge transfer and ion drift inside the channel has been modelled by Tybrandt et. al.[3], using modified versions of equations (*1*) and (*3*). Unfortunately, the computer available for this work was not powerful enough to compute the Nernst-Planck equation on a 2-dimensional domain, which is necessary to model the movement of ions deeper into the channel, and towards the D electrode, at the same time as modelling the drift

of holes across the length of the channel. Due to this, an older and less accurate model by Bernards and Malliaras[4] had to be used. In this model, the hole concentration p [m^{-3}] is considered to be a function of the electric charge Q [C], of ions exchanged between the electrolyte and the channel (equation *4*):

$$p = p_0 \left(1 - \frac{Q}{q p_0 v}\right), \qquad (4)$$

where v is the volume of the polymer material [m^3]. After the ion exchange is taken into account, the conductivity σ [S m^{-1}] can be calculated and the electric current density **J** [A m^{-2}] is give by Ohm's law (*5*):

$$\mathbf{J} = \sigma \nabla V \, , \sigma = q p \mu, \qquad (5)$$

where μ is the charge carrier mobility [cm^2 V^{-1} s^{-1}].

In addition, the model had to be split into three parts, due to scale differences – the transistor diameter was in the order of 1 mm, while the PEDOT:PSS layer thickness was in the order of 100 nm. These scale differences make meshing the domain for finite element computing nearly impossible. Figure 2 shows an OECT, which the model was based on. The device was housed in a 10.9 mm chimney well microplate.

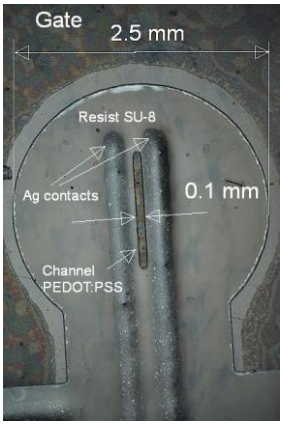

Fig. 2. **The OECT that served as a basis for this model**

In the first part, the electric field in the electrolyte above the OECT was computed. This part can also be considered the macroscopic part of the model, since it deals with the entire device. The device was considere to be fully circular, to take advantage of symmetry for easier computing. Due to this, it was possible to only compute the electric field in one half of the device. The rest can be obtained by mirroring. Figure 3 shows the the model geometry.

The values of electric potential along the top of the channel and inside the channel were gained from this part of the model, and used in further modelling. Figure 4 shows electric potential on top of the channel for several combinations of V_D and V_G. This figure also demonstrates how electric field superposition affects the potential, as the potential values influenced by a negatively biased G are lowered on most of the channel, while those influenced by a positively biased G are raised. In some cases (such as a relatively high V_G and a V_D sufficiently close to

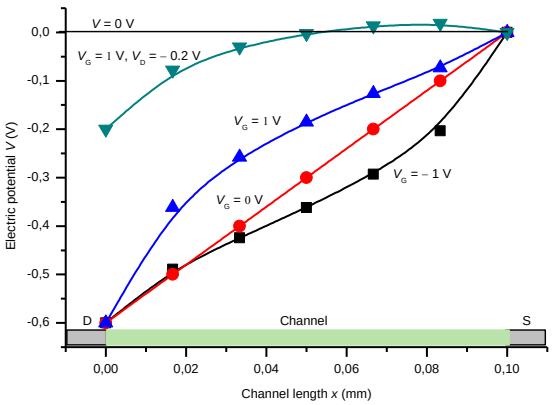

Fig. 4. **Electric potential on top of the channel for $V_D = -0.6$ V**

zero), as illustrated by the green curve on fig. 4, the potential values near the S electrode become positive. In this case, electrolyte cations actually drift away from the channel, resulting in an increase of conductivity. Furthermore, living cells have proven to be sensitive to the electric potential and doping of a PEDOT:PSS surface, which they adhere to[5]. Therefore, modelling the electric potential of PEDOT:PSS structures may help to predict their biocompatibility.

In the second part of the model, the EDL above the PEDOT:PSS channel was modelled. The EDL was expected to have a thickness consistent with the Debye length λ_D [m] (*6*):

$$\lambda_D = \sqrt{\frac{\varepsilon_{sol} RT}{2F^2 c_i}}. \qquad (6)$$

Within a distance λ_D from the channel, the changes of ion concentration and electric potential were computed, based on equations (*1*) and (*3*). Everywhere else, the bulk electrolyte was supposed to be electroneutral (there is no local difference in concetrations, and therefore $\rho_v = 0$ C). The EDL was supposed to consist of a compact Stern layer close to the electrode, with thickness λ_S of the electrolyte ion radius, and the Diffuse layer, with thickness λ_D. The Stern layer consists mainly of polarized solvent molecules, and because there are generally no ions present in this layer (they are expected to immediately transfer into the channel, or into the bulk electrolyte), the space charge density is also expected to be zero. The greatest potential drop in an EDL is expected to occur in the Stern layer[2].

In OECTs for biological applications, phosphate buffered saline (PBS) is typically used as the electrolyte. For ease of computation, the electrolyte in this model was supposed to be a NaCl solution, with bulk concentration $c_0 = 137$ mol m^{-3}. The potassium and phosphate ions were omitted, due to their low concentration[6].

Since it was not possible to model the EDL above the channel as a 2D domain, the channel had to be divided into subdomains, and the EDL was approximated by a 1-dimensional interval for each one. As indicated by fig. 5, the PEDOT:PSS

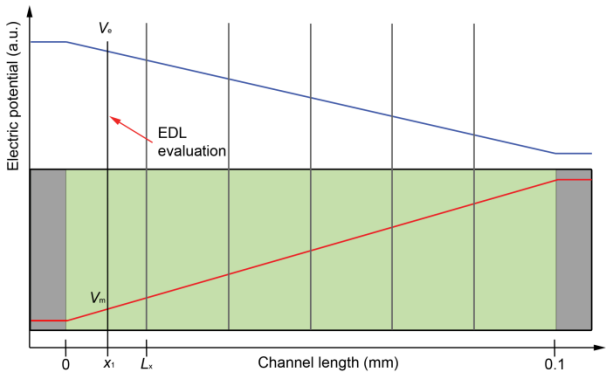

Fig. 5. **Division of the polymer layer into subdomains for EDL modelling; the blue line signifies potential on top of the channel, the red line signifies potential inside the channel**

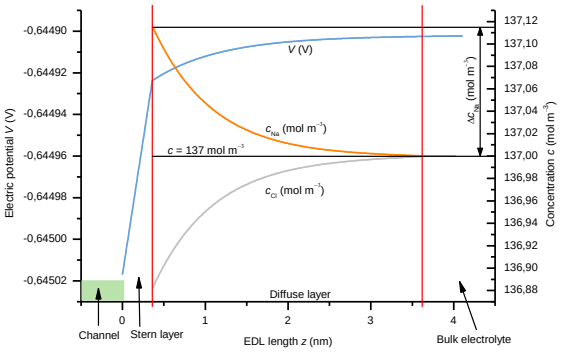

Fig. 6. **Gradient of the concentration and the electric potential in the EDL; the blue line signifies the potential change in the EDL; the orange and grey lines show the concentration of Na^+ and Cl^- ions respectively; the red lines show boundaries of the Stern and Diffuse layers; the black lines demonstrate the difference Δc_{Na}**

channel was split into several subdomains of length L_x and for each of the subdomains, potential values V_m within the channel and V_e in the electrolyte, which correspond to some point x of the channel, were chosen. Based on these values, the EDL at the point x was computed as a 1D case. This process was then carried out for the rest of the subdomains.

After the computation was finished, the change in ion concentration was determined for each subdomain. Figure 6 shows the ion concentration gradient and the potential gradient across the EDL for the case V_G = 1 V, V_D = – 1 V, close to the D electrode (around 0.017 mm away). These values were chosen, because they provide the largest potential change possible in the model and in turn the largest concentration changes. The potential curve has the expected shape[2]. The concentration change Δc_{Na} is highlighted in the figure, as it is used to compute the conductivity. The concentration gradient is similar for other values of V_G and V_D. However, if the polarity is reversed (i. e. $V_G < V_D$) at some point x of the channel length, there is a negative value of Δc_{Na} – the Na^+ ions are pushed away from the electrode and the EDL. When the concentration change in an EDL subdomain of length L_x, width 0.1 mm and thickness λ_D was determined, the exchanged charge is given by the Faraday constant.

Based on this, the hole concentration and subsequently the conductivity was evaluated for each subdomain. Then, the curves of conductivity along the channel were constructed from the evaluated data.

In the third part, the Ohm's law (*5*), together with the Poissons equation (*1*), and the conductivity values gained earlier were used to model the transport of electric charge inside the channel and determine the output current. Due to the presence of ions in the polymer, the channel is expected to have a space charge density, given by equation (*7*) [3]:

$$\rho_v = (V(x) - V_G)C^* , \qquad (7)$$

where C^* is the volumetric capacitance of the polymer [F m^{-3}]. Table I shows the parametres and constants, used in the model.

Results and discussion

Figures 7 and 8 show the conductivity values for different V_G and V_D combinations. In these figures, the moving front of the dedoped polymer can be observed. It is possible to say, that the V_G value controls the absolute values of conductivity (i.e. the difference from the curve V_G = 0 V), while V_D controls the shape of the curve. In all cases, where $V_G < V_D$, the electric field gradient is reversed on the entire channel domain and the conductivity is therefore never lower than the base value. As a baseline, the value σ_0 = 320 S m^{-1} was chosen, based on literature[7,9]. The highest value of conductivity produced by the model was 348 S m^{-1}; the lowest value was 280 S m^{-1}. Note, that the base conductivity value is largely theoretical, based on hole concentration and mobility taken from different pieces of literature. Since the properties of PEDOT:PSS are strongly dependent on treatment during deposition, the σ_0 value represents a weak point of the model.

In the third part, representing the processes inside the PEDOT:PSS layer, the transfer curves of the OECT were modelled (see figs. 9 and 10). The transfer curves and current-voltage characteristics are realistic in the sense that the output

Table I, parametres and constants used in the model

Constant	Value
PEDOT:PSS relative permittivity[7]	2.2
NaCl solution relative permittivity[8]	78.3
PEDOT:PSS hole concentration[7]	$1 \cdot 10^{21}$ m^{-3}
PEDOT:PSS hole mobility[9]	2 m^2 V^{-1} s^{-1}
Na^+ diffusion coefficient[10]	$1.33 \cdot 10^{-9}$ m^2 s^{-1}
Cl^- diffusion coefficient[10]	$2.03 \cdot 10^{-9}$ m^2 s^{-1}
Bulk electrolyte concentration[6]	137 mol m^{-3}
PEDOT:PSS volumetric capacitance[11]	40 F cm^{-3}

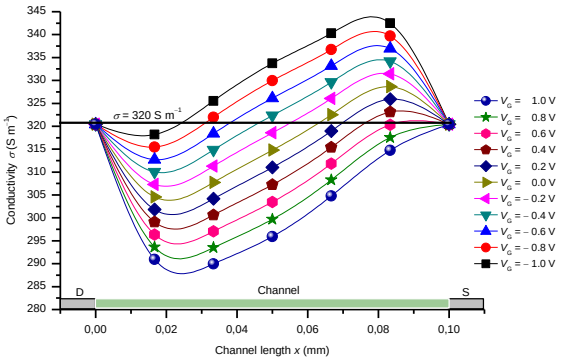

Fig. 7. **Conductivity values for $V_D = -0.6$ V and varying V_G values**

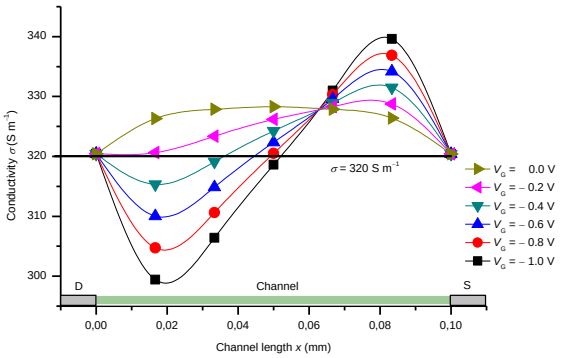

Fig. 8. **Conductivity values for $V_G = -0.4$ V and varying V_D values**

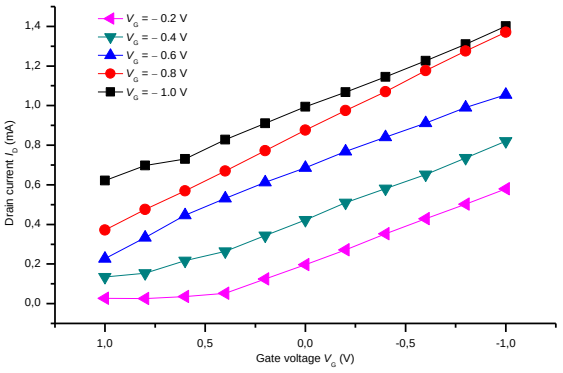

Fig. 9. **Transfer curves of the modelled OECT**

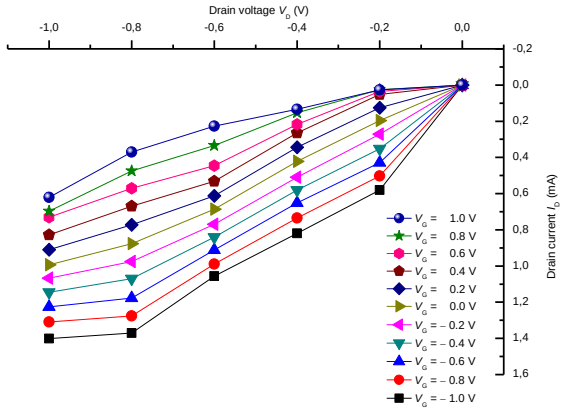

Fig. 10. **Current-voltage characteristics of the modelled OECT**

current is higher for lower values of V_G, and the shape of the curves bears some similarity to those of a real OECT. However, only the transfer curve taken for $V_D = -0.2$ V shows saturation (the I_D values becoming constant for sufficiently low or high voltages, due to complete dedoping or doping of the channel), and only in the positive V_G values. For the other curves, it is unclear whether they would show saturation for higher values of V_G and V_D. In any case, they do not match the behaviour of a real OECT.

Conclusion

A mathematical model of an organic electrochemical transistor was created, using the finite element method and utilizing the Poisson and Nernst-Planck differential equations. It is likely, that the improper modelling of saturation behaviour was caused by the simplification of the model and splitting due to low computer performance. This model effectively shows, how closely is it possible to match the behaviour of a real device without properly taking into account the hole drift and ion diffusion into the channel (i. e. computing only the transport processes in the EDL, and approximating the rest).

The research was supported by the Czech Science Foundation project no. GA17-24707S, the infrastructure was supported by the National Program for Sustainability I (MEYS CR) project no. REG LO1211.

REFERENCES

1. Rivnay J., Inal S., Salleo A., Owens R. M., Berggren M., Malliaras G. G.: Nat. Rev. Mater. *2*, 17086 (2018).
2. Pilon L., Wang H., D'Etremont A.: J. Electrochem. Soc. *5*, (2015), doi: 10.1149/2.0211505jes.
3. Tybrandt K., Zozoulenko I. V., Berggren M.: Sci. Adv. *12*, 3659 (2017).
4. Bernards D. A., Malliaras G. G.: Adv. Funct. Mater. *17*, 3538 (2007).

5. Löffler S., Libberton B., Richter-Dahlfors A.: J. Mater. Chem. B *3*, 4979 (2015) .
6. http://cshprotocols.cshlp.org/content/2006/1/pdb.rec8247, downloaded 18. 8. 2017
7. Rutledge S.A., Helmy A. S.: J. Appl. Phys. *13*, 133708 (2013).
8. Gavish N., Promislow K.: Phys. Rev. E *1*, 2611 (2016).
9. Inal S., Malliaras G. G., Rivnay J.: Nat. Commun. *1*, (2017), doi: 10.1038/s41467-017-01812-w.
10. https://medicalsciences.med.unsw.edu.au/research/research-services/ies/ionicmobilitytables, downloaded 18. 9. 2017.
11. Rivnay J. and 13 co-authors: Sci. Adv. *4*, 1400251 (2015).

FRYING QUALITY CHARACTERISTICS OF RAPESEED OIL USED FOR FRENCH FRIES PRODUCTION

LUCIA ZELEŇÁKOVÁ[a], MÁRIA ANGELOVIČOVÁ[a], MAREK ŠNIRC[b], JANA ŽIAROVSKÁ[c], STANISLAV KRÁČMAR[d], BRANISLAV GÁLIK[e]

[a]*Department of Food Hygiene and Safety, Faculty of Biotechnology and Food Sciences, Slovak University of Agriculture, Tr. A. Hlinku 2, 949 76 Nitra, Slovak Republic, lucia.zelenakova@uniag.sk*
[b]*Department of Chemistry, Faculty of Biotechnology and Food Sciences, Slovak University of Agriculture, Tr. A. Hlinku 2, 949 76 Nitra, Slovak Republic*
[c]*Department of Genetics and Plant breeding, Faculty of Agrobiology and Food Resources, Slovak University of Agriculture Tr. A. Hlinku 2, 949 76 Nitra, Slovak Republic*
[d]*College of Business and Hotel Management (CBHM), Bosonožská 9, 625 00 Brno, Czech republic*
[e]*Department of Animal Nutrition, Faculty of Agrobiology and Food Resources, Slovak University of Agriculture, Tr. A. Hlinku 2, 949 76 Nitra, Slovak Republic*

Keywords: rapeseed oil, deep-frying, total polar compound, peroxide and acid value, fatty acid methyl ester, oil deterioration

Abstract

The goal of this study was to analyse thermo-degradative changes of rapeseed oil during deep-frying French fries. In this context the purpose of our experiment was to examine the effect of deep-frying process on fatty acids composition, acid value, peroxide value and content of TPCs in used oil. TPCs values measured by Testo 270 grown in oil continuously since the first deep-frying. TPCs content in the fresh rapeseed oil was 3.3% and the threshold (24%) was achieved on the fourth day. The total time for the deterioration of deep-frying rapeseed oil was $23^{½}$ hours. Throughout the deep-frying process were in rapeseed oil measured acid values and peroxide values. At the beginning of deep-frying French fries in rapeseed oil, the acid number was 0.374 mg KOH/g and 1.271 mg KOH/g at the fourth day of depp-frying. The measured peroxide value was 4.3 mEq O_2/kg at the beginning and at the end of deep-frying 10.5 mEq O_2/kg. It should be note, than the acid values and peroxide values, respectively, in the fresh oil used in this study were below the limit of refined oil according to Slovak legislation (peroxide value – not more than 10 mEq O_2/kg, acid value – not more than 0.6 mg KOH/g). However, detected values varied during deep-frying process. Monounsaturated fatty acids were predominatly observed in fresh rapeseed oil (61.22%). The initial content of saturated fatty acids (SFA) in rapeseed oil was 6.94%, over the deep-frying process increased to 7.14, 7.33, 7.59 and 8.03%. The important groups of fatty acids in fresh rapesed oil were polynusaturated fatty acids (PUFA) which have in principle a significant effect on oil deterioration. The content of PUFA in oil was reduced by about 9.42% while the initial content was 28.14%.

Introduction

Frying is a more efficient process than other cooking methods and has gained a high popularity both in restaurants and in industry because of its speed and operational simplicity. Even though deep-frying is an old and very popular process, it is still poorly understood. Proper frying practice and the most appropriate frying oil are generally determined by experience[43,41,20,31]. Deep frying is classified as hot-fat cooking method (170°C – 200°C). Typically, deep frying cooks food quickly: all sides of a food are cooked simultaneously as oil has a high rate of heat conduction[36,3,38]. Deep frying is commonly utilized for food preparations such as frozen pre-fried foods, snack foods and fast foods[17,21,10].

The frying-process is a complex system depending on the extent of chemical reactions like oxidation, polymerization of triglycerides (TAGs), and hydrolysis where the physical and chemical properties of the heated fat are altering. It is difficult to estimate the extent of influence of each factor and to keep the frying conditions at an optimum level. Excellent reviews are published in the scientific literature describing the oxidative and hydrolytic changes during frying process[15,20,5,41].

Moisture in foods induces and accelerates oxidation with the hydrolytic compounds. Foods with high water content like potato and foods with breading or battering materials cause faster hydrolysis of frying oil. During frying, the fat of chicken or pork that is released into frying oil alters the fatty acid composition and increases the degradation rate of the oil[2,12]. TPCs content in deep-fried oils is an accurate and reliable indicator of oxidative degradation of frying oils. Herein, the determination of TPCs content has been widely used to evaluate the quality of frying oils. Although the formation of TPCs in different kinds of oils during frying process has been extensively studied[44,4,26,27,8,9] the comparison of the TPCs in deep-fried oils and the oils extracted from frying substance has not been done.

The content of total polar compounds and acid value are the most predominant indicators for oil quality and are widely used in many international regulations[18]. The contents of free fatty acid (FFA) and total polar compounds were commonly used for initial oil quality assurance and after-use frying oil quality assessment, respectively[23,24,10]. Several states reported an interest in passing legislation or amending regulations to require food establishments to inform customers of oil cooking type

used in food preparation and the percentage of saturated fat present in the cooking oil.

Materials and methods

Deep-frozen French fries were purchased at a local supermarket and stored in the freezer at -18 °C until being anylzed. The total quantity of French fries that were used in the experiment was 2.5 kg. For deep-frying French fries were used edible rapeseed oil bougt from market. This oil has wide spectrum of using in long-term and short-term thermal preparation of food (cooking, steaming, frying, baking) as well as in cold kitchen (salads, marinades, sauces etc.).

A commercial deep-fat fryer (Siemens TG 15001/01 Kreis Pinneberg, Germany) of capacity 2 L was used for the frying of French fries samples. Fresh rapeseed oil was loaded into the fryer separately and heated to 170 °C before frying. The same batch of French fries (100 g) was deep-fried and the same frying conditions (4 min, 170 °C) were applied. Afterwards, the French were placed in a plate and extra oil was sucked using tissue paper. The frying procedure was held constantly for 4 continous days (6 h per day according to reached 24% TPCs content). At the end of each day of frying the deep fryer was shut off and the oil was cooled down. Then, the oil was filtered to remove the solid residues. Time of oil sampling was different according to examinated parameters (explained below). All experiments were done at least in duplicates. All analyzes oil samples were carried out at Department of food hygiene and safety, FBFS, SUA in Nitra and at Department of animal nutrition, FAFR, SUA in Nitra as well.

Measurement of TPCs content by oil tester Testo 270 The TPCs content (total polar compounds) enables a statement on the deterioration of deep-frying oils due to the effects of heat. For quality analysis used oil samples (fresh and deep-fried) were taken every 30 min throughout the deep-frying process. Measurement of TPCs content in oils was carried out at an oil temperature 130 °C. Analyzes were terminated when the TPCs content reached ≥ 24%, which means oil wear.

Determination of peroxide value according to ISO 3960:2007 (EN) The peroxide value (PV) expressed in milliequivalents of active oxygen per kilogram (mEq O_2/kg) was calculated by the following equation:

$$PV = \frac{(V - V_0)\ x\ cthio\ x\ cstand\ x\ 1000}{m}$$

where:

V – is the volume of the 0.01 N sodium thiosulfate standard solution used for the determinantion, in millilitres

V_0 – is the volume of the 0.01 N sodium thiosulfate standard solution used for the blank test, in millilitres

c_{stand} – is the exact concentration of the 0.01 N sodium thiosulfate standard solution, in moles per litre

c_{thio} – is the approximate concentration of the 0.01 N sodium thiosulfate standard soludion, in moles per litre (= 0.01)

m is the mass of the test sample, in grams

For quality analysis used oil samples were taken in fresh state as well as deep-fried every 60 min throughout the deep-frying process.

Determination of acid value according to ISO 660:2009 (EN) An acid number of fat was expressed in mg KOH per g (mg KOH/g).

$$AV = \frac{56.1\ x\ Vx\ c}{m}$$

Where

AV: acid value

V – is the volume of the potassium hydroxide standard solution, in millilitres

c – is the exact concentration of the potassium hydroxide standard solution, in moles per litre m is the mass of the test sample, in grams

For quality analysis used oil samples were taken in fresh state as well as deep-fried every 60 min throughout the deep-frying process.

Determination of fatty acids composition by gas chromatography according to ISO 12966-1:2014 ISO 12966-1:2014 gives an overview of the gas chromatographic determination of fatty acids, free and bound, in animal and vegetable fats and oils following their conversion to fatty acid methyl esters (FAMEs). The bound fatty acids of the triacylglycerols (TAGs) and, depending on the esterification method, the free fatty acids (FFA) and other lipids, are converted to fatty acid methyl esters (FAMEs), which are determined by capillary gas chromatography. Depending on the number of different fatty acids (theoretically more than 50 different fatty acids can be present) capillary columns with a length of 10 m to 100 m are used for a separation.

For quality analysis used oil samples were taken in fresh state as well as deep-fried every day after 6-hour of deep-frying process.

Statistical analysis Mathematical and statistical evaluation of the results was realized by the SAS Enterprise Guide Version 1.5 system program. Measurements of duplicate samples were expressed as means ± standard deviation. The data were subjected to the analysis of variance (ANOVA) in the general linear models (GLM) and Pearson correlation coefficients (r_{xy}). The level of significance associated to the statistical test was 0.05.

Note: Oil sampling time: A/B/C/D – first/ second/ third/ fourth day of deep-frying 08/14 – at 8 am/at 2 pm

Results and discussions

Both, goal setting and implementation of the experiment itself were based on requirements of Slovak legislation[13]. It requires that deep-fat frying be carried out in accordance with good manufacturing practice and frying fats should not be heated above 180 °C (not longer than 24 hours of continuous frying). The law specifically forbids preparation of fried foods in equipment not provided with temperature control. However, practice shows that, especially, operators of fast food restaurants often violate these requirements and use "frying" oils for several days.

TPCs in oils during deep-frying French fries As was mentioned, TPCs content and polymer TAGs are the most reliable parameters for this purpose. Recommended and widely accepted limits are 24% for TPcs and 12% for PTG. As is shown

in Figure 1, TPCs values measured by Testo 270 grown in rapeseed oil continuously since the first deep-frying. TPCs content in the fresh oil was 3.3% and the threshold (24%) was achieved on the fourth day. The total time for the deterioration of deep-frying rapeseed oil was 23½ hours.

The statistical analysis (Scheffe´s test) showed that TPCs content was similar or lower at 8 o´clock compared to previous day (at 14 o´clock). However, this finding was not statistically significant (>0.05). Deeper analysis using Pearson correlation coefficients (r_{xy}) by Cohen (1988) showed that between days and hours of deep-frying French fries in rapeseed oil was found high positive linear correlation (P<0.001) between A08 and B08, C14; B08 and C14; B14 and C08. The other linear correlations were other medium negative (P>0.05) or none. In other results were no linear correlations. However, it can be said that deep-frying process directly increases TPCs content (<0.05).

For public health concerns, the content of total polar compounds in frying oil is regulated at not more than 25%, in Taiwan[23,24]. Some authors have published that the contents of TPCs in soybean oil and palm olein, respectively, were shown to exceed the limit of 25% after 48 h of frying with foods[10]. The other reported that the TPCs content in the above mentioned oils used to fry potato chips reached 25% after 20 h[26]. Simillar research was realized by[41].

As it was mentioned, over the frying process, TPCs increased linearly with the frying time. As shown Figure 1, level of detection reliability was 99.4% and between the time of deep-frying and TPCs content was found high positive linear correlation r = 0.997 (Table 1). The slope of regression line over time for oil frying with French fries was 0.79.

Similar results were also recorded by[10] during frying French fries, chicken leg fillets and pork chops. The content or TPCs in both soybean oil and palm olein increased linearly with frying time.

As was discussed in the 6th International Symposium on Deep-Frying in Hagen, polar compounds and polymeric triglycerides remain the most reliable chemical indicators for the chemical analysis of frying oils and fats[45].

Polar compounds and TAG oligomers which produced during deep-fat frying course with content range of 20 – 27% and 10 – 16%, respectively have been proposed to determinate the rejection of frying oil[42]. However, the measurement of polar compounds doesn't represent the whole content of reaction products formed during the deep-fat frying and the reaction products are not detailed in these indices. Some products were considered as potential detrimental substances to the human body from the nutritional aspect[35,40].

Therefore, it is quite necessary and useful to know more systematic precise information about the nature and quantity of the new compounds formed during the deep-fat frying course.

Acid and peroxide value in oils during deep-frying French fries The acid value and peroxide value are routinely used as a selective indicators for the degradation status. These parameters were measured in our research throughout the deep-frying process. At the beginning of deep-frying French fries in rapeseed oil, the acid number was 0.374 mg KOH/g and 1.271 mg KOH/g at the fourth day of depp-frying. The measured peroxide value was 4.3 mEq O_2/kg at the beginning and at the end of deep-frying 10.5 mEq O_2/kg. It should be note that both parameters were below the limit of refined oil according to Slovak legislation[14]. However, detected values varied during deep-frying process. In particular, peroxides are known to be unstable and volatile, as can be seen from Figure 2.

As it was mentioned, over the frying process, TPCs increased linearly with the frying time in both oils. The linear regression was also used in evaluating the reliability of peroxide and acid value detection (Figures 2 and 3). However, unlike TPCs detection, in these detections was found a lower reliability indicated by R^2. The determination coefficients were 0.8711 (peroxide value) and 0.7847 (acid value) in rapeseed oil. No significant differences in the peroxide value of rapeseed oil were observed in the first two days of frying. The first significant differences were found between B14 and A08, B08. Interestingly, no significant differences in the peroxide value were observed at the beginning of the third frying day and A08, A14, B08 and B14, but there were significant differences at the end of the third frying day and A08, A14, B08, C08. At the beginning of the last frying day, there were observed significant differences compared with A08, A14, B08 and C08. The peroxide value was significant different at the end of the last frying day compared with the first three frying days.

In the determination of acid value in oil, there were no significant differences among days and hours of deep-frying rapeseed oil.

During deep-frying process (125 °C), rapid oxidation occurs (accumulation of hydroperoxides) and peroxide value increased. However, but upon further heating at high frying temperatures, the peroxide value again decreases, because accumulated hydroperoxides are decomposed more rapidly and other secondary degradation products are formed. The rise of the peroxide value therefore occurs at a time when the oil cools and is not used. It can be concluded that measurement of the peroxide value is more suitable for measuring the quality of fresh oil than for measuring the quality of oil during frying and

Table I: Parameters of linear regression for TPCs, peroxide value and acid value in rapessed oil during deep-frying French fries

Summary output	TPCs (%)	Peroxide value (mEq O_2/kg)	Acid value (mg KOH/g)
Model	y = 3.04 + 0.7942x	y = 3.48 + 0.2481x	y = 0.31 + 0.038x
Multiple R (r)	0.997	0.933	0.886
R Square (R^2)	0.994	0.871	0.785
P- value	$5.24.10^{-57}$	$4.49.10^{-13}$	$3.71.10^{-10}$
Intercept	3.04	3.48	3.11
Slope	0.794	0.25	0.038

deep-frying, respectively[5]. For public health concerns, the acid value in frying oil is regulated at not more 2.0 mg KOH/g, in Taiwan[23,24]. From the results of[10,11] soybean oil contained 0.03 mg KOH/g of acid value, while palm olein contained slightly higher acid value (0.071 mg KOH/g). Other studies[19,39] also showed that the acid value in palm olein were higher than those in soybean oil.

Fatty acid methylesters composition in oils during deep-frying French fries In the present study, fatty acid profiles in rapeseed oil were analysed and compared over the deep-frying process of French fries at temperature 170 °C. As is shown in the table 2, in the fresh rapeseed oil was predominatly observed monounsaturated fatty acids (MUFA) (61.22%) and it was found a slight increase of MUFA (from 61.22 to 62.1) during depp-frying process. The initial content of saturated fatty acids in rapeseed oil was 6.94%, over the deep-frying process increased to 7.14, 7.33, 7.59 and 8.03%. The important groups of fatty acids in fresh rapesed oil were polynusaturated fatty acids (PUFA) which have in principle a significant effect on oil deterioration. The content of PUFA in oil was reduced by about 9.42% while the initial content was 28.14%.

The impact of the fatty acid composition on lipid oxidation was evaluated by measuring the relative percentage of unsaturated, polyunsaturated and saturated fatty acids. [34]studied the effect on PUFA/MUFA ratio in sunflower oil. They reported a higher reactivity of PUFA than MUFA (-linolenic acid > linoleic acid > oleic acid), as had previously been shown by different studies[30,33].

The major fatty acid in fresh rapeseed oil was oleic acid (59.64±0.00 %). A slight increase of oleic acid (C18:1) was observed in fried oil. At the end of frying period, oleic acid increased by 1.5%.

In contrary, amount of oleic acid decreased slightly from 38.70% to 32.06% in palm oil over the frying process. However, oleic acid content in the other two kinds of oils (palm kernel oil and coconut oil) remained unchanged (approximately 17% and 8%, respectively) during frying period[25]. The high oleic acid is reported as a better oil compared to regular sunflower, soybean, corn and peanuts oils due to its good thermal and oxidative stability during traditional frying[37,1,29,34].

In the case of palmitic (C16:0) and stearic acids (C18:0), they increased with the increase of frying time (from 4.52 to 5.11% and 1.49 to 1.75%, respectively, in rapeseed oil). Notably, even though no caprylic acid was observed in fresh rapeseed oil, it increased to 0.12% at the end of the frying procedure. The similar results were found in content of myristic acid (C14:0).

What is interesting, caprylic acid and capric acid were observed reduced in refined palm kernel oil and refined coconut oil. The medium-chain fatty acids are volatile under the high temperature[7]. Thus, the decrease of caprylic acid and capric acid in refined palm kernel oil and refined coconut oil could be explained by its evaporation during frying process.

In our study fresh rapeseed oil was found to have 18.96% of linoleic acid (C18:2) and 9.19% of linolenic acid (C18:3). The linoleic acid content was almost unchanged during frying process in rapeseed oil. The deterioration of (α) linolenic acid was more pronounced, with its contents being decreased by 30.25% in the last deay of deep-frying French fries in rapeseed oil. Similar results were found by[11] who detected by 20.86% lower linolenic acid content in palm oil. [3]reported decreases of 13.3% in linoleic acid and 47.1% in linolenic acid when fresh canola oil was heated at 215 °C for 7 days.

Fresh soybean oil was reported to have 21.5% of oleic acid (C18:1), 53.4% of linoleic acid (C18:2) and 5.1% of linolenic acid (C18:3) and saturated fatty acid[22]. It is important to note that soybean oil is commonly used for deep fat frying by Korean school meal services. Considering that linoleic acid (C18:2) has been more susceptible to oxidation than palmitic acid C16:0, the ratio of C18:2/C16:0 has been used as an indicator of the oxidative deterioration status in fried oils[32,3,6,8,44].

In our study, rapeseed oil has n-6/n/3 ratio around 2. This result is similar to this from Dubois et al. (2007) who analysed soybean oil (around 6). Since flaxseed oil stands out for containing high levels of n-3, and safflower oil stands out for introducing high n-3 values, the mixture of these oils may result in a mix with higher concetnrations of polyunsaturated fatty acids and different n-6/n-3 ratios.

Industrial food producers should understand the thermoxidative changes in their frying oils, especially below 15% polar compounds. In fast food restaurants where the products are prepared for the direct consummation the limits of degradation are much higher (i.e. 24% polar materials) and may be monitored by units that measure and related dielectric constant to the degree of degradation[45].

Conclusions

Our results, supported by other studies, provided the basis for choosing the suitable vegetable oil as well as rapid-measuring device to control the quality of frying oil in restaurants.

Based on our findings, we suggest:

for frying and deep-frying to use only oils for that purpose,

to keep the set temperatures and time with respect to the type of food,

to keep the established ratio between food and oil,

to filter the used oil at the end of the frying day to remove food debris,

to store the oil in a dark and cool place,

regularly check the oil quality, immediately to change oil showing the deterioration (exceeded smoke point and TPCs of 24%).

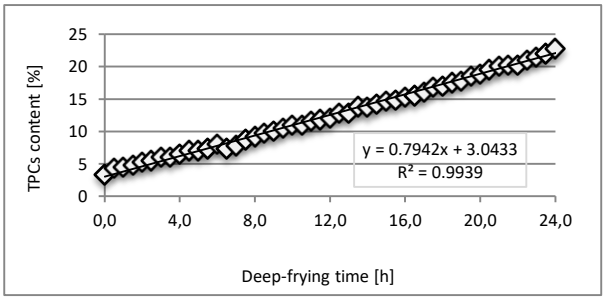

Fig. 1. **Determination of TPCs content in rapeseed oil during deep-frying French fries**

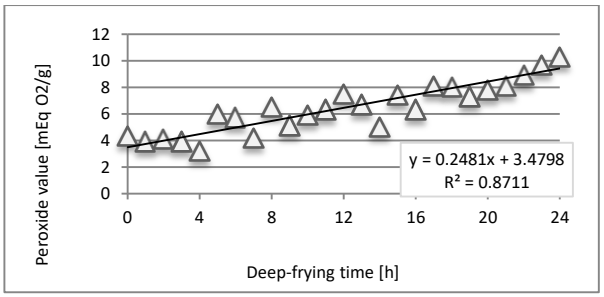

Fig. 2. **Determination of peroxide value in rapeseed oil during deep-frying French fries**

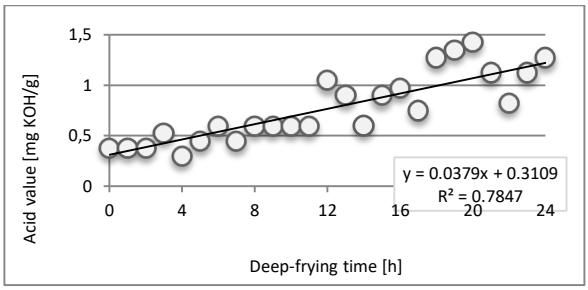

Fig. 3. **Determination of acid value in rapeseed oil during deep-frying French fries**

Fig. 4. **French fries and rapeseed oil after 4-days of deep-frying**

Table II: Fatty acids composition (%) of deep-fried rapeseed oil during frying process

FAMEs (wt %)	Rapeseed oil				
	fresh oil	after 1 day	after 2 days	after 3 days	after 4 days
palmitic acid C16:0	4.52±0.00	4.64±0.00	4.76±0.01	4.91±0.00	5.11±0.01
stearic acid C18:0	1.49±0.00	1.55±0.00	1.59±0.00	1.67±0.00	1.75±0.01
oleic acid C18:1cis n9	59.64±0.00	59.97±0.01	60.29±0.01	60.48±0.01	60.54±0.02
linoleic acid C18:2cis n6	18.96±0.00	19.00±0.00	18.92±0.00	18.93±0.01	18.89±0.01
arachidic acid C20:0	0.52±0.00	0.52±0.00	0.53±0.00	0.54±0.00	0.55±0.00
cis-11-eicosenoic acid C20:1 n9	1.23±0.00	1.23±0.00	1.23±0.01	1.22±0.00	1.21±0.00
behenic acid C22:0	0.31±0.00	0.31±0.00	0.32±0.00	0.34±0.00	0.36±0.00
lignoceric acid C24:0	0.11±0.01	0.12±0.00	0.12±0.00	0.13±0.00	0.15±0.00
caprylic acid C8:0	-	-	-	-	0.12±0.00
myristic acid C14:0	-	-	-	-	-
palmitoleic acid C16:1	0.22±0.00	0.22±0.00	0.23±0.00	0.23±0.00	0.23±0.00
α-linolenic acid C18:3 n3	9.19±0.00	8.58±0.00	8.00±0.00	7.28±0.01	6.41±0.02
erucic acid C22:1 n9	0.13±0.00	0.13±0.00	0.14±0.00	0.14±0.00	0.14±0.01
cis-13.16-docosadienoic acid C22:2	-	-	-	0.06±0.08	0.19±0.00
PUFA polyunsaturated fatty acids	28.14	27.58	26.92	26.26	25.49
MUFA monounsaturated fatty acids	61.22	61.56	61.88	62.06	62.11
SFA saturated fatty acids	6.94	7.14	7.33	7.59	8.03
ratio Σn3/Σn6	0.48	0.45	0.42	0.38	0.34
ratio Σn6/Σn3	2.07	2.22	2.36	2.60	2.95

Data are presented as means±standard deviations (SD). Every day were French fries deep-fried 6 hour except the last day (5.5 hour)

This study was supported by the Project KEGA No. 007SPU-4/2017 „Linking theory and practice in the study program Food safety and control by implementing modern didactic technologies within various forms of learning“.

REFERENCES

1. Abdulkarim S. M., Long K., Lai O. M., Muhammad S. K. S., Ghazali H. M.: Food Chemistry *105*, 1382 (2007).
2. Akoh, C. C., Min, D. B.: *Food Lipids.* Marcel Dekker, New York 2002.
3. Aladedunye F. A., Przybylski R.: Journal of the American Oil Chemists´ Society *86*, 149 (2009).
4. Aladedunye F. A., Przybylski R.: European Journal of Lipid Science and Technology, *116*, 144 (2014).
5. Alander J. et al.: Vegetable oils and fats. 2nd edition. Jan – Olof Lidefelt, Sweden 2007.
6. Alireza S., Tan C. P., Hamed M., Che Man Y. B.: International Food Research Journal *17*, 295 (2010).
7. Amri I. N., in book *Vegetable oils in food technology composition, properties and uses*, F. D. Gunstone (Ed.), A John Wiley Sons Ltd., Chiechester 2011.
8. Aniołowska M., Kita A.: Journal of the American Oil Chemists´ Society *92*, 1621 (2015).
9. Aniołowska M., Kita A.: Food Chemistry *203*, 95 (2016).
10. Chen W. A., Chiu Ch. P., Cheng W. Ch., Hsu Ch. K.: Journal of Food and Drug Analysis *21*, 58 (2013).
11. Chen Y., Yang Y., Nie S., Yang X., Wang Y., Yang M., Le Ch., Xie M.: Food Control *44*, 191 (2014).
12. Choe E., Min D. B.: Journal of Food Sciences *72*, 77 (2007).
13. Decree of the Ministry of Health of the Slovak Republic no. 125/2017 which amends Decree no. 533/2007 laying down requirements for mass caterers
14. Decree of the Ministry of Agriculture and Rural Development of the Slovac Republik no. 424/2012 laying down requirements for edible vegetable fats and edible vegetable oils and their products, including requirements for their production, labeling and division
15. Dobarganes C., Marquez-Ruiz G., Velasco J.: European Journal of Lipid Science and Technology *102*, 521 (2000).
16. Dubois V., Breton S., Linder M., Fanni J., Parmentier M.: European Journal of Lipid Science and Technology *109*, 170 (2007).
17. Fellows, P. J.: *Food Processing Technology*. (3th ed.), Woodhead Publishing, Oxford 2009.
18. Firestone D. in: *Deep Frying: Chemistry, Nutrition, and Practical Applications*, Erickson, M. D. (Eds.) AOCS Press, Urbana 2007.
19. Gerde J. A., Hardy C. L. M., Hurburgh C. R., White P. J.: Journal of American Oil Society *84*, 519 (2007).
20. Gertz, C.: European Journal of Lipid Science and Technology *116*, 669 (2014).
21. Gertz C.: European Journal of Lipid Science and Technology *102*, 566 (2000).
22. Juárez M. D., Osawa C. C., Acuña M. E., Sammán N., Gonçalves L. A. G.: Food Control *22*, 1920 (2011).
23. Lee C. H.: Taiwan Food News *232*, 38 (2009a).
24. Lee C. H.: Taiwan Food News *234*, 70 (2009b).
25. Li X., Jinwei L., Young W., Peirang C., Yuanfa L.: Food chemistry *237*, 98 (2017).
26. Man Y. B. C., Liu J. L., Jamilah B., Rahman R. A.: Journal of Food Lipid *6*, 181 (1999).
27. Mareček J., Fikselová M., Frančáková H., Muchová Z.: Chemické listy *102*, 718 (2008).
28. Mareček J., Mauerová J., Frančáková H., Mendelová A., Líšková M., Poberézny J.: Potravinárstvo *2*, 57 (2010).
29. Marmesat S., Morales A., Velasco J., Dobarganes M. C.: Food Chemistry *135*, 2333 (2012).
30. Martin-Polvillo M., Parquez-Ruiz G., Dobarganes M. C.: Journal of the American Oil Chemists ´Society *81*, 577 (2004).
31. Neethu K. C., Sharma A., K., Pushpadass H. A., Emerald F. M. E., Manjunatha M.: Innovative Food Science and Emerging Technologies *34*, 275 (2016).
32. Normand L., Eskin N. A. M., Przybylski R.: Journal of the American Oil Chemists´ Society *78*, 369 (2001).
33. Parker T. D., Adams D. A., Zhou K., Harris M., Yu L.: Journal of Food Science *68*, 1240 (2003).
34. Roman O., Heyd B., Broyart B., Castillo R., Maillard M.: Food Science and Technology *52*, 49 (2013).
35. Saguy I. S., Dana D., Journal of Food Engineering *56*, 143 (2003).
36. Seppanen C. M., Sarri-Csallany A.L: Journal of the American Oil Chemists´ Society *79*, 1033 (2002).
37. Smith S. A., King R. E., Min D. B.: Food Chemistry *102*, 1208 (2007).
38. Srivastava Y., Semwal A. D.: Journal of Food Science and Technology *52*, 984 (2015).
39. Tabee E., Jägerstad M., DuttA P. C.: Journal of the American Oil Chemists´ Society *86*, 885 (2009).
40. Totani N., Burenjargal M., Yawata M., Ojiri Y.: Journal of Oleo Science *57*, 153 (2008).
41. Zeleňáková L., Pastyriková S., Židek R., Mura L.: Potravinárstvo *6*, 45 (2012).
42. Zhang Q., Saleh A. S. M., Chen J., Shen Q.: Chemistry and physics of lipids *165*, 662 (2012).
43. Ziaiifar A. M., Achir N., Courtois F., Trezzani I., Trystram G.: International Journal of Food Science and Technology *43*, 1410 (2008).
44. Zribi A., Jabeur H., Aladedunye F., Rebai A., Matthäus B., Bouaziz M.: Journal of Agricultural and Food Chemistry *62*, 10357 (2014).
45. 6th International Symposium on Deep-Frying: Errors and Myths of Industrial and Catering Frying, 22-24 May 2011, Hagen Germany

LIST OF AUTHORS

CZECH CHEMICAL SOCIETY SYMPOSIUM SERIES • ročník/volume 16 (2018), čís./no. 6 • ISSN 2336-7202 (Print), ISSN 2336-7210 (On-line) • ISSN 2336-7229 (CD-ROM) • evidenční číslo MK ČR E 21999 • Vydává Česká společnost chemická jako časopis Asociace českých chemických společností ve spolupráci s VŠCHT Praha, s ČSPCH a ÚOCHB AV ČR za finanční podpory Rady vědeckých společností ČR, Akademie věd ČR, Nadace Český literární fond a kolektivních členů ČSCH • IČO 444715 • Published by the Czech Chemical Society • VEDOUCÍ REDAKTOR/EDITOR-IN-CHIEF: B. Kratochvíl • REDAKTOŘI/ EDITORS: J. Barek, Z. Bělohlav, E. Benešová, P. Drašar, P. Holý, P. Chuchvalec, Z. Kolská, J. Masák, J. Podešva, V. Vyskočil; Webové stránky: V. Vyskočil • TECHNICKÁ REDAKTORKA/EDITORIAL ASSISTANT: R. Řápková • Redakce čísla (ISSUE EDITOR) M. Vala • ADRESA PRO ZASÍLÁNÍ PŘÍSPĚVKŮ/MANUSCRIPTS IN CZECH, SLOVAK OR ENGLISH CAN BE SENT TO: Chemické listy, Novotného lávka 5, 116 68 Praha 1; tel./phone +420 221 082 370, +420 222 220 184, e-mail: chem.listy@csvts.cz • PLNÁ VERZE NA INTERNETU/FULL VERSION ON URL: http://www.ccsss.cz • TISK: Garamon s.r.o., Wonkova 432, 500 02 Hradec Králové • SAZBA, ZLOM: ČSCH, Chemické listy • Copyright © 2018 Czech Chemical Society Symposium Series/Česká společnost chemická • Cena výtisku 180 Kč • This journal has been registered with the Copyright Clearance Center, 2322 Rosewood Drive, Danvers, MA 01923, USA, where the consent and conditions can be obtained for copying the articles for personal or internal use • Pokyny pro autory najdete na http://www.ccsss.cz , zkratky časopisů podle Chemical Abstract Service Source Index (viz http://cassi.cas.org/search.jsp) • Molekulární námět na obálce: Vladimír Palivec • Dáno do tisku 11.12.2018.